HU ISSN 1785-6892 in print
HU ISSN 2064-7522 online

DESIGN OF MACHINES AND STRUCTURES

A Publication of the University of Miskolc

Volume 12, Number 2 (2022)

Miskolc University Press
2022

EDITORIAL BOARD

CONTENTS

Design of Machines and Structures, Vol. 12, No. 1 (2022), pp. 5–13.
https://doi.org/10.32972/dms.2022.008

THE VIKOR ALGORITHM IN MATERIAL DECISION SUPPORT

JUDIT ALBERT[1] – ÁGNES TAKÁCS[2]

University of Miskolc, Institute of Machine and Product Design
H-3515, Miskolc-Egyetemváros
[1]szalai.judit@student.uni-miskolc.hu, [2]takacs.agnes@uni-miskolc.hu
[1]https://orcid.org/0000-0001-8043-5503, [2]https://orcid.org/0000-0002-3210-6964

Abstract: The paper presents how to deal with frequent decision conflicts between design criteria that arise when selecting complex materials. The results show that the VIKOR model, in this case study, can also be used for extensive exploration of trade-offs and design return points, such as changes in environmental, material performance, and cost characteristics for the decision maker during design. In this paper, we examine the problem-solving algorithm for implementation.

Keywords: *Multi-Criteria Decision Making (MCDM), VIKOR, design theory, design methodology*

1. INTRODUCTION

Nowadays, the use of Multi-Criteria Decision Making (MCDM) in material selection processes has become an intensive research area in product development.
The study presents the application of a multi-aspect decision-making method designed for development needs that supports the work of engineers involved in the design and material selection tasks of hip prostheses. Opricovic [1] was the first to examine VIKOR (Vise Kriterijumska Optimizacija I Kompromisno Resenje), a method published in 1998, which focuses on the ranking of alternatives and their compromise selection for difficult-to-reconcile criteria. The advantages and limitations of the decision support application of the VIKOR method are presented using a design theory case study.
After presenting the results, we draw conclusions and make suggestions for further applications of the methodology (Figure 1).
In order to select the right materials, even in the case of alternatives to the simplest products, it is necessary to simultaneously consider many conflicting criteria when ranking them, which is usually a complex problem solution for decision-makers (DMs) (Figure 2).

The select of material is often limited or often based only on experience intended for practical purposes based on the available material properties, which can result in potential underutilization of materials or a reduction in life cycle.

2. REVIEW OF DECISION SUPPORTING METHODOLOGIES

Decision-making tasks are characterized by the fact that each alternative can have positive and negative sides, and the aspects can be both quantitative and non-quantifiable.
The VIKOR decision support method searches for the solution closest to the ideal solution, which is still feasible, from a set of alternatives with contradictory and non-comparable criteria (e.g., attributes with different measurement units).

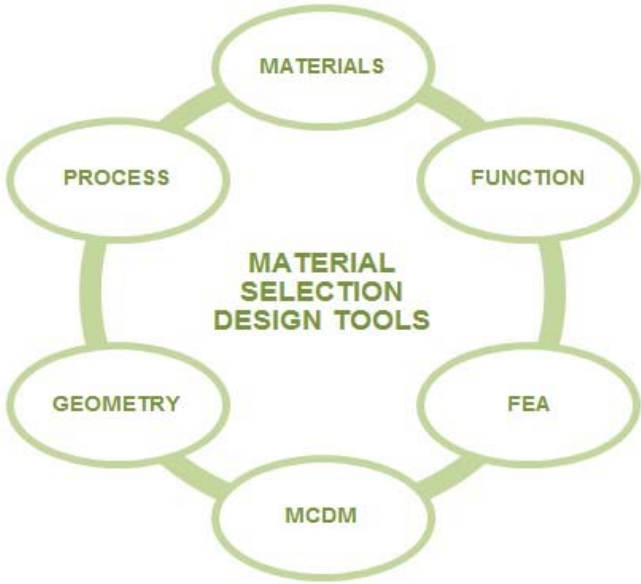

Figure 1. *MCDM as a material design / selection tool [2]*

Its basic concept is based on the definition of positive and negative ideal points in the solution space, and the degree of relative "closeness" to the "ideal" solution. The solution derived in this way is the selection of the alternative that is closest to the positive ideal solution and farthest from the negative ideal solution.
Due to the nature of the task, the model of the interval-based target value VIKOR method may be suitable for selecting the optimal alternative to be determined in our example, since it can be calculated separately whether the point value of each

alternative is significantly higher, that is, whether it can actually be considered better from the point of view of the decision maker. Another advantage is that, in the case of criteria that are difficult to reconcile, by focusing on the ranking and selection of the alternatives, a relatively small amount of data enables a sufficient comparison between the alternative.

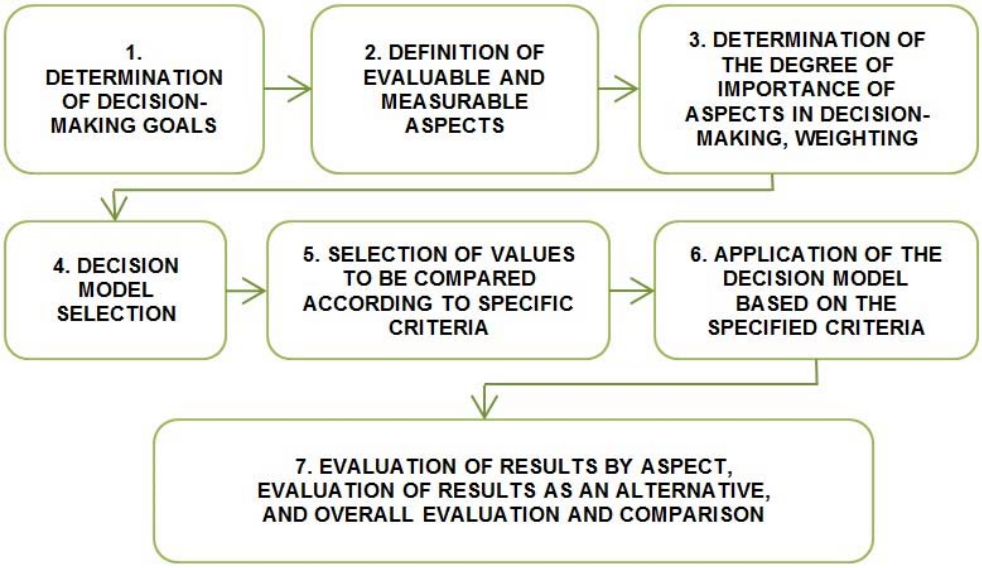

Figure 2. *Flowchart of decision support methodology [2]*

This study presents a method for the selection of hip prosthesis materials, suitable for handling decision conflicts between frequently encountered design criteria, and we illustrate how to be determined the optimal material alternative, with the interval-based target value VIKOR method. It was chosen because it can be calculated separately, whether the score of an alternative is significantly higher, that is, whether it can actually be considered better, in terms of material selection decision. [2]

A further advantage is that, in the case of difficult-to-reconcile criteria, focusing on the ranking and selection of alternatives, a relatively small amount of data allows for a sufficient degree of comparison between the alternatives. The essence of multi-criteria decision support methods is that, in general, conflicting impact criteria must be met at the same time, taking into account the limits of the available data.

The mathematical foundations of the algorithm are presented below, and illustrate the application of the method, whose model is shown in Equations (1) and (2).

$$\begin{array}{cccc} & \boldsymbol{A_1} & \cdots & \boldsymbol{A_n} \\ \boldsymbol{C_1}\ \boldsymbol{w_1} & \boldsymbol{u_i(a_{11})} & \cdots & \boldsymbol{u_1(a_{1n})} \\ & \vdots & \ddots & \vdots \\ \boldsymbol{C_m}\ \boldsymbol{w_m} & \boldsymbol{u_m(a_{m1})} & \cdots & \boldsymbol{u_m(a_{mn})} \\ & \boldsymbol{x_1} & \cdots & \boldsymbol{x_n} \end{array} \tag{1}$$

and

$$y_j = \sum_{i=1}^{n} \boldsymbol{w_i u_j}\left(\boldsymbol{a_{ij}}\right) u_{(x)} \tag{2}$$

where

$\boldsymbol{A_j}$: j[th] alternative;
$\boldsymbol{C_i}$: i[th] aspect;
$\boldsymbol{w_i}$: weight of the i[th] aspect;
$\boldsymbol{a_{ij}}$: value of the j[th] alternative according to the i[th] aspect;
$\boldsymbol{u_i}$: the evaluation (utility) function for the i[th] aspect;
$\boldsymbol{x_j}$: score of the j[th] alternative (place in the ranking).
Below, we present the mathematical foundations of the compromise ranking algorithm of VIKOR1. The $\boldsymbol{x_{ij}}$ elements of the $m \times n$ decision matrix determine the score that can be assigned to the ith alternative and the jth aspect. The decision matrix (3)

$$x = \left(\bar{x}_{ij}\right)_{m,n} \tag{3}$$

Step 1: Determination of the priority values of the aspects (4).

$$\bar{x}_{ij}{}^{+} = \max_{i}\left(\bar{x}_{ij}\right), \qquad \bar{x}_{ij}{}^{-} = \min_{i}\left(\bar{x}_{ij}\right), \tag{4}$$

where, $\bar{x}_{ij}{}^{+}$ aspect j is the best and $\bar{x}_{ij}{}^{-}$is the worst value of aspect j.

Step 2: Calculation of the level of utility and the level of individual dissatisfaction based on equations (5) and (6):

$$\boldsymbol{S_i} = \sum_{\boldsymbol{j=1}}^{\boldsymbol{n}} \boldsymbol{w_j} \frac{(\bar{x}_j{}^{+} - \bar{x}_{ij})}{(\bar{x}_j{}^{+} - \bar{x}_j{}^{-})} \tag{5}$$

$$\boldsymbol{R_i} = \underset{\boldsymbol{j}}{\boldsymbol{max}} \left[\boldsymbol{w_j} \frac{(\bar{x}_j{}^{+} - \bar{x}_{ij})}{(\bar{x}_j{}^{+} - \bar{x}_j{}^{-})} \right] \tag{6}$$

where, $\boldsymbol{w_j}$ is the weighting of the aspects, $\boldsymbol{S_i}$ is the measure of utility and $\boldsymbol{R_i}$ is the measure of individual dissatisfaction.

Step 3: Determination of the value of $\boldsymbol{Q_i}$ based on equation (7):

$$\boldsymbol{Q_i} = v \left(\frac{\boldsymbol{S_i} - \boldsymbol{S^+}}{\boldsymbol{S^-} - \boldsymbol{S^+}} \right) + (\boldsymbol{1} - v) \left(\frac{\boldsymbol{R_i} - \boldsymbol{R^+}}{\boldsymbol{R^-} - \boldsymbol{R^+}} \right) \tag{7}$$

when,

$$\boldsymbol{S^+} = \underset{\boldsymbol{i}}{\boldsymbol{min}} [(\boldsymbol{S_i}),\ \boldsymbol{i = 1, 2, \dots, m}]$$

$$\boldsymbol{S^-} = \underset{\boldsymbol{i}}{\boldsymbol{max}} [(\boldsymbol{S_i}),\ \boldsymbol{i = 1, 2, \dots, m}]$$

$$\boldsymbol{R^+} = \underset{\boldsymbol{i}}{\boldsymbol{min}} [(\boldsymbol{R_i}),\ \boldsymbol{i = 1, 2, \dots, m}]$$

$$\boldsymbol{R^-} = \underset{\boldsymbol{i}}{\boldsymbol{max}} [(\boldsymbol{R_i}),\ \boldsymbol{i = 1, 2, \dots, m}]$$

where, v gives the weighting of the decision-making strategy of 'the majority of criteria' (or 'the maximum group utility'), the value of which varies between 0-1, and the decision-maker determines its value. The decision-maker can also apply the maximization of the criteria's usefulness (v =1) and the minimum individual dissatisfaction strategy, i.e., the maximization of the individual dissatisfaction values of aspects considered to be of lower importance (v=0). (Another compromise can be given by v 'majority vote' ($v > 0.5$), 'consensus' ($v = 0.5$) or 'veto' ($v < 0.5$). In general, a v value of 0.5 is preferred. In this paper, the value of v is 0.5 (this value gives a result with sufficient accuracy, since most decision-making processes include both decision strategies.)

Step 4: The alternatives are ranked based on the $\boldsymbol{Q_i}$, VIKOR index value, according to which the lower the value, the better the ranking of the given alternative.

3. RESULTS OF OPTIMIZATION SUPPORTING PROCESS

In the decision situation examined in our example, the decision maker evaluates a finite number of alternatives based on a finite number of criteria. The alternatives are denoted by $\boldsymbol{A_1} \ldots \boldsymbol{A_n}$, and the aspects by $\boldsymbol{C_1}, \boldsymbol{C_2}, \boldsymbol{C_3}$ ..., $\boldsymbol{C_m}$.
When evaluating the alternatives, the most basic aspect to be taken into account is the cost aspect, and an important aspect is also the availability of the necessary materials. Another essential aspect is the reliability of the alternatives, as well as their guaranteed lifespan.
As the first step in the choice of material for the hip prosthesis examined in our example, we mapped the hip prosthesis materials found in medical practice (Table 1) and their material characteristics. The optimal load absorption of the material selection alternatives can be measured by the structural utilization, i.e. the over- or under-sizing resulting from each design can be specified at this point. The suitability of the basic material of the hip prosthesis can be examined on the basis of several aspects [3, 4]. With the interconnected open pores and large surface area of Porous NiTi alloys are emerged to be one of the promising biomaterials for prosthesis.[5] The hip prosthesis performs such complex functions, where relevant requirements include tolerance, corrosion resistance, compliance with mechanical requirements, flexible compatibility, and weight and cost. Since all material is generate a 'foreign body reaction' when implanted in the body, therefore, biocompatibility is directly related to the corrosion behaviour of the material in a specified solution and the tendency for the alloy to release potential toxic ions [6, 7].
In our case, in the decision situation, denote the material properties n and the number of possible materials m. The evaluation criteria were density (g/cm3), tensile strength (MPa), modulus of elasticity (GPa), elongation (%), corrosion resistance, wear resistance and ossification efficiency. (Table 2) The aim is to find the most suitable raw material based on the selected criteria, or to establish a ranking among the raw materials, which one meets the given expectation (8). Let it be

$$\left[x_{ij}^{L}, X_{ij}^{U}\right] \tag{8}$$

the interval for the jth characteristic of the ith material, where i= 1, ..., m, j = 1, ..., n. In order to make a decision, we need a target value with the properties of the ideal material.
Mark each target value T1, T2, ..., Tn. In order to approximate the target values, the corresponding weighting is required (9), which specifies how important each feature is, and therefore the weights associated with each feature w_1, ..., w_n, mark where $w_j \geq 0$, j=1,..., n and

$$\sum_{j=1}^{n} w_j = 1 \tag{9}$$

When we want to maximize or minimize a criterion, we can select a maximum or minimum of data for a particular characteristic of the target values (Table 3).

Table 1

Material alternatives considered in the comparative process

Materials	
A_1	Stainless steel L316 (annealed)
A_2	Stainless steel L316 (cold worked)
A_3	Co-Cr alloys (wrought Co-Ni-Cr-Mo)
A_4	Co-Cr alloys (castable Co-Cr-Mo)
A_5	Ti alloys (pure Ti)
A_6	Ti alloys (Ti-6A1-4V)
A_7	Ti-6A1-7Nb (IMI-367 wrought)
A_8	Ti-6A1-7Nb (Protasul-100 hot-forged)
A_9	NiTi SMA
A_{10}	Porous NiTi SMA

Table 2

Evaluations criteria of materials

Evaluation criteria	
C_1	Density (g/cm3)
C_2	Tensile strength (MPa)
C_3	Modulus of Elasticity (GPa)
C_5	Elongation (%)
C_6	Corrosion resistance, biocompatibility
C_7	Wear resistance
C_8	Osseointegration

By processing the properties of the alternatives, we ranked the alternatives in an Excel implementation using the mathematical model of the VIKOR method. Table 4 presents the results of the evaluation process.

Table 3

Aspects taken into account during the process of comparing alternatives and their importance value

Evaluation c	w_i importance	Target value	Max	Min
C_1	0.071429	1.3	9.13	4.3
C_2	0.1071429	1240	1240	517
C_3	0.1428571	16	240	15
C_4	0.1071429	54	54	10
C_5	0.1785714	0.955	0.955	0.665
C_6	0.202381	0.955	0.955	0.59
C_7	0.190476	0.955	0.955	0.5

Table 4

S, R and Q scores and rank

Weight of aspects	0.5	Criteria's usefulness	0.5				
Materials	S_i^L	S_i^U	R_i^L	R_i^U	Q_i^L	Q_i^U	Rank
A_1	0.852931	0.8529314	1	1	1	1	10
A_2	0.784044	0.7840443	1	1	0.9382489	0.9382489	9
A_3	0.623685	0.6723866	1	1	0.7945014	0.8381578	8
A_4	0.651828	0.7005293	0.9955556	1	0.8001732	0.8633852	7
A_5	0.475071	0.4750706	1	1	0.6612816	0.6612816	5
A_6	0.478275	0.4782752	0.9545455	0.9545455	0.4641542	0.4641542	3
A_7	0.492118	0.501642	1	1	0.6765632	0.6851005	6
A_8	0.453479	0.4804736	0.8863636	1	0.1419267	0.6661249	2
A_9	0.360503	0.360503	1	1	0.5585819	0.5585819	4
A_{10}	0.295151	0.2951514	0.545455	0.9545455	0.3	0.3	1

As a result of the ranking of the VIKOR method, among the alternatives, the tenth alternative A_{10} Porous NiTi SMA (Shape Memory Alloy) was ranked the best, ahead of the A_8 and A_6 titanium alloys, and the first alternative A_1 Stainless steel L316 (annealed) was the one that came to the bottom of the ranking.

4. SUMMARY

By applying a ranking method that supports the selection of different alternatives, based on an individual decision-maker's evaluation criteria system, based on our results, it can be stated that the VIKOR method can be effectively used to support the design processes of hip prostheses.
During the evaluation, it can be established that the disadvantages of the method include the fact that the result only gives a ranking between the alternatives, so there is not enough information available about the magnitude of the difference between the alternatives, so the decision-maker receives a certain ranking, but does not have information about the proportions of the differences. Therefore, it would be advisable to use the AHP (Analytical Hierarchy Process) for the further development of the methodology, which makes this information determinable, thereby increasing the effective support of decision makers.

REFERENCES

[1] Opricovic, S. (1998). *Multicriteria Optimization of Civil Engineering Systems*, PhD Thesis, University of Belgrade.

[2] Ali, J. et al. (2016). *Multicriteria Decision Analysis for Supporting the Selection of Engineering Materials in Product Design*, Butterworth Heinemann, ISBN 9780081005361.

[3] De Jonge, T. et al. (2018). Elülső feltárásból végzett minimál invazív csípőprotézis beültetéssel szerzett kezdeti tapasztalatok, *Magyar Traumatológia Ortopédia Kézsebészet Plasztikai sebészet*, Vol. 61, No. 3-4, ISSN 1217-3231, https://doi.org/10.21755/mto.2018.061.0304.005.

[4] Wu, S. L. et al. (2006). Surface characteristics, mechanical properties, and cytocompatibility of oxygen plasma-implanted porous nickel titanium shape memory alloy, *Journal of Biomedical Materials Research*, Vol. 79A, No. 1, ISSN 1552-4965, https://doi.org/10.1002/jbm.a.30705.

[5] Ghazali, M. J. et al. (2015). Surface modification and their effects on titanium dental implants, *Biomed Research International*, Vol. 2015, Article ID 791725, ISSN 2314-6141 (Online), https://doi.org/10.1155/2015/791725.

[6] Duerig, T. et al. (1999). An overview of nitinol medical applications, *Materials Science and Engineering A*, Vol. 273-275, ISSN 0921-5093, https://confluent-medical.com/wp-content/uploads/references/029.pdf.

Design of Machines and Structures, Vol. 12, No. 1 (2022), pp. 14–24.
https://doi.org/10.32972/dms.2022.009

ANALYTICAL AND EXPERIMENTAL STUDY OF BEAM BENDING VIBRATION

IYAD F. AL-NAJJAR[1], LÁSZLÓ E. KOLLÁR[2], KÁROLY JÁLICS[3]

[1,3]University of Miskolc, Institute of Machine and Product Design, Miskolc-Egyetemváros
[2]Savaria Institute of Technology, ELTE Eötvös Loránd University, Budapest
[1]iyad.al-najjar@uni-miskolc.hu, [2]kl@inf.elte.hu, [3]machijk@uni-miskolc.hu
[2]https://orcid.org/0000-0002-0589-9575, [3]https://orcid.org/0000-0003-0749-7569,

Abstract: This study presents free bending vibration analysis of beams of glass epoxy material. The analytical and the modal model (experimental) methods were used to conduct the investigation. The experiment represents basic concepts of the modal model analysis method, which allows us to find the beam's natural frequencies and vibrational mode shapes. The analytical solution was found using Maple and compared to the frequencies obtained experimentally.

Keywords: *Transverse vibration, Modal analysis, Analytical solution, Free-Free beam, Cantilever Beam.*

1. INTRODUCTION

Vibrational problems are critical in most engineering applications. Hence, understanding the vibration effects in an application is essential. In the last decades, the Modal analysis has become one of the most used methods for determining and optimizing the dynamic characteristics of engineering applications and different fields such as mechanical, aeronautical, civil, biomechanical, acoustic engineering and music instruments, transportation, and many other areas. Modal analysis determines the dynamic properties of a given system in the frequency domain.
Free vibration happens when no external vibration force is applied on the system. The system, in this case, the beams, starts vibrating due to initial displacement or by using a tool like a shaker. The first part of this investigation consists of the exact solution for the two boundary conditions (constraints on the beam due to its supports). They are the Free-Free and Fixed-Free beams. Maple was used to find the exact solution and plot each case's mode shapes.
In recent decades, modal analysis has been used in many specialized engineering fields related to dynamic structural analysis [1]. In the experiments, the system

vibrates due to a shaker then the displacement is measured in time using a sensor. The sensor is attached to the system, either transducer (accelerometer) or noncontact like lasers or cameras. When the shaker starts vibrating the beam, the accelerometer will collect data as displacement (amplitude) in time for the specific point of the beam. This data is sent and displayed on a computer.
This study aims to understand the vibration of a simple model (geometry) for wind turbine blades: the fixed-free beam, also known as the cantilever beam. After that, in future studies, the system will be improved into a more complicated beam by adding more conditions or changing the beam, such as a change in the cross-section area, pre-bending, moving mass on the beam, or attaching a spiral spring to the beam.

2. ANALYTICAL STUDY

In this section, the equation of motion and boundary conditions are given, which are used to obtain the characteristic equation and eigenvalues. Then the mode shapes are plotted.

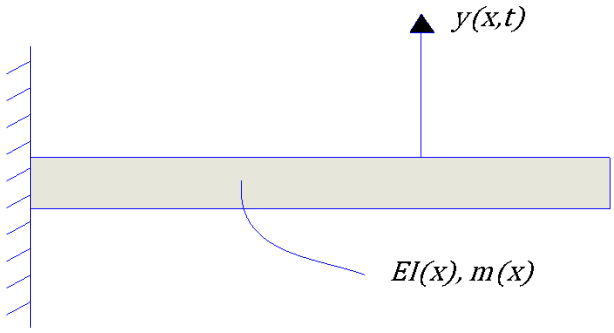

Figure 1. *Cantilever Beam*

Figure 1 shows the schematic setup of the problem (cantilever beam). By applying the Euler–Bernoulli theory on the system to derive the equation of motion, the following equation is obtained [2]:

$$EI\,\frac{\partial^4}{\partial x^4}y(x,t) + \rho A\,\frac{\partial^2}{\partial x^2}y(x,t) = 0. \tag{1}$$

The constants of this equation are E (Young's modulus of elasticity), I (the moment of inertia), ρ (the density of the beam), and A (the cross-section area), while

$y(x,t)$ is the deflection function. By using the method of separation of variables and rearranging some terms, the following equation is obtained:

$$\frac{d^4}{\mathrm{d}x^4} y(x) - \beta^4 y(x) = 0. \tag{2}$$

The wave number β in this equation can be expressed as follows

$$\beta^4 = \omega^2 \frac{m}{EI}, \tag{3}$$

where ω is the angular frequency, and m(x) shown in Figure 1 is the mass per unit length that is constant for our case, i.e., m(x)=m.
The spatial part of the solution can be presented as follow:

$$y(x) = A\sin(\beta x) + B\cos(\beta x) + C\sinh(\beta\, x) + D\cosh(\,\beta\, x). \tag{4}$$

The boundary conditions, the characteristic equation, and the eigenvalues are presented in Table 1. The characteristic equation for each case is obtained by using the solution in equation (4) to solve the equation of motion (1) using the boundary conditions in Table 1. Further details can be found in [3].

Table 1

Boundary conditions, Characteristics equation, and Eigenvalues for Free-Free and Fixed-Free beams

Free-Free		**Fixed-Free**	
Right end	**Left end**	**Right end**	**Left end**
$\frac{\mathrm{d}^2}{\mathrm{d}x^2}\, y(x) = 0$	$\frac{\mathrm{d}^2}{\mathrm{d}x^2}\, y(x) = 0$	$y(x) = 0$	$\frac{\mathrm{d}^2}{\mathrm{d}x^2}\, y(x) = 0$
$\frac{\mathrm{d}^3}{\mathrm{d}x^3}\, y(x) = 0$	$\frac{\mathrm{d}^3}{\mathrm{d}x^3}\, y(x) = 0$	$\frac{d}{dx}\, y(x) = 0$	$\frac{\mathrm{d}^3}{\mathrm{d}x^3}\, y(x) = 0$
Characteristics equation	$\cos(\beta_n L)\cosh(\beta_n L) - 1 = 0$ $n = [0,1,2,\dots]$	$\cos(\beta_n L)\cosh(\beta_n L) + 1 = 0$ $n = [1,2,\dots]$	
Eigenvalues(β_nL)	[0., 4.730, 7.853, 10.99, 14.137,]	[1.875, 4.694, 7.854, 10.995, 14.137]	

Natural frequencies are calculated from the eigenvalues listed in Table 1 and they are compared with the frequencies obtained experimentally as shown in Table 3 and Table 4, whereas the mode shapes are obtained from the deflection function.
The free-vibration solution for the beam with free-free ends is obtained as follows

$$y(x) = -\frac{(\cos(\beta l) - \cosh(\beta l))\sin(\beta x)}{sin(\beta l) - \sinh(\beta l)} + cos(\beta x) - \frac{(\cos(\beta l) - \cosh(\beta l))\sinh(\beta x)}{sin(\beta l) - \sinh(\beta l)} + \cosh(\beta x). \quad (5)$$

The first five mode shapes for the free-free ends are plotted in Figure 2.

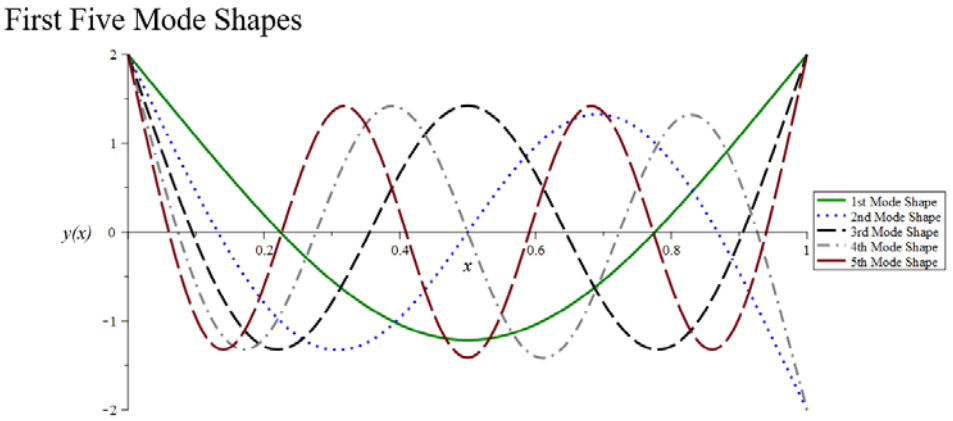

Figure 2. *First Five mode shapes for Free-Free beam. The x-axis presents the dimensionless length, while the y-axis is the deflection*

The free vibration solution for the cantilever beam is the following:

$$y(x) = \frac{(\cosh(\beta x) - \cos(\beta x))\sinh(\beta l)}{\sin(\beta l) + sinh(\beta l)} + (\cosh(\beta x) - \cos(\beta x))\sin(\beta l) - \left(\cos(\beta l) + \cosh(\beta l)\right)(\sinh(\beta x) + \sin(\beta x). \quad (6)$$

The first five mode shapes for the cantilever beam are plotted in Figure 3. Figure 2 and Figure 3 illustrate the beam's deflection y(x) along the x-axis for the first five mode shapes for the Free-Free and Fixed-Free cases, respectively. For instance, when the beam gets excited at the first natural frequency, the beam will be deflected into the shape of the first mode shape in the figure.

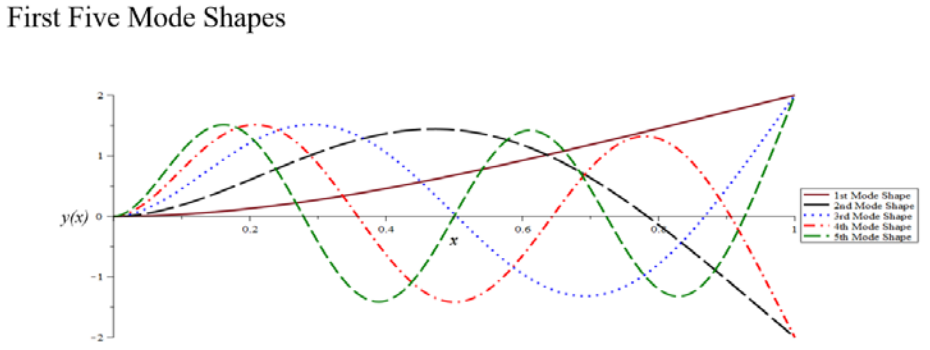

Figure 3. *First Five mode shapes for Cantilever beam. The x-axis presents the dimensionless length, while the y-axis is the deflection*

3. EXPERIMENTAL METHOD (MODAL MODEL ANALYSIS)

Modal analysis studies the dynamic properties of systems in the frequency domain. Such analysis is carried out to study the free vibration of machines and structures such as a car, a turbine blade, or a wind turbine. The experiments need the following items to be carried out:

- Sensors like transducers (accelerometers) or noncontact like lasers or cameras to measure the system answer caused by an excitation.
- Force transducer to measure the excitation force.
- An analog-to-digital converter front end (DAQ) and a host PC are to view the data in which Fourier series is used to analyse the data where the resulting transfer function demonstrates the natural frequencies.

The experiment for this study consists of the following items shown in Figure a:

1. A shaker.
2. Data acquisition board (DAQ).
3. Impedance head (accelerometer and force transducer in one housing).
4. A computer.

The measurements are carried out with the following software setup:

- Frequency range: 0 – 18750 Hz
- Frequency resolution: 0.732 Hz
- Excitation signal: white noise
- Number of averages: 30 (linear average)
- Hanning window
- Measuring transfer functions (FRF): a/F; v/F, and for each FRF also the coherence function

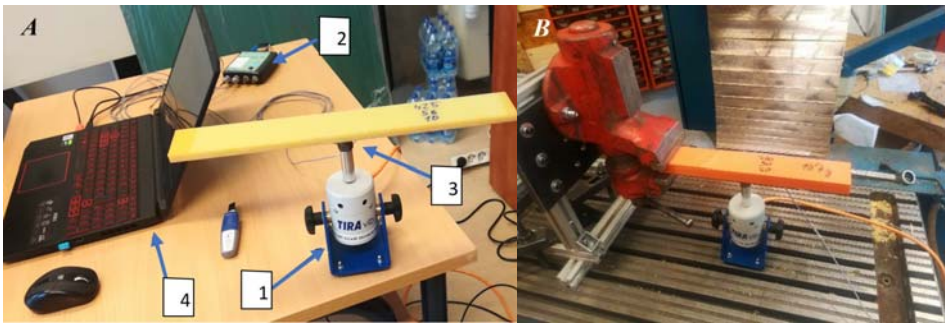

Figure 4. *Experimental setup for (A) Free-Free beam and (B) Cantilever beam*

In order to determine the modal parameters (natural frequencies, damping, and mode shapes) of a specimen, the so-called frequency response functions (FRF) have to be constructed from the measurements. The FRFs are functions that are constructed, in this case, from the excitation force and from the response function of the system to the excitation. The response functions are in this measurement the acceleration (in the excitation point measured with impedance head) and the velocity (at the end of the beam, measured with laser vibrometer). The FRFs are in general, recorded in several points of the specimen geometry, so the mode shapes can also be calculated. In our case, we only measured 2 points, so the experimental mode shapes could not be calculated.
Three specimens are selected for the modal model analysis with the data in Table 2. The data was imported into MATLAB to plot figures for different cases. These figures are followed by tables showing the experimental and analytical (theoretical) values of the natural frequencies and the error between them.

Table 2
Parameters for the three specimens

Specimen	**Material**	**Dimensions (m)**			**Mass (kg)**	**Young's Modulus (GPa)**
		Length	**Width**	**Height**		
1	Glass epoxy	0.390	0.06	0.015	0.655	10.5
2	Glass epoxy	0.425	0.058	0.01	0.462	12
3	Printed	0.3	0.05	0.02	0.197	14

Glass epoxy has a range of different values for Young's modulus in the transverse direction. In papers [4], [5], and [6] a range for its possible values can be found. For our purposes, we selected the values in table (2), which minimizes the error among a large number of frequencies.

Two different boundary conditions were applied for every specimen (Free-Free, and fixed-free), and the experimental results were compared to the exact solution for each case.

Figure 5 illustrates the behaviour of the first specimen (15 mm) in the Frequency-Acc/Force domain, where the peaks in the figures represent the resonance frequencies. The left part is for the free-free case, while the right side is for the fixed-free beam.

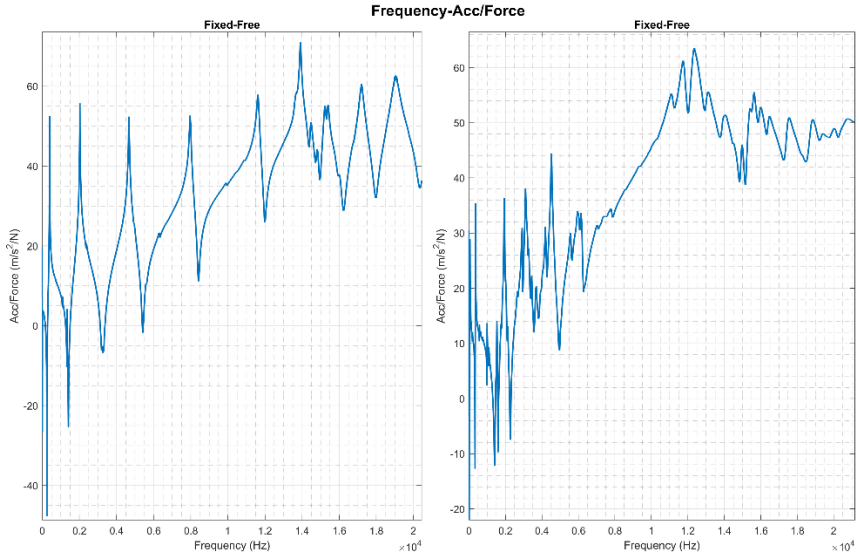

Figure 5. *Frequency-Acc/Force domain for the first specimen (15 mm)*

Table 3

Experimental and analytical results for different frequencies and the error between them for the first specimen (15 mm)

15 mm	Experiment (rad/sec)	Analytical (rad/sec)	Error %
	Fixed-Free		
ω_1	361.2	380.2	4.988
ω_2	2245.7	2382.7	5.747
ω_4	12135.3	13073.7	7.177
	Free-Free		
ω_1	2475.8	2419.3	2.335
ω_3	12733.5	13073.9	2.603
ω_5	29346.5	32284.3	9.099

Table 3 represents the values for different natural frequencies analytically and experimentally with the error for the first specimen (15 mm). The unit of the frequency in the experiment is Hz, so it was converted into rad/sec to compare it with the analytical value.
Figure 6 illustrates the first beam's behaviour in the Frequency-Acc/Force domain. The left part is for the Free-Free case, while the right side is for the Fixed-Free beam.
Table 4 represents the values for different natural frequencies analytically and experimentally with the error for the second specimen.

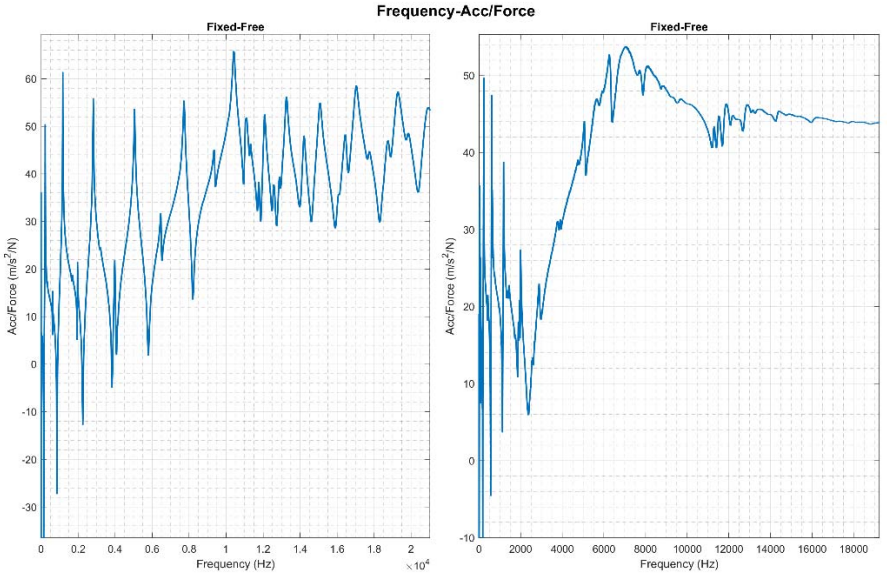

Figure 6. *Frequency-Acc/Force domain for the second specimen (10 mm)*

The error increases with the increase in frequency due to two main reasons. The first one is the inhomogeneous elasticity of the material, and the second one is an assumption applied in the mathematical model considered for the system. The shaker is attached to the beam at a specific point. At that point, the shaker acts as a pin-support, yet the shaker's force on the beam is assumed to be zero in the mathematical model. At higher frequency (displacement), the force increases, which increases its effect on the system and the error's value as well.

Table 4

Experimental and analytical results for different frequencies and the error between them for the second specimen (10 mm)

10 mm	Experiment (rad/sec)	Analytical (rad/sec)	Error %
	Fixed-Free		
ω_1	227.6	218.1	4.360
ω_2	1417.3	1366.8	3.698
ω_4	3815.0	3827.1	0.318
	Free-Free		
ω_1	1389.7	1387.8	0.138
ω_3	7367.7	7499.8	1.761
ω_5	17708.2	18519.9	4.382

In paper [7], the researchers compared the natural frequencies obtained by the FEM and the experimental method. The error between the frequencies from both methods kept increasing with the increase in the number of the natural frequencies. This might be because the FEM uses a complete mathematical model. Nevertheless, the increase in error might be due to the used material, human error, or numerical errors.

4. RESONANCE FREQUENCIES FROM THE MODAL METHOD

The modal model method can be used to construct the mode shapes of the beam experimentally [8] by placing sensors (for example, accelerometers) at different points along the beam and comparing the results.

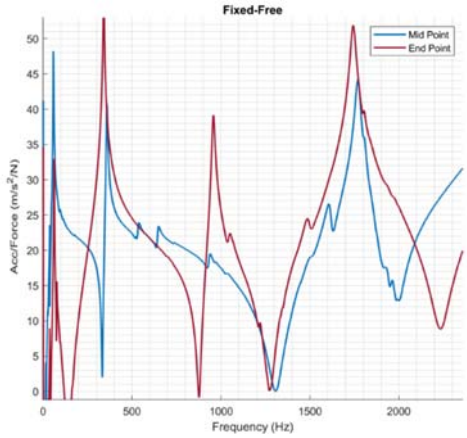

Figure 7. *The resonance frequencies from the experimental data*

In Figure 7, we can see the data obtained in the same experiment for two different points. One point is at the beam's free end, while the other one is in the middle. The beam has zero displacements at the middle point for the third natural frequency. Hence, the sensor could not detect any significant movement (deflection). The mode shapes can be built by tracking such pieces of information from the experimental data and from the geometrical location of the sensors.

5. SUMMARY AND CONCLUSION

The free vibration of a Free-Free Beam and a Cantilever beam has been investigated analytically and experimentally with glass epoxy material. The relative error between the exact theoretical solution and experimental values is at its minimum (less than 1%) at small frequencies and increases at higher frequencies to more than 10%. This is due to the inhomogeneity of the material and the mathematical model, which does not accommodate the force between the beam and the shaker. The paper also showed the possibility of building the vibrational mode shapes from the experimental data.

ACKNOWLEDGEMENTS

Project no. TKP2021-NVA-29 has been implemented with support from the Ministry of Innovation and Technology of Hungary from the National Research, Development and Innovation Fund, financed under the TKP2021-NVA funding scheme.

REFERENCES

[1] He, J. – Fu, Z. F. (2001). *Modal Analysis*, Butterworth-Heinemann, Oxford, ISBN 0750650796.

[2] Rao, S. S. (2007). *Vibration of Continuous Systems*, John Willey & Sons, Hoboken, ISBN 9780471771715.

[3] Meirovitch, L. (2001). *Fundamentals of Vibrations*, McGraw-Hill, New York, ISBN 0-07-041345-2.

[4] Benzarti, K. et al. (2001). Transverse properties of unidirectional glass/epoxy composites: influence of fibre surface treatment, *Composites Part A: Applied Science and Manufacturing*, Vol. 32, No. 2, ISSN 1359-835X, https://doi.org/10.1016/S1359-835X(00)00136-6.

[5] Muhit, I. B. et al. (2017). Aluminium and E-Glass Epoxy Plates Behaviour Subjected to Shock Loading, *Advances in Materials Research*, Vol. 6, No. 2, ISSN 2234-0912, https://doi.org/10.12989/amr.2017.6.2.155.

[6] Fadhil, B. M. (2013). Effect of Plies Stacking Sequence and Tube Geometry on the Crush Behaviour of Tube under Low Velocity Impact – Numerical Study, *International Journal of Mechanics and Applications,* Vol. 3, No. 2, ISSN 2165-9281, https://doi.org/10.5923/j.mechanics.20130302.02.

[7] Chaphalkar, S. P. et al. (2015). Modal analysis of cantilever beam structure using finite element analysis and experimental analysis, *American Journal of Engineering Research*, Vol. 4, No. 10, ISSN 2320-0936.

[8] Dossing, O. (1988). Structural Testing Part1: Mechanical Mobility Measurements, Brüel & Kjaer, Nearum.

Design of Machines and Structures, Vol. 12, No. 1 (2022), pp. 25–32.
https://doi.org/10.32972/dms.2022.010

A SPINDLE SYSTEM ANALYSIS USING SYSTEMS RECEPTANCE COUPLING APPROACH

MOHAMMAD ALZGHOUL[1], FERENC SARKA[2], FERENC J. SZABÓ[3]

University of Miskolc, Department of Machine and Product Design
H-3515, Miskolc-Egyetemváros
[1]mohammadzgoul90@gmail.com, [2]machsf@uni-miskolc.hu, [3]machszf@uni-miskolc.hu
[1]https://orcid.org/0000-0002-4673-3328, [2]https://orcid.org/0000-0003-3136-4248,
[3]https://orcid.org/0000-0002-6694-8959

Abstract: The goal of this study is to dynamically simulate a turning-centre main spindle system utilizing the systems receptance coupling technique to determine the spindle system's first three resonant frequencies in the event of transverse vibrations. The findings are then confirmed using the finite element technique using ANSYS software. The significance of analysing the spindle system described in this study is that it can be utilized to optimize the spindle system in terms of resonance frequencies for improved performance in terms of spindle vibration while the turning centre is in operation.

Keywords: *dynamical analysis, turning centre, spindle system*

1. INTRODUCTION

Nowadays, it is essential to dynamically simulate machine tools systems. The objective is to increase the accuracy and productivity of these devices [1]. The basic goals of dynamical analysis are usually to monitor, analyse, and reduce mechanical vibrations in machine tools [2]. A mathematical model is often used to validate the model that is simulated using CAD 3D modelling and modal analysis [3]. The dynamical analysis and modelling of a CNC turning centre focus specific attention on defining the spindle's dynamical behaviour and the impacts of each component that is coupled to it [4]. Spindle models have recently been introduced to facilitate more precise dynamical evaluations, ranging from spindle models assume having rigid bearings [5] to models assume having flexible bearings [6] offering a much clearer view of the behaviour of this critical part of a turning-centre.

2. MATHEMATICAL MODELLING

For the spindle system considered, the main assumption is that the bearings are attached to a rigid frame, which implies that the rest of the machine structure is also quite rigid. The spindle's flexural (transverse) vibration will also be assumed to be in a single plane. The spindle may be broken down into several subsystems, such as shaft components and bearings, which can then be reassembled to form the entire spindle as illustrated in Figure 1.

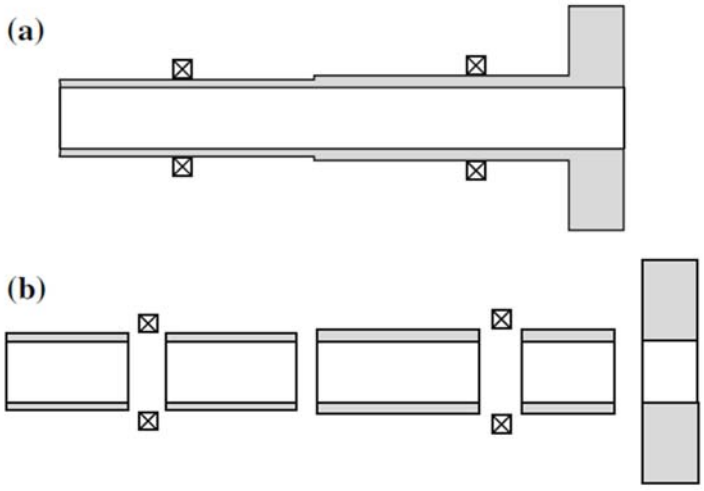

Figure 1. *Typical spindle (a), subsystem component (b) [7]*

Enforcing equilibrium and compatibility criteria at the joins is a part of the subsystem's addition process. There are two coupling connections between each subsystem because the connected ends of each subsystem's coupled ends must have compatible displacement and slope due to bending for the transverse bending vibration of shafts.

2. 1. RECEPTANCE DEFINITION AND SYSTEMS ADDITION

Receptances are used in systems approach, the receptance is defined as:

$$\alpha_{12} = \frac{X_1 e^{i\omega t}}{F_2 e^{i\omega t}} = \frac{X_1}{F_2} \tag{1}$$

where X_1 is the steady-state response of a system at the position and in the direction specified by the subscript 1 and is oftenly a complex number that indicates a phase with respect to the steady exciting force $F_2 e^{i\omega t}$ that is applied to the system at the position and in the direction specified by the subscript 2. The receptance of shafts including shear and rotary inertia effects were derived by Potter and Stone [8] and Stone [9]. Also, the receptance of bearings was derived taking into consideration their stiffness.

For adding systems, the process consists of breaking the combined system A into its component systems, or subsystems B and C, and applying forces to each subsystem at coordinate 1, causing the separate systems to behave exactly as they would when they were combined as illustrated in Figure 2.

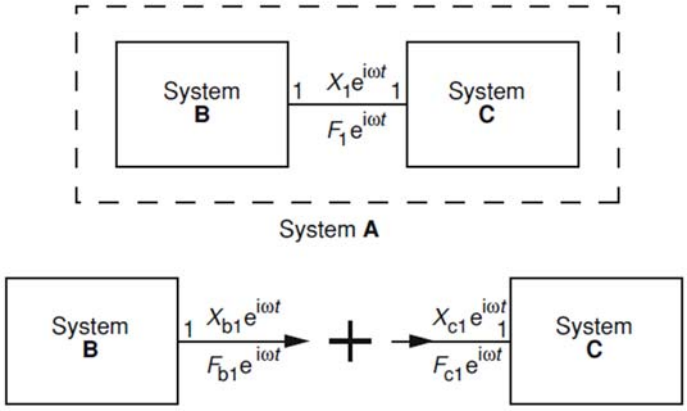

Figure 2. *The addition of two subsystems [7]*

3. THE PROPOSED MODEL

After deriving the receptance of all the required components of a spindle system, the spindle system illustrated in Figure 3 is analysed using systems receptance coupling approach. The shaft elements and the chuck are modelled as hollowed circular sections while the workpiece is modelled as a cylinder.

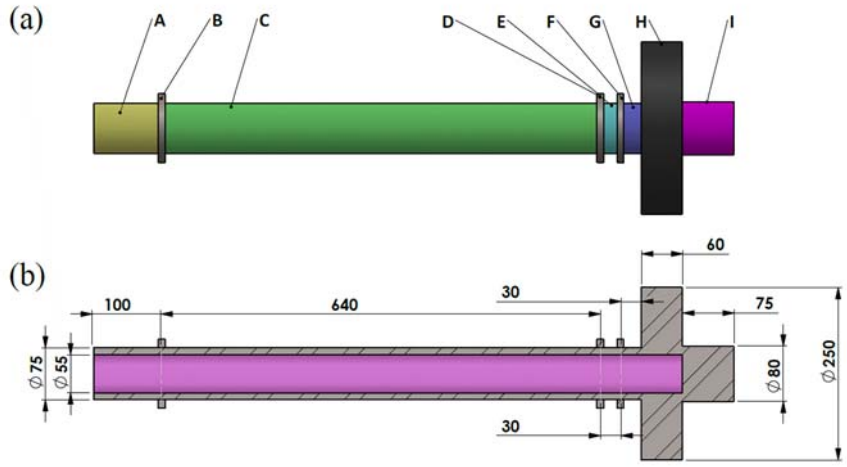

Figure 3. *The spindle system including the subsystems(a), the model dimensions(b)*

Figure 4 illustrates the block diagram of the spindle system including the shaft segments, the bearings, the chuck, and the workpiece. Symbols, D, F represent the bearings, H represents the chuck, Symbol I represents the workpiece and the rest of the subsystems represent the shaft segments. The used material of the spindle is assumed to be ASTM A36 steel. The stiffness of the bearing used in the analysis is 4.85x10^7 N/m [7].

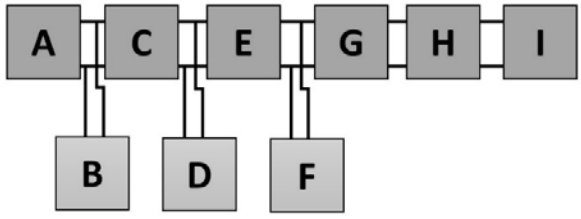

Figure 4. *Addition of shaft and bearing subsystems*

4. RESULTS

A code utilizing systems receptance coupling approach for analysing the spindle system presented in Figure 3. Is written to obtain the response of the system over a frequency range of 950 Hz as illustrated in Figure 5, the values of the first three

resonant frequencies can be extracted and it can be observed that the relationship between the values of the resonant frequencies are not linear. The values of the resonant frequencies are listed in Table 1.

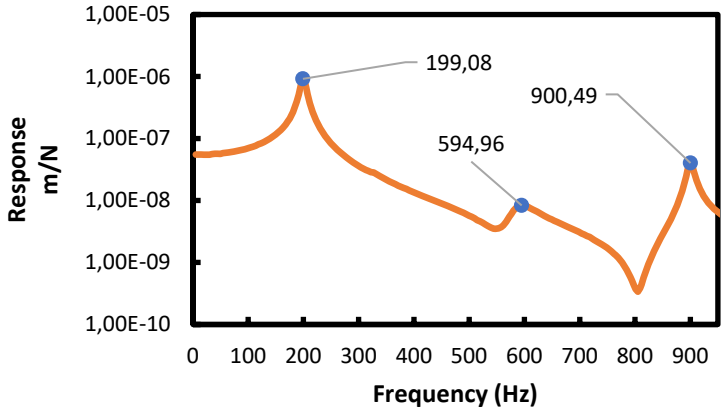

Figure 5. *Response of the proposed spindle system.*

Based on these results, resonance will take place in the spindle system when the excitation frequency meets one of the resonant frequencies listed in Table 1.

Table 1
Resonant frequency values

Mode number	Frequency Value [Hz]
1	199.08
2	594.96
3	900.49

Finite element modal analysis of the proposed model was performed using ANSYS V19 software to compare the results. Table 2 lists the first three resonant frequency values.

Table 2
ANSYS resonant frequency results

Mode number	Frequency Value [Hz]
1	199.26
2	590.36
3	901

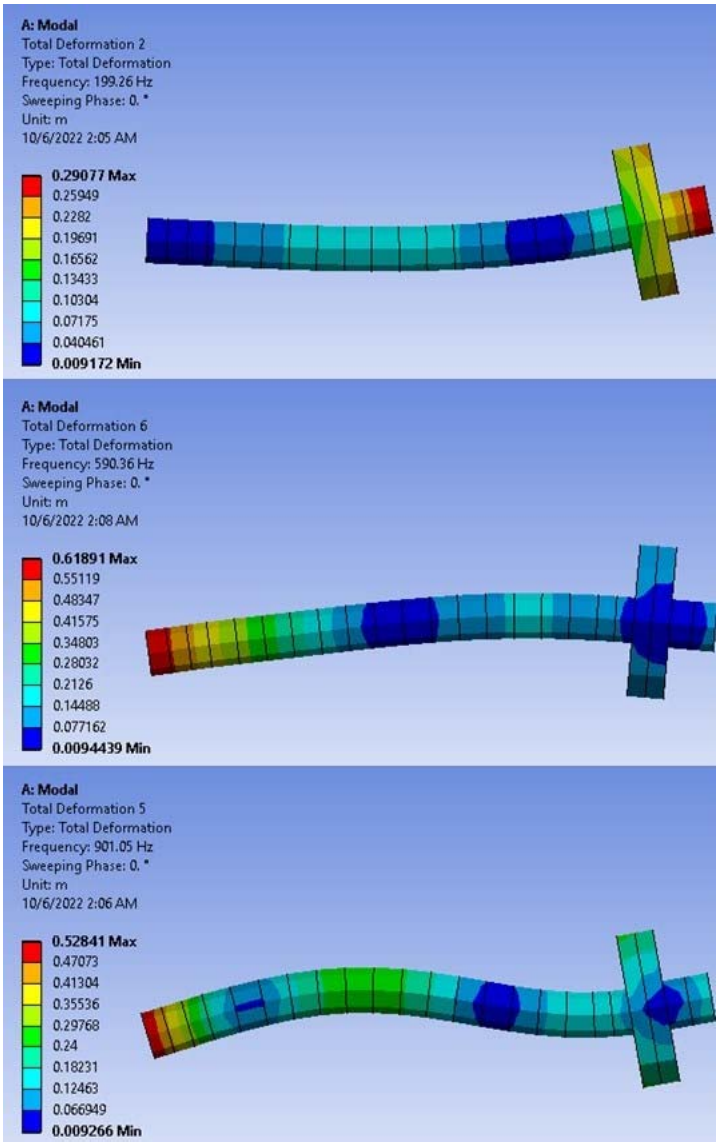

Figure 6. *ANSYS 19 spindle system mode shapes.*

Figure 6. shows the first three resonant frequency mode shapes obtained from ANSYS 19. Table 3 compares the results of first three resonant frequencies [Hz] of the spindle system using the systems receptance; coupling approach and the results from the finite element analysis using ANSYS software.

Table 3
Results comparison

Mode number	Receptance approach	ANSYS	Error %
1	199.08	199. 26	0.09%
2	594.96	590.36	0.78%
3	900.49	901.05	0.62%

5. CONCLUSIONS

A spindle system supported on three bearings is analysed using systems receptance coupling approach. The analysis takes into consideration the stiffness of the bearings. The main results are the first three resonant frequencies. The same spindle system is analysed using the finite element method using ANSYS software. The results of the two approaches then were compared. The comparison of the results shows a very good agreement in the values of the resonant frequencies. The code written to analyse the spindle system suing the systems receptance coupling approach can be modified to take into account for different bearing stiffness (different kinds of bearings) values and location and different lengths and diameters of shaft segments, chuck and workpiece which can be helpful in the process of optimizing the spindle system in terms of resonant frequencies values.

REFERENCES

[1] Holub, M. et. al. (2016). Geometric errors compensation of CNC machine tool, *MM Science Journal*, Vol. 9, No. 6, ISSN 1805-0476, https://doi.org/10.17973/MMSJ.2016_12_2016194.

[2] Hadas, Z, et. al. (2012). Stability analysis of cutting process using of flexible model in ADAMS, *Proceedings 15th International Symposium on mechatronics*, ISBN 978-80-01-04987-7.

[3] Brezina, T. et al. (2011). Using of Co-simulation ADAMS-SIMULINK for Development of Mechatronic Systems, *14th International Conference Mechatronika*, ISBN 978-80-8075-477-8, https://doi.org/10.1109/MECHATRON.2011.5961080.

[4] Fortunato, A. – Ascari, A. (2013). The virtual design of machining centers for HSM: Towards new integrated tools, *Mechatronics*, Vol. 23, Nr. 3, ISSN 0957-4158, https://doi.org/10.1016/j.mechatronics.2012.12.004.

[5] Alzghoul, M. et al. (2022). Dynamic modelling of a simply supported beam with an overhang mass, *Pollack Periodica,* Vol. 17, Nr. 2, ISSN 1788-3911, https://doi.org/10.1556/606.2022.00523.

[6] Lambert, J. R. et al. (2006). Some characteristics of rolling-element bearings under oscillating conditions. Part 1: Theory and rig design, *Proceedings of the Institution of Mechanical Engineers, Part K: Journal of Multi-body Dynamics*, Vol. 220, Nr. 3, ISSN 1464-4193, https://doi.org/10.1243/1464419JMBD12.

[7] Stone, B. (2014). *Chatter and Machine Tools*, ISBN 978-3-319-05236-6, Springer Cham, Switzerland.

[8] Soon, M. P. – Stone, B. J. (1998). The stiffness of statically indeterminate spindle systems with nonlinear bearings, *The International Journal of Advanced Manufacturing Technology*, Vol. 14, Nr. 11, ISSN 1433-3015, https://doi.org/10.1007/BF01350763.

[9] Stone, B. (1992). The Receptances of Beams, in Closed form, Including the Effects of Shear and Rotary Inertia, *Proceedings of the Institution of Mechanical Engineers, Part C: Journal of Mechanical Engineering Science*, Vol. 206, Nr. 2, ISSN 0954-4062, https://doi.org/10.1243/PIME_PROC_1992_206_102_02.

Design of Machines and Structures, Vol. 12, No. 1 (2022), pp. 33–43.
https://doi.org/10.32972/dms.2022.011

ANALYTICAL AND EXPERIMENTAL TECHNIQUES FOR CHATTER PREDICTION, SUPPRESSION AND AVOIDANCE IN TURNING: LITERATURE SURVEY

MOHAMMAD ALZGHOUL[1], FERENC SARKA[2], FERENC J. SZABÓ[3]

University of Miskolc, Department of Machine and Product Design
H-3515, Miskolc-Egyetemváros
[1]mohammadzgoul90@gmail.com, [2]machsf@uni-miskolc.hu, [3]machszf@uni-miskolc.hu
[1]https://orcid.org/0000-0002-4673-3328, [2]https://orcid.org/0000-0003-3136-4248,
[3]https://orcid.org/0000-0002-6694-8959

Abstract: Chatter is a self-excited vibration that takes place during turning operations. It is either to be avoided or reduced for its negative impact on the machine-tool, the work-piece surface finish, and the cutting tool life. A lot of research has been carried out in this domain to understand this phenomenon, which leads to finding ways to detect, identify, avoid, reduce, and control chatter in turning processes. In this paper, chatter research related to turning processes is reviewed and summarized. The main goal of this review paper is to compare different chatter prediction, suppression, and avoidance techniques to find out the most effective technique, so a scope of a work related to turning processes chatter is defined.

Keywords: *Chatter, Vibration, Stability, Turning, Spindle*

1. INTRODUCTION

Chatter has four main types, regenerative chatter, mode coupling chatter, frictional chatter and force -thermal chatter. In machining when chatter is present, the surface quality is poor, the tool life is shorter and the productivity decreases [1].The earliest work related to chatter was performed by Arnold. He investigated experimentally and analytically the behaviour of a cutting tool during the cutting process of a lathe machine and came up with an explanation about the chatter generation mechanisms. It was shown that the chatter is a result of the forces generated during the cutting process, not a result of external periodic forces. In the recent years, various methods were suggested to suppress chatter. Yao proposed a method for chatter identification before it is fully developed based on wavelet and support vector machine. Anderson developed a passive adapter to suppress resonance

vibrations of an end mill cutter. Albizuri proposed a method to reduce chatter vibrations using actively controlled piezoelectric actuators. Dohner used the so-called active control approach for mitigating chatter. Chen used active magnetic bearings for the aim of suppression of machining chatter. Wu [2], Otto [3] and Kambiz [4] studied using variable spindle speed machining to suppress chatter. Yang [5] used multiple tuned mass dampers to suppress machine tool chatter. Tobais explained that a machine-tool system including the cutting tool, the tool holder and the workpiece witnesses free, forced and self-excited vibrations. Free and forced vibrations can be detected and suppressed since they are the results of shocks and unbalances respectively. Due to the complex nature of self-excited vibrations in machining processes and due to their harmful effects, they are in interest of research. Chatter that results from the self-excited vibrations is classified into two main categories, primary and secondary chatter. Primary chatter is less of interest as it is the result of mainly the interaction between the cutting tool and the workpiece. When it comes to the secondary chatter as it is the result of the regeneration of the wavy surface on the just machined workpiece surface, it is in more interest of research and investigation. Moreover, compared to the other types of vibrations, this one is the most harmful one. Figure 1 illustrates the difference between chatter occurrence and smooth turning. In this paper, some of the analytical and experimental techniques for chatter prediction and avoidance are reviewed specifically for turning processes.

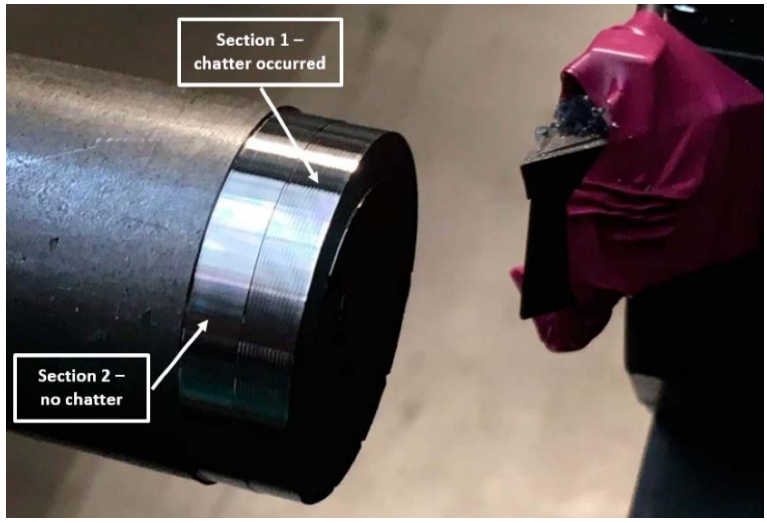

Figure 1. *Chatter occurrence in turning process [6]*

2. ANALYTICAL CHATTER PREDICTION TECHNIQUES

For the analytical techniques of chatter prediction, A lot of models are available in the literature. The main three ones are the construction of stability lobes diagram (SLD), Nyquist plots and the finite element method. These analytical techniques are reviewed in this paper.

2. 1. Stability Lobes Diagram (SLD)

Stability lobe diagrams are essential tools that are used in optimizing some turning processes parameters for maximizing the rate of material removed while keeping stable cutting conditions. In SLD, the stable and unstable areas are distinguished by the graph itself as illustrated in Figure 2. Chatter takes place at high chip widths. The depth of cut (chip width) is the most important factor of cutting in terms of chatter presence. The maximum value of depth of cut without having chatter depends on the workpiece material, cutting speed and feed, and on the geometry of the tool.

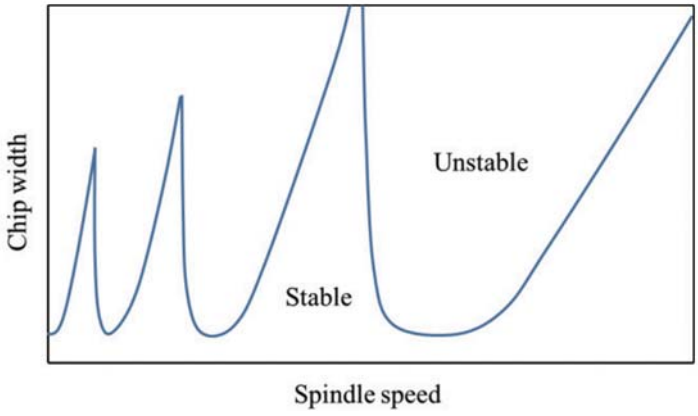

Figure 2. *Example stability lobe diagram*

Analytical models were presented by many researchers based on the number of DoF (degrees of freedom) of the cutting process. Starting with the SDoF (single degree of freedom) models, Hanna and Tobias introduced a model with a time delay-differential equation. The model takes into consideration the cutting force and the structural stiffness. Chatter is predicted in three categories, unconditionally stable, conditionally stable, and unstable which is affected by the width of cut. In the model, even in the stable category there is a presence of unstable periodic motions which is considered a weakness point of the model. Suzuki et al

introduced a model defining equivalent transfer function in order to understand the effects of the cutting force ratio and the cross-transfer function on the stability of cutting. An interesting finding is that the critical width of cut in the clockwise and the counter clockwise rotation is different from each other in the experiment. The stability limits were estimated from the vector diagram of the equivalent transfer function. Dombovari et. al [7] analysed large-amplitude motions by introducing a SDoF model that deals with orthogonal cutting. The main equation of the model takes into consideration the non-smoothness when contact between the cutting tool and the workpiece is lost and the regenerative effect of the turning process.

When it comes to the 2DoF models, Chandiramani and Pothala used a 2DoF model of the cutting tool to deal with the dynamics of chatter. The main finding of that model is that increasing the width of cut results in the occurrence of frequent tool-leaving-cut events and the occurrence of increased chatter amplitudes. Suzuki et al introduced a 2DoF model with the same idea of his SDoF which was mentioned before; it is interesting that both of his models the SDoF one and the 2DoF one gave the same solutions. Chen and Tsao introduced a 2DoF model of a cutting tool with the tailstock supported workpiece and without the tailstock supported workpiece using beam theory. The workpiece is treated as a continuous system and under different spindle speeds, the effect of the critical chip width was studied. The strength of this model is that the ability of predicting the stability and evaluating the influence of the elastic deformation and the workpiece natural frequency on the critical chip width for two different workpiece end conditions.

When it comes to the 3DoF models, tool chatter taking into consideration turning dynamics was studied by Dassanayake by employing a 3DoF model at which the workpiece is modelled as a system of three regions, machined, being machined, and unmachined regions connected by a flexible shaft. It was found that for better results, the workpiece vibration (which is not included in the model) should be considered along with tool vibrations for more accurate results. Eynian and Altintas introduced a 3DoF model of turning by modelling the transfer matrix between the displacements and cutting forces in order to predict the stability regions. Nyquist criterion was used to analytically predict stability regions.

When comparing these analytical models (DoF models), it can be seen that there is no point of going with models that are more than a SDoF unless they result in noticeable higher accuracy. The accuracy of the SDoF models show quite acceptable results in terms of predicting chatter stability for the turning process. However, it would be a good achievement to have a SDoF model with an enhanced accuracy.

2. 2. Nyquist Plots

A complex vibration frequency response function can be visualized using Nyquist chart. The dynamic behaviour close to resonances is shown by charting the real and imaginary parts of the response as illustrated in Figure 3. This offers a way to distinguish the modes and provides insight into how they are coupled. Hardware used for frequency analysis frequently incorporates mathematical models like the Nyquist analysis.

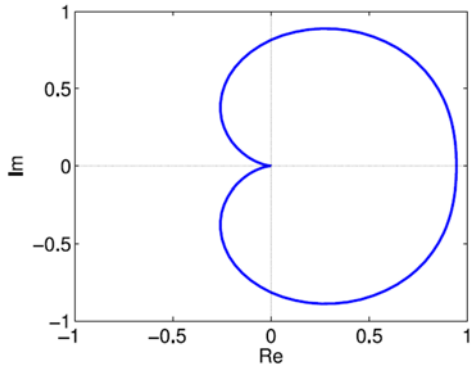

Figure 3. *Nyquist plot example*

Many researchers used control theory to predict chatter vibrations and they implemented Nyquist plots. By modelling the process using an oriented transfer function using τ decomposition forms, Turkes et al. [8] was able to predict chatter vibrations in orthogonal cutting with a SDoF turning system. The stability of the system was investigated using Nyquist criterion in conjunction with an oriented transfer function and a τ decomposition form. Finally, Nyquist technique which is an analytical technique was compared with the time domain simulation technique.

Eynian and Altintas –as mentioned earlier– used Nyquist criterion to analytically predict stability regions. Based on the feedback control theory, Merritt proposed a method that uses Nyquist criterion to predict the stability. Using the same concept and based on the feedback control theory as in Merritt, Nigm introduced another method that has the benefit of taking the dynamics of the cutting process into consideration. The analysis approach could account for the whole spectrum of regeneration and was robust enough to be implemented either analytically or graphically. Nigm used Nyquist criterion to predict the stability. Instead of plotting the open-loop frequency response locus as required by the Nyquist criterion, the method only requires plotting the operative receptance. Even faster than

plotting the open-loop frequency response locus is plotting the operative receptance. The critical stability parameter was found by Minis et al. It was derived by using the Nyquist criterion, the criterion was used as an alternative approach by finding the left-most intersection of the Nyquist plot with the negative real axis. Only two-dimensional orthogonal machining could be used with this approach. Also, stability analysis using the Nyquist criterion was performed by Wang and Cleghorn and Altintas et al.

2. 3. The Finite Element Method

The literature presents a variety of additional methodologies for the improvement of analytical stability analysis. FEM/FEA is one of them. Urbikain et al. created a FE model for the workpiece in ANSYS using 3D 10-node tetrahedral solid elements type SOLID92. A final workpiece with 35,516 elements was produced after several geometries were designed and analysed. The model parameters were then periodically adjusted to include workpiece evolution during machining into account inside the stability algorithm, which was followed by a FE analysis to create a workpiece. Brecher et al. proposed a 3-dimensional turning model based on FEA. This 3D-FEA model has the capability of predicting the cutting forces that will be generated even for complex-shaped tool geometries. Focusing on the thrust and feed forces, a method was employed to shorten the calculation time by employing characteristic diagrams for the computed process forces in the FEA-model. In any production environment, the FEM/FEA approach is very helpful for predicting stability at the design stage of any process, saving time and money. Mahdavine- jad used finite element analysis and ANSYS software to predict the stability of a turning operation. This FEA model takes into account the flexibility of the machine's structure, workpiece, and tool. Baker and Rouch used ANSYS software to build a structural model of the machine tool system and used the FEM approach to investigate the instability of a machining process. However, the validity of the results is not supported by experimental data. Without considering the dynamics of the cutting process models, the impact of structural parameters on machine instability was examined. However, the approach described allows the analysis to take into account the flexibility of both the cutting tool and the workpiece. Airao and Chandrakant used the FEA to analyse a turning process and to understand the effect of temperature, vibration amplitude, frequency and cutting speed on the machining responses.

3. EXPERIMENTAL CHATTER PREDICTION TECHNIQUES

When it comes to chatter prediction experimental techniques, two main methods have received researchers' attention, the first one is the on-line chatter classification, detection, and monitoring and the second one is the traditional experimental techniques for chatter avoidance.

3. 1. On-Line Chatter Classification, Detection, and Monitoring

In order to minimize or suppress chatter in real-time applications before it completely develops, it is essential to identify it early on. For this reason, it is crucial that CNC controllers and other external devices provide a time-efficient technique for monitoring vibration or/and process signals. For chatter recognition based on pattern recognition, a variety of methods have been employed, such as support vector machines, sensor-less methods based on power-factor theory indexes, topological data analysis, or the use of regression neural networks when non-linear effects must be addressed.

A method for sensor-less chatter detection was presented by Yamato et al. They achieved this by using two evaluation measures, a mechanical energy factor (MEF) and a mechanical power factor (MPF), both of which are helpful for tracking unstable cutting. The phase difference between the dynamic cutting force and velocity-displacement is shown by these indicators. The authors were able to identify chatter vibration from experimental tests in a precision lathe using only a few calculations. Topological Data Analysis (TDA) and supervised machine learning were integrated by Khasawneh et al. [9]. to provide an indicator of chatter's impending presence. In this method, deterministic and stochastic turning models (with different cutting coefficients) work together. Tansel used a neural network technique to study a three-dimensional turning process. In comparison to traditional time series models, their model demonstrated superior nonlinear effect representation. In addition, precision was improved at higher cutting speeds since there is more space between the lobes. Cherukuri et al. evaluated the behaviour of implementing an artificial neural network (ANN) when it comes to modelling stability in turning. The datasets needed to train the ANN were created using the stability boundaries as a starting point. They discovered that over 90 % of the time, the ANN was successful in predicting stability. With the aid of an artificial neural network and a mathematical model of responses based on response surface methodology (RSM), Kumar and Singh analysed the relationship between cutting parameters and chatter degree (ANN). Wavelet Transform was used to eliminate noise from the raw data, and the results demonstrated that ANN was more reliable than RSM. Chatter severity was detected by obtaining a chatter index. Similar methods were employed by Shrivastava et al., who used the wavelet

transformation to denoise the raw signal, identify chatter frequency, and calculate chatter index. An operational modal analysis was proposed by Kim and Ahmadi to predict the start of chatter in turning operations. They employed a stability margin of the process, allowing them to predict the start of chatter before the vibrations became intolerable.
In a turning system, the reliability probability of chatter was computed by Liu et al. They compared their results with a Monte Carlo simulation that presented a modified version of conventional stability lobes, using the first order second moment method (FOSM) and fourth moment method. They coded deeper cuts to cross the stability boundary limitations for the experimental validation. Similar to this, Huang et al. used the Laplace transform to calculate the depth of cut to spindle speed ratio utilizing the Monte Carlo method and advanced first order second moment method. Their predictions were verified by real experiments. With adequate precision, Jimenez Cortadi et al. employed the Linear Mixed Model (LMM) for chatter prediction as well as for wear prediction. A neural network analysis for identifying chatter vibration in turning was carried out by Tian. It was proven that this approach was more effective and reliable than the frequency domain approach.

3. 2. Experimental Techniques for Chatter Avoidance

When it comes to the experimental techniques for chatter avoidance, it specifically means optimizing the cutting parameters of machining. A time-varying delay can be produced using the spindle speed variation (SSV) approach by distorting chip thickness. As a result, the chatter feedback mechanism is reduced by new, more desirable phase delays between inner and outer chip modulation. There are other approaches to change the head's rotational speed, but the most effective ones introduce a sinusoidal SSV, in which the spindle speed oscillates sinusoidally at a favourable frequency and amplitude.
The method is adaptable to various cutting systems and dynamics. However, when the variation is used, certain previously stable regions of the stability lobe diagram may become unstable. The high spindle accelerations and decelerations, as well as the difficulty in adjusting the frequency and amplitude of the variation, are additional disadvantages of this method. SSV was initially presented in scientific literature to enhance milling processes stability. Al-Regib et al. introduced a simple criterion for determining the ideal amplitude ratio was proposed, along with a heuristic criterion to assist in the process' stability. Based on an energy analysis of the process, Zhang et al. suggested a criterion for determining the ideal SSV amplitude. They also suggested a stability increment index (SII) of SSV in relation to constant spindle speed (CSS). The Ideko-IK4 research team produced various

works on the SSV technique used in milling and grinding operations. In some circumstances, such as those involving small workpiece diameters, this approach might be challenging to use. The reference spindle speed, which is limited by the workpiece diameter and work material, is frequently correlated with the SSV amplitude. High spindle speeds are required for smaller workpiece diameters in order to maintain acceptable cutting speeds. Additionally, the variations in spindle speed cause spindle speeds to increase.

A comprehensive formulation for modelling stability in turning and milling operations utilizing SSV for the semi-discretization approach was presented by Insperger et al. in. However, according to some researchers, the SSV approach is more effective in turning than milling since turning naturally involves slower cutting speeds. The tool's stability analysis was created by Wu et al. utilizing a discrete angle approach. The workpiece's angular position is given by C-axis works as the independent variable in this method. Along with using a stability index criterion, they examined the impact of variable speed machining on the stability of noncircular turning. A closed-loop dynamic model of the noncircular turning process was added by Wu and Chen to the earlier work. They found that both constant and variable spindle speeds led to some improvements in the stability of noncircular turning.

As demonstrated by Yilmaz et al., the most unstable eigenmode was strongly dampened and stabilized in turning. An interesting model for the prediction of stability lobes using the SSV approach was proposed by Otto and Radons [3] in turning. They outlined the procedures for putting this technology into practice and noted that, as compared to milling processes, turning processes may achieve greater stable chip widths. Additionally, they suggested advantageous circumstances to regulate the spindle speed's maximum acceleration. The outcomes of the experiments were not included in that research. Adapting the Chebyshev collocation approach and the Homotopy Perturbation Method (HPM) for chatter onset prediction, Urbikain et al. investigated the use of varying turning speeds during the turning of a piece to mitigate this. Speed functions of the sine-wave variety were created and tested for validity using a laser tachometer. Good agreements were reached for chatter types A and B. However, they did not take into account temperature effects on spindle speed in their investigation.

It is well known that the stability boundaries depend on a specific spindle speed and uncut chip load combination; nevertheless, the single time-varying parameters (STVP) approach has demonstrated chatter reduction by, for example, time-varying tool rake angle and time-varying federate. However, the Multiple Time-Varying Parameter (MTVP), which in certain circumstances gave chatter reductions up to 80 %, can be used to strengthen the resilience of this method, according to the authors.

4. Conclusions

The first focus of the literature review was stability prediction using analytical and numerical techniques. As a result, specific sections that highlight the key developments in these techniques (analytical and experimental) are presented. Numerous scholars attempted to generalize the problem of chatter in turning since it is not a problem with many chatter types and variations. SLDs are the most practical method of chatter vibration process prediction. Even SLDs created using a basic SDoF orthogonal turning model produces results and prediction accuracy that are acceptable. Nyquist Plots is a good method when dealing with chatter, still it is in less interest compared to SLDs. The finite element method gives interesting results, yet with the development of the fields with high capabilities, the results are expected to be enhanced. Experimental techniques are an adequate and practical alternative when analytical modelling becomes very complicated and challenging. Among the mentioned experimental techniques, the SSV is a promising one and still have room for further development.

References

[1] Yan, B. – Zhu, L. (2019). Research on milling stability of thin-walled parts based on improved multi-frequency solution, *The International Journal of Advanced Manufacturing Technology*, Vol. 102, No. 1, ISSN 1433-3015, https://doi.org/10.1007/s00170-018-03254-0.

[2] Wu, D. – Chen, K. (2010). Chatter suppression in fast tool servo-assisted turning by spindle speed variation, *International Journal of Machine Tools and Manufacture*, Vol. 50, Nr. 12, ISSN 0890-6955, https://doi.org/10.1016/j.ijmachtools.2010.09.001.

[3] Otto, A. – Radons, G. (2013). Application of spindle speed variation for chatter suppression in turning, *CIRP Journal of Manufacturing Science and Technology*, Vol. 6, Nr. 2, ISSN 1755-5817, https://doi.org/10.1016/j.cirpj.2013.02.002.

[4] Hajikolaei, K, et. al. (2010). Spindle speed variation and adaptive force regulation to suppress regenerative chatter in the turning process, *Journal of Manufacturing Processes*, Vol. 12, Nr. 2, ISSN 1526-6125, https://doi.org/10.1016/j.jmapro.2010.08.002.

[5] Yang, Y. et. al. (2010). Optimization of multiple tuned mass dampers to suppress machine tool chatter, *International Journal of Machine Tools and Manufacture*, Vol. 50, Nr. 9, ISSN 0890-6955, https://doi.org/10.1016/j.ijmachtools.2010.04.011.

[6] Jasiewicz, M. – Miądlicki, K. (2019). Implementation of an Algorithm to Prevent Chatter Vibration in a CNC System, *Materials*, Vol. 12, Nr. 19, ISSN 1996-1944, https://doi.org/10.3390/ma12193193.

[7] Dombovari, Z. et. al. (2011). On the global dynamics of chatter in the orthogonal cuttingmodel, *International Journal of Non-Linear Mechanics*, Vol. 46, Nr. 1, ISSN 0020-7462, https://doi.org/10.1016/j.ijnonlinmec.2010.09.016.

[8] Turkes, E. et. al. (2011). Linear analysis of chatter vibration and stability for orthogonal cutting in turning, *International Journal of Refractory Metals and Hard Materials*, Vol. 29, Nr. 2, ISSN 0263-4368, https://doi.org/10.1016/j.ijrmhm.2010.10.002.

[9] Khasawneh, F. et al. (2018). Chatter Classification in Turning using Machine Learning and Topological Data Analysis, *IFAC-PapersOnLine*, Vol. 51, Nr. 14, ISSN 2405-8963, https://doi.org/10.1016/j.ifacol.2018.07.222.

Design of Machines and Structures, Vol. 12, No. 1 (2022), pp. 44–53.
https://doi.org/10.32972/dms.2022.012

DESIGN OF EQUIPMENT SUITABLE FOR MEASURING THE NATURAL FREQUENCY OF A ROTATING SHAFT

SÁNDOR APÁTI[1], GYÖRGY HEGEDŰS[2]

University of Miskolc, Institutional Department of Machine Tools
H-3515, Miskolc-Egyetemváros
[2]hegedus.gyorgy@uni-miskolc.hu
[2]https://orcid.org/0000-0002-0081-8019

Abstract: In this paper, the construction and operation of a measuring bench for measuring the vibration state of a rotating shaft and the evaluation of the measurement results are presented. The design of the measuring bench was aimed at measuring the vibration generated by the excitation effects on the shaft. The effect of the imbalance and the position of the disc on the vibration characteristics is shown in diagrams. It is also observed that at higher speeds the vibration plotted shows an irregular shape. This is due to the excitation effects on the whole structure.

Keywords: *natural frequency, critical speed, shaft*

1. INTRODUCTION

It is advisable to test the rotating parts of machines used in the technical field with experimental and practical methods. Energy accumulates in these components, and these energies force the system to vibrate. In the alternating evolution of potential and kinetic energies, such as in the case of vibration of a system or a structural element, the frequency of the excitation effect determines the speed of the energy transitions. Depending on the excitation effects on the drive chain, the amount of stored energy can be increased. The time-varying excitation effects cause a vibrating motion of the structure, which is damped either by the material or by the damping of the structure.
The vibration amplitude of the drivetrain depends on the excitation effects, the degree of damping, and the proximity of the excitation to the natural frequency. The excitation effects are caused by the operating characteristics of the drive chain (e.g., universal joint or any reciprocating element) and manufacturing or assembly error causing the eccentricity of the rotating elements. Resonance can be avoided

by adjusting the eigenfrequencies of the drive train and excitation frequencies far from each other.

The purpose of building the test bench was to measure the effect of excitation on the vibration level. A test bench appears to provide measurement results in operation, is subject to mischaracterization in practice, and effectively reduces the corresponding capabilities. This provides a visual representation of the conflicting placement that allows for practical use and results in satisfactory accuracy.

When designing rotating shafts, care must be taken to reduce vibrations, considering their sources. In addition, the intensity of vibration, the critical speed of the shaft, stability and other parameters affecting the properties of the system must be considered. The effects of the mentioned parameters should be examined especially at the critical speed, since the vibration properties of the system change significantly, which can cause damage to the shaft, premature failure of rotating parts and bearings [1].

Vibrations affecting the service life of shafts include torsional vibrations of varying degrees. High levels of torsional vibration can damage or cause rotating equipment to fail, causing costly downtime. Comprehensive torsional vibration analysis is the typical method for designing a torsional system that eliminates such problems. Torsion system design requirements are defined by various standards; however, a certain degree of uncertainty is always present in analytical data, modelling techniques, and excitation and damping assumptions [2].

The predictive calculation of the torsional natural frequencies of the shaft is performed to avoid torsional resonance problems. However, it is often delicate to select the appropriate excitation frequencies and to determine the modal damping factors that must be considered in the calculation. A further inaccuracy is caused by neglecting the elasticity of the bearings in the boundary conditions, which makes the results uncertain. In practice, it is therefore often useful to experimentally measure the torsional natural frequencies to validate the calculations [3].

Every elastic system is characterized by its own period of oscillations, which is determined by its stiffness and its own mass. If such a system is subjected to forced vibrations because of forces and torques changing due to unbalanced masses or other reasons, and if the frequency of change of these forces and disturbing moments is equal to the frequency of the vibrations or a multiple thereof, then the amplitude of the vibrations increases rapidly, and resonance occurs. In the case of shafts, longitudinal, torsional, and transverse vibrations may occur depending on the forces and disturbing torsional moments. From a practical point of view, it is most often only the latter two types of vibration, because in general the longitudinal restoring forces are very large, and the amplitude of the longitudinal vibrations is small. In most cases, transverse vibrations occur due to transverse forces, which are periodically repeated [4] - [6].

In practice, there are also tasks where the critical speed of axes with asymmetrically concentrated mass (e.g., gear shafts, main shafts of cone crushers) must be determined [7].
Analytical methods may also be suitable for testing torsional vibrations. Two methods were developed to examine the power transmission shaft of a ship propeller, of which the shaft line was modelled as a two-mass system in the first, approximate method. In the second procedure, the multi-degree-of-freedom problem of the entire system was solved using the Rayleigh-Ritz method. The outlined analytical procedures can be used to estimate shaft torsional vibrations in the conceptual design phase, as well as for equipment already in operation [8].
Torsional vibrations are inherently present in all rotating drivetrains. Torsional vibrations can be significantly amplified in resonant conditions. A typical method of reducing torsional vibration, especially at resonance, is to modify the torsional natural frequencies by designing the component. In general, a simple way of modification is to adjust the torsional stiffness of the elements incorporated in the drive [9].

2. CONSTRUCTION OF THE LOAD BENCH

Based on the studies and research reviewed in the introduction, the examination of the critical speed of the rotating shafts and the various vibrations of the shafts is an extremely important task. The experimental measurements were carried out on the load bench shown in Figure 1. As shown in Figure 1, a disc can be mounted on the shaft along the longitudinal axis, which can be fixed in any position on the shaft. There is a 15x∅150xM8 threaded hole on the disc, with the help of which the mass mounted on the rotating shaft can be placed, because of which the moment of inertia and imbalance of the system can be changed.
The mass and moment of inertia of the disk, as well as its location on the shaft, are parameters that influence the natural frequencies of the shaft. The imbalance of the disk ensures the excitation effects when the shaft rotates.
The test bench is driven by a 300 W electric motor, the speed of adjusted using a variable frequency drive (VFD) in the range of 0-5000 rpm. The load of the drive chain is provided by a car generator with a power of 500 W, which can be increased with 3 additional loads of 25 W in discrete steps. When the test bench is in operation, a Hottinger Baldwin Messtechnik Ltd. data acquisition system ensures the registration of measurements and the collection of measurement data. The basis of the measurement is a Spider8 device, which is a multi-channel PC measuring electronics for the computerized collection of parallel, dynamic measurement data. Spider8 contains everything needed for measurement in a compact design.

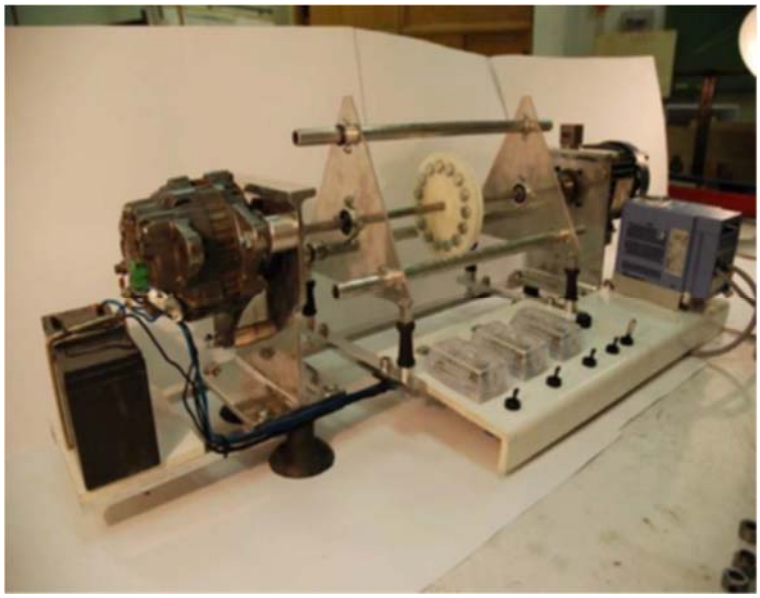

Figure 1. *The design of the measuring bench and the measurement data collection system*

Such a measurement system does not require additional connection and wiring installations, nor large configuration presets. The processing and direct display of the measured data is made possible by a CATMAN EASY measuring software. The system offers the user several prepared measurement programs with evaluation diagrams, which speeds up the evaluation of the measured data. The bending vibration of the shaft placed on the load bench can be measured in two ways. In one method, the values occurring during loading can be measured along three axes with a piezoelectric accelerometer, which is fixed on the two end plates of the stand. In the other measurement method, a complete bridge created with 4 strain gauges measures the changes in shape due to vibration. During measurement, depending on the angular velocity relative to the natural frequencies of the shaft, the transducers generate an electrical signal proportional to the amplitude of the vibration. The natural frequencies of the shaft can be measured by increasing the speed of the shaft and checking the amplitude of the vibration. The natural frequency (or critical speed) is the angular velocity at which the maximum value of the vibration occurs.

3. MEASUREMENT RESULTS

The measurements were carried out in various arrangements, the direction x acceleration of the piezoelectric accelerometer, as well as the magnitude of the vibration amplitude as a function of the speed were measured during the measurements. The piezoelectric accelerometer and strain gauges were fixed so that their measurement direction was the same (direction x).

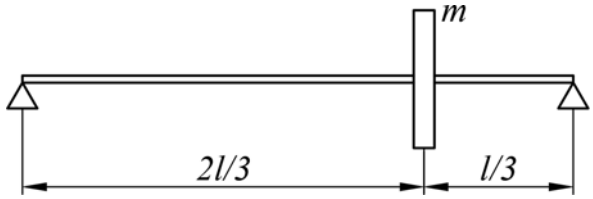

Figure 2. *Schematic figure of the measurement arrangement I.*

3. 1. Measurement result I.

In this measuring arrangement, the disk was fixed at 1/3 of the length of the shaft (Figure 2), the fastening elements were installed in the threaded holes of the disk, thus the assembled mass of the disk was 300 g. The measurement result shows that the maximum vibration acceleration reaches its highest value at 1950 rpm. The magnitude of the vibration amplitude can be inferred from the electrical signal provided by the strain gauge stamps proportional to the displacement.

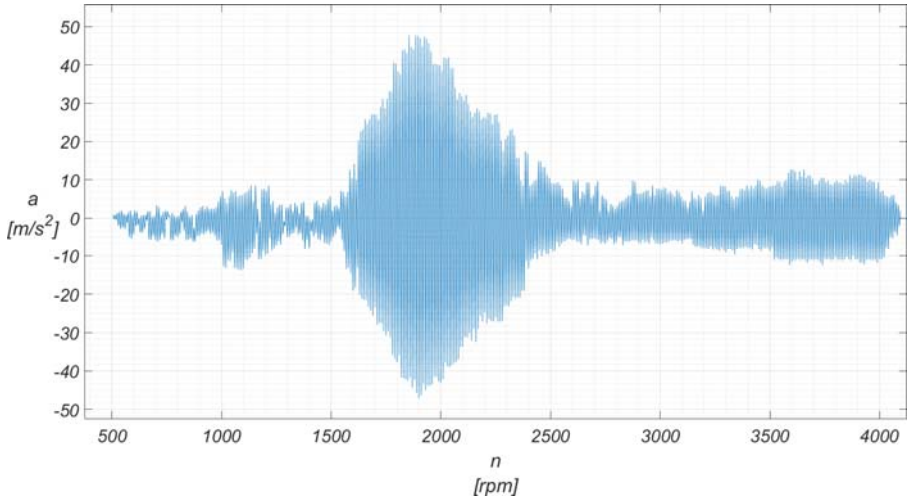

Figure 3. *The vibration acceleration as a function of the speed (Measurement I.)*

Figure 3 shows the measurement result of the vibration acceleration as a function of the speed. The measurement was performed by fixing the disc at 1/3 of the shaft length and removing 3 fasteners from the disc, which caused the disc to be unbalanced and resulted in reduced weight. The figure shows that due to the reduced mass, the natural frequency was generated at a higher frequency (~2000 rpm), and due to the increased excitation effects, the vibration amplitude decreased minimally after the critical speed was exceeded.

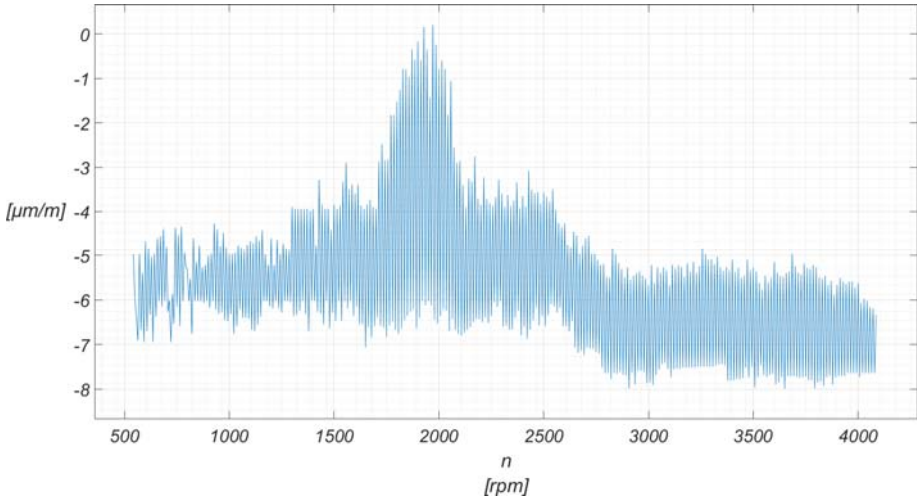

Figure 4. *Vibration amplitude as a function of speed (Measurement I)*

Figure 4 shows the measurement result of the vibration amplitude as a function of the speed. At higher revolutions the measurement result shows an uncertain vibration range. The reason for this may be that the whole structure was affected by the excitation effect.

3. 2. Measurement result II.

In this case, the arrangement of the measurement is the same as the measurement described in the previous case. However, the measured system differs from the previous one in that the disc here is unbalanced and weighs 290 g. Figure 5 shows that the value of the maximum vibration acceleration already appears at ~1800 rpm and a slight increase in deflection can be observed from ~3300 rpm.

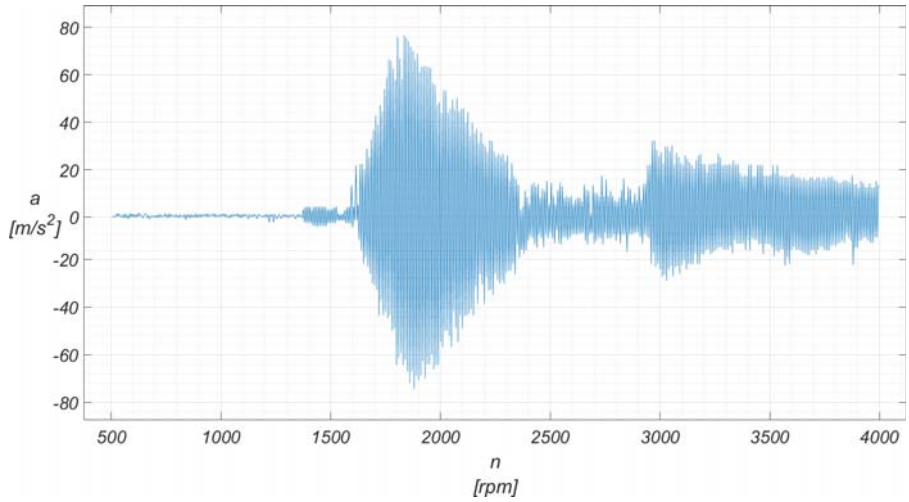

Figure 5. *The vibration acceleration as a function of the speed (Measurement II)*

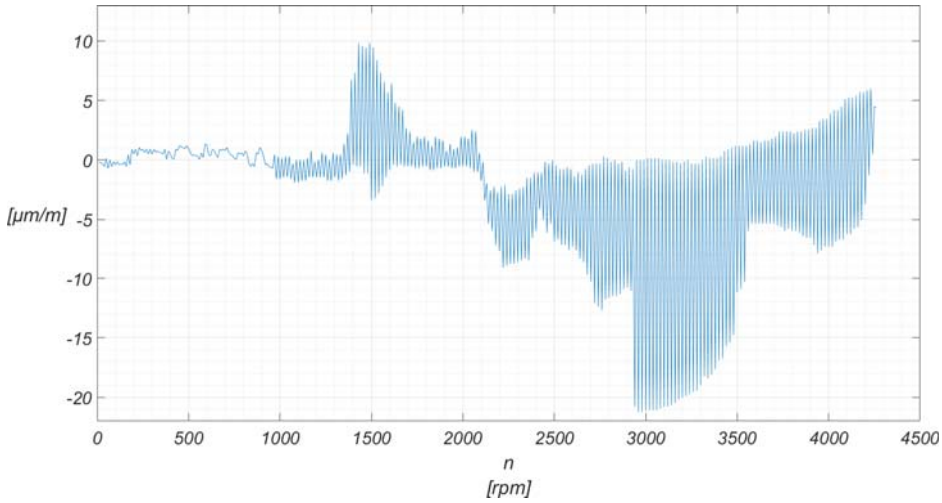

Figure 6. *Vibration amplitude as a function of speed (Measurement II)*

Figure 6 illustrates the measurement result registered by the measuring bridge formed by the strain gauge stamps for the same measurement arrangement. It can be observed that even with this configuration, the largest vibration deflection occurs at ~1800 rpm. Compared to Figures 3 and 4, the measurement results show higher and more irregular vibration acceleration and vibration deflection, which can be explained by the fact that the pulley became unbalanced when the fasteners

were removed, which significantly increased the vibration of the shaft. It can also be seen in this figure that at ~3300 rpm the measured maximum value at which the vibration peaks occur is displayed.

3. 3. Measurement result III.

In this measurement setup, it shows acceleration in the x direction as a function of speed. The vibration maxima are clearly visible in Figure 7. The graph recorded by the piezoelectric accelerometer shows that there are several maximum accelerations in the range of ~3500 rpm and ~4700 rpm. The measurement results detected by the strain gauges are illustrated in Figure 8.
It can be observed that the diagram registered by the strain gauges gives a slightly more accurate picture of where the frequencies are where the system tends to resonate. The increase in acceleration and vibration values already occurs at lower speeds. From this, it can be concluded that the eccentric disc is located halfway between the two clutches, affecting the vibration conditions of the shaft, as when it was placed closer than one third to the bearing bracket. The displacement - speed diagram shows that the vibration peaks at low speed already appear around ~1000 rpm.

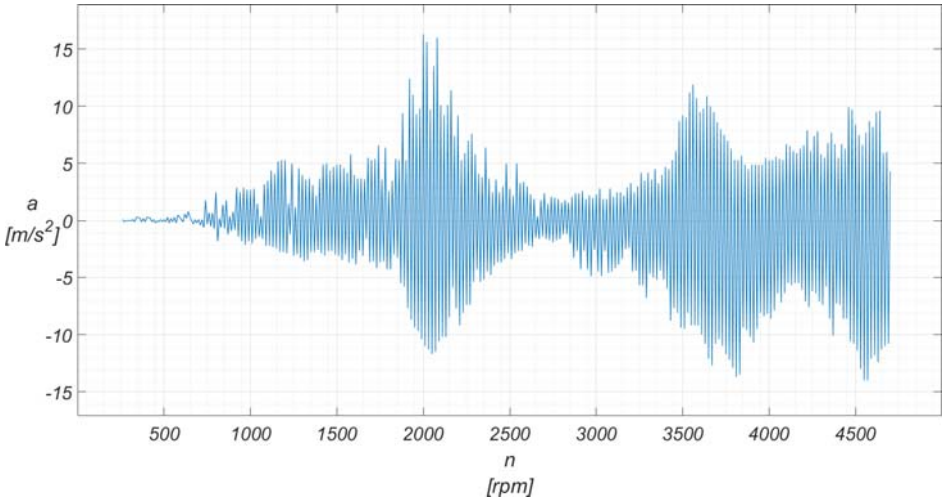

Figure 7. *The vibration acceleration as a function of the speed (Measurement III)*

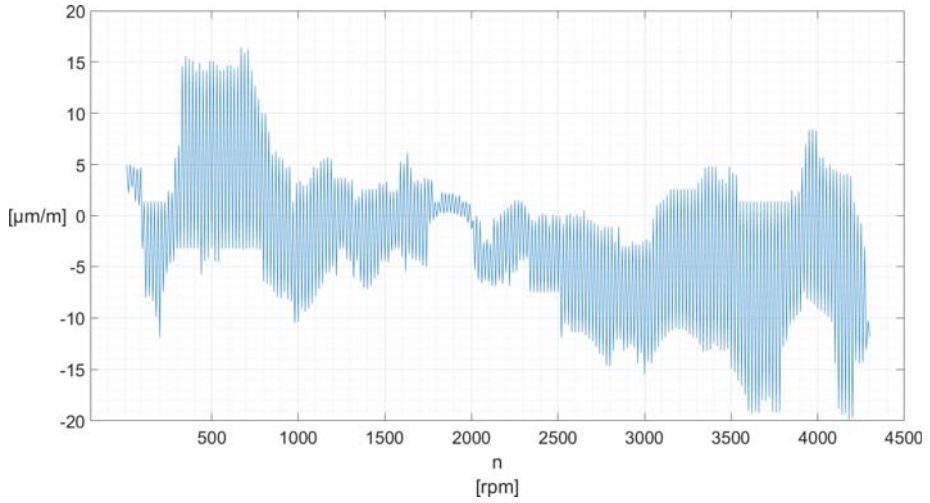

Figure 8. *Vibration amplitude as a function of speed (Measurement III)*

4. SUMMARY

In this article, the construction and operation of a measuring bench suitable for measuring the vibration state of a rotating shaft, as well as the evaluation of the measurement results were presented. The purpose of the measuring bench was to measure the vibration caused by the effects that excite the shaft. The effects of unbalance and disc position on vibration characteristics are shown in the diagrams. It can also be observed that at higher revolutions the depicted vibration shows an irregular shape. The reason for this is that the whole structure is affected by the excitatory effects.

REFERENCES

[1] Choong-Yul S. et al. (2008). A study on the vibration characteristics of critical speed for rotor shaft, *Transactions of the Korean Society for Noise and Vibration Engineering*, Vol. 18, Nr. 9, ISSN 1598-2785, https://doi.org/10.5050/ksnvn.2008.18.9.961.

[2] Wang, Q. et al. (2012). Torsional Natural Frequencies: Measurement Vs. Prediction, *Proceedings of the Forty-First Turbomachinery Symposium*, https://doi.org/10.21423/R1RM09.

[3] Vasselin, J.-L. (2013). Practical methodologies for on-site measurements of torsional natural frequencies – application to industrial cases, *Surveillance 7 – International Conference.*

[4] Huang, Z. – Han, B. (2015). Effective approach for calculating critical speeds of high-speed permanent magnet motor rotor-shaft assemblies, *IET Electric Power Applications*, Vol. 9, Nr. 9, ISSN: 1751-8679, https://doi.org/10.1049/iet-epa.2014.0503.

[5] Geonea, I. et al. (2017). Analytical and numerical study of critical speed for right shafts, *Acoustics and Vibration of Mechanical Structures – Proceedings of the 14th AVMS Conference*, ISBN 978-3-319-69823-6, https://doi.org/10.1007/978-3-319-69823-6_49.

[6] Song, H. et al. (2022). Rotor strength and critical speed analysis of a vertical long shaft fire pump connected with different shaft lengths, *Scientific Reports*, Vol. 12, Article ID. 9351, ISSN 2045-2322 (online), https://doi.org/10.1038/s41598-022-13320-z.

[7] Gorbatyuk, S. et al. (2019). Influence of critical speed when working shafts with asymmetrically located monolithic weighting on the accuracy of work surfaces, *Materials Today: Proceedings*, Vol. 19, Nr. 5, ISSN 2214-7853, https://doi.org/10.1016/j.matpr.2019.07.222.

[8] Senjanović, I. et al. (2019). Analytical procedures for torsional vibration analysis of Ship Power Transmission System, *Engineering Structures*, Vol. 178, ISSN: 0141-0296, https://doi.org/10.1016/j.engstruct.2018.10.035.

[9] Kinnunen, K. et al. (2022). Method for adjusting torsional natural frequencies of powertrains with novel coupling design, *Machines*, Vol. 10, Nr. 3, ISSN 2075-1702 (online), https://doi.org/10.3390/machines10030162.

Design of Machines and Structures, Vol. 12, No. 1 (2022), pp. 54–60.
https://doi.org/10.32972/dms.2022.013

GENERATIVE DESIGN: AN OVERVIEW AND ITS RELATIONSHIP TO ARTIFICIAL INTELLIGENCE

BORSODI, ESZTER[1] – TAKÁCS, ÁGNES[2]

University of Miskolc, Department of Machine and Product Design,
H-3515, Miskolc-Egyetemváros
[1]borsodies@gmail.com, [2]takacs.agnes@uni-miskolc.hu
[1]https://orcid.org/0000-0002-3955-2182, [2]https://orcid.org/0000-0002-3210-6964

Abstract: The paper deals with generative design. It presents the definition and the process of generative design and mentions the differences from traditional design method. The application areas are also discussed with real life examples and collection of possible application cases. Furthermore, the article analyses the connection between Artificial Intelligence and generative design and gives a suggestion for adapting Deep Learning in the evaluation and selection phase.

Keywords: *generative design, Artificial Intelligence, Machine Learning, Deep Learning*

1. INTRODUCTION

Generative design was developed in the 1990's, but software supporting this design method are appeared in the 2010's [1]. The computing capacity back in the past was not enough for run these complicated algorithms, but nowadays with the power of cloud computing this problem is solved. The development of additive manufacturing technologies also supported the realization of structures with complex geometry created by generative design.
Generative design is mainly based on nature-mimicking algorithms and operate similar to the evolutionary process [2]. To achieve this, generative design implements Artificial Intelligence. With these properties, generative design can create the best solutions for different consumer needs and redefine the engineering design.

2. GENERATIVE DESIGN

2. 1. Definition

According to the general definition of generative design, parameters are given in a programme, which creates all versions of the output that meet the input criteria. Generative design is used in many areas, the output can be, for example, sound, image or 3D model [3]. In this paper, generative design means the production of 3D models by generative design in CAD software.
Approached from this aspect, it can be defined as a design process which iteratively, with the help of an algorithm creates all the models that are optimized for the requirements we set [4].

2. 2. The process of generative design

There are programmes especially created for generative design (e.g., Generate from Frustrum), CAE software supporting generative design (e.g., OptiStruct from Altair) and parametric design systems with a generative design module (e.g., Fusion 360 from Autodesk from) [5]. The steps of generative design are illustrated in Figure 1, which is based on the Autodesk Fusion 360 Generative Design framework, but other generative programmes work similarly.
First, we need to define the initial geometry. The starting geometry can be specified from scratch by selecting the areas to be retained and the areas of empty spaces, or we can import a traditionally designed 3D model (in this case we also have to mark off preserve and obstacle regions). The next step is defining the location and magnitude of the constraints and loads acting on the areas to be preserved. After that, objective of the design (maximize stiffness or minimize mass) can be selected. This is followed by the choosing of the manufacturing method, so that the programme takes into account the characteristics of different production technologies when generating the model, thus reducing the production costs. The last step in specifying the generative parameters is selecting the material.
The software checks the entered data before generation and warns in case of incorrect or missing information. If the result of the check is positive, the generation process can come, which provides a number of 3D models corresponding to the input parameters. The generation process takes place in the cloud, and then the designer's computer receives the results. We can filter these outputs according to different properties and choose the one that best meets our requirements. It is possible to export the selected model and modify it using traditional CAD tools, but in this case additional FEA is recommended after the editing.

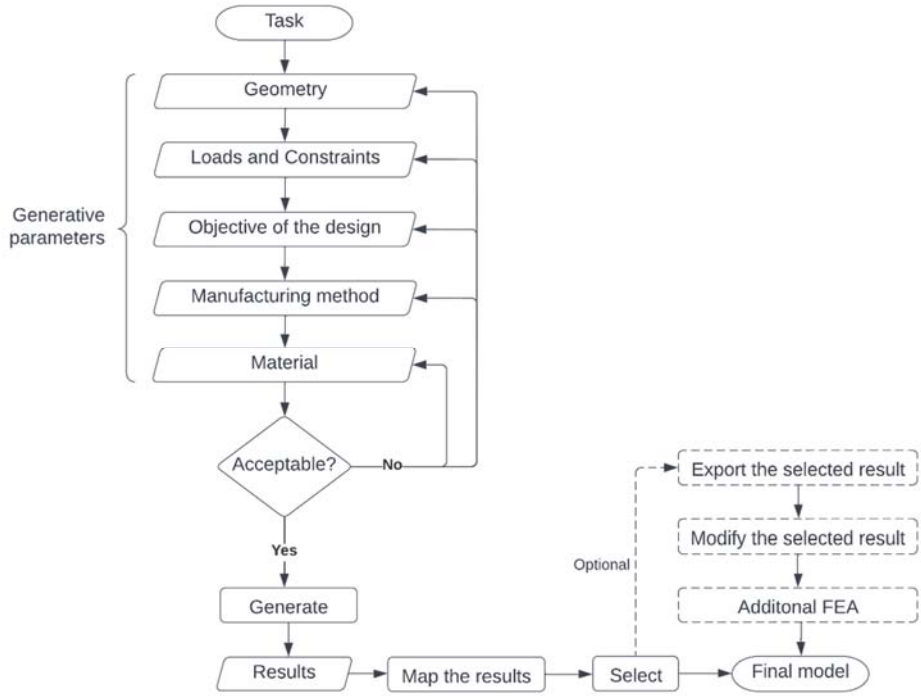

Figure 1. *Flowchart of the generative design method*

In the case of traditional design, only a few concepts are created. After that, the adequacy with given parameters and manufacturability of the conceptual models are examined, and during this several modifications or redesigns may be necessary. In contrast, generative design reduces the time of product development and market launch because it creates a large number of models that meet the given requirements and takes into account the manufacturability.

2. 3. Application areas

Generative design has already been used successfully by several companies. Airbus created a partition wall for the A320 aircraft with generative design. The algorithm of the wall's frame imitates the growth pattern of the slime mold, and the algorithm of the frame's inner structure was based on the lattice structure of the mammal bones which densely fills the space with material at the stress points, while less densely elsewhere. General Motors produced automotive parts, Under Armor created lightweight running shoes using generative design. NASA has also

used this design method, for example, they designed a space exploration lander (Figure 2) with generative design.
Several studies have already dealt with the practical application of generative design, for example Seregi and Ficzere designed a weight-reduced drone frame using this method [6].

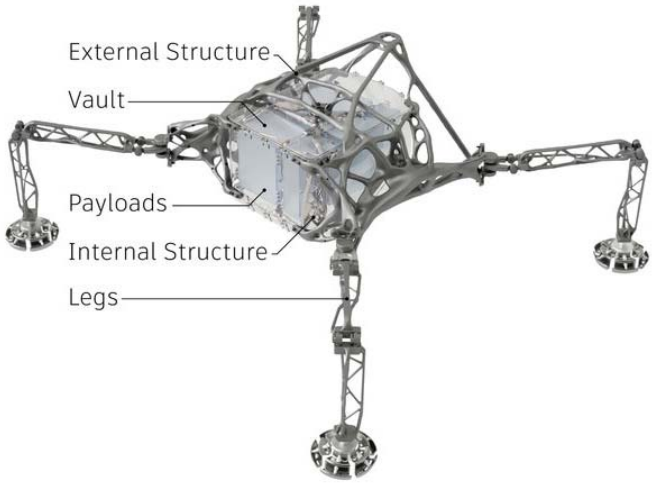

Figure 2. *Space exploration lander created with generative design by NASA*

Considering the characteristics of the generative design, engineers can exploit the potential of this method in the following cases:

- Industries, where minimizing mass but achieve same performance is the key issue (e.g.: automotive industry, aviation industry, space industry, competitive sports)
- When the goal is to reduce fuel consumption thus emissions (e.g.: aviation industry)
- When the goal is to reduce material usage thus material costs
- When sustainability is an important factor
- When the goal is to increase performance and load capacity
- When the product is unique and exposed to special loads, and it is sufficient to produce it in small series
- When reduction of product development time and quick market launch is important

- When highly automatized design process is required
- When unique, nature imitated design is the goal
- When we want consolidate parts, which also simplifies supply chains and maintenance
- Design tasks with high complexity

3. Connection between generative design and Artificial Intelligence

3. 1. Fundamentals of Artificial Intelligence, Machine Learning, and Deep Learning

Artificial Intelligence (AI) is a technique demonstrated by machines which imitates human thinking and behaviour with algorithms to solve problems as humans would do, or with even better performance [7]. The ability to learn is part of the intelligent behaviour, AI's subfield, Machine Learning focuses on this topic.
Machine Learning (ML) trains computers with mathematical data models without direct human supervision. It uses algorithms to identify patterns in the data, and then makes predictions based on the observed patterns and/or improves itself. [8]
Deep Learning (DL) is an advanced type of machine learning that uses multi-layers of algorithmic networks, called neural networks, inspired by the structure of the human brain. A deep artificial network consists of nested neural nodes, and each question answered leads to another connected questions in the nested hierarchy. The difference between ML and DL is Deep Learning automatically perceives the identification properties, while these features have to be given by human in the case of Machine Learning. [9]

3. 2. Generative design and Artificial Intelligence

According to the Autodesk Generative Design Primer open-source project, generative design and Machine Learning are not the same, but generative design relies on Machine Learning. Machine Learning finds patterns and predicts, while generative design creates models.
The programme makes an initial model with random input values in the beginning of the generative process and after that continuously optimizes it according to the given requirements. If large amount of data available, Deep Learning can be a great support of generative design to create better initial design based on accurate historical dataset.

3. 3. Application of Artificial Intelligence in the evaluation and selection phase of generative design

After the generation process, we have to select from the models. This raises a tough question: which one should we choose, since they all meet our requirements of geometry, mechanical properties, material and manufacturing method? Artificial Intelligence can play a role in this phase as well, because if a sufficient amount of data is accessible, Deep Learning can help the choice between concepts.
The data is the key point here: we have to provide information about factors that was not included in the generative parameters, because generative design focuses on the performance. These data can derive from the life-cycle analysis of similar parts, from the following areas:

- Mechanical and other kind of test results.
- Experiences of manufacturing.
- Maintenance, service.
- Logistics and transportation.
- Packaging.
- Assembling, disassembling.
- Recyclability.
- Ergonomic aspect.
- Economic aspects (e.g.: marketability).
- Customer feedback.
- Experiences from long-term usage.

4. SUMMARY

The most important features of generative design were briefly described above. The generative design process based on the Autodesk Fusion 360 Generative Design framework was presented. Practical applications of generative design were mentioned, and the areas of possible applications were collected according to the properties of this method. It can be highlighted that generative design method could be used if we want to achieve a lower weight or better mechanical properties. The article also presented the connection between generative design and Artificial Intelligence, and finally we made suggestions regarding the further application of Deep Learning related to generative design.
Further task could be to develop an Artificial Intelligence based evaluation system for the selection phase of the generative design method.

REFERENCES

[1] Szabó, K. – Hegedűs, Gy. (2020). A generatív tervezés lépései integrált CAD rendszerekben, *Multidiszciplináris tudományok*, Vol. 10, No. 4, ISSN 2062-9737, https://doi.org/10.35925/j.multi.2020.4.43.

[2] Singh, V. – Gu, N. (2012). Towards an integrated generative design framework, *Design studies*, Vol. 33, No. 2, ISSN 0142-694X, https://doi.org/10.1016/j.destud.2011.06.001.

[3] Bohnacker, H. et al. (2012). *Generative Design: Visualize, Program, and Create with Processing*, ISBN 9781616890773, Princeton Architectural Press, New York.

[4] Kallioras, N. A. – Lagaros, N. D. (2020). DzAIℕ: Deep learning based generative design, *Procedia Manufacturing*, Vol. 44, ISSN 2351-9789, https://doi.org/10.1016/j.promfg.2020.02.251.

[5] Szabó, K. – Hegedűs, Gy. (2020). A generatív tervezést támogató szoftverek rövid áttekintése, *Multidiszciplináris tudományok*, Vol. 10, No. 3, ISSN 2062-9737, https://doi.org/10.35925/j.multi.2020.3.39.

[6] Seregi, B. L. – Ficzere, P. (2021). Weight Reduction of a Drone Using Generative Design, *Hungarian Journal of Industry and Chemistry*, Vol. 49, No. 2, ISSN 2450-5102, https://doi.org/10.33927/hjic-2021-16.

[7] Russell, S. J. – Norvig, P. (2021). *Artificial Intelligence: A Modern Approach*, ISBN 9780134610993, Pearson Education, Hoboken.

[8] Mohri, M. et al. (2018). *Foundations of Machine Learning*, ISBN 9780262039406, The MIT Press, Cambridge.

[9] Goodfellow, I. et al. (2016). *Deep learning*, ISBN 9780262035613, The MIT Press, Cambridge.

Design of Machines and Structures, Vol. 12, No. 1 (2022), pp. 61–69.
https://doi.org/10.32972/dms.2022.014

DEVELOPMENT AND MILESTONES OF ALTERNATING CURRENT HYDRAULIC DRIVES

TAMÁS FEKETE

University of Miskolc, Department of Machine Tools
H-3515, Miskolc-Egyetemváros
fekete@uni-miskolc.hu
https://orcid.org/0000-0002-2699-2621

Abstract: The energy transfer at the hydraulic drives can be solving with direct current hydraulic drives and alternating current hydraulic drives. At the direct current hydraulic drives, the operating fluid flow in one way besides the alternating current hydraulic drives, where it is alternating periodically between the hydrogenerator and the hydromotor. In this research, I would like to examine the evolution and milestones of this scientific field.

Keywords: *hydraulic system, hydraulic drive, milestone*

1. INTRODUCTION

Man has been preoccupied since ancient times to create the conditions for himself to make a living. Over time, based on the personal and ancestral experiences of his ancestors, he sought to develop the means necessary for his livelihood in all areas, thus saving the effort of human strength in order to achieve his goals.
The 20th century can be considered an era of scientific, technical, health and social development. We can also refer to it as the age of world wars, which also had innumerable consequences for posterity. The mechanization of production and services began in the 19th century, and the construction of global communications networks continued at an ever-accelerating pace in the 20th century. In this century, all areas of life have fundamentally changed and the whole of human society has changed considerably.
The development of hydraulic and pneumatic technology is due to this process. Hydraulic and pneumatic technology has undergone an explosive development in the 20th century because it has been essential for various industries to increase the level of technology in terms of productivity. The rapid mechanization and automation of production processes, the increasing complexity of the kinematic design of machines, and the need to increase transmitted power have placed increasing

demands on energy transmission and control. Different energy transmitters can be used for the mode of energy transmission. The selection of the appropriate energy transmission technology is based on different criteria and should be compared with the specific characteristics of the energy transmission modes, which may limit their scope. The use of a liquid energy transfer medium, the simple change of the characteristic parameters of the transmitted energy (force, torque), the simple protection against overload and the extremely high specific power make the hydraulic systems suitable for the fulfilment of highly and rapidly changing requirements.
After the Second World War, developments that were still secret at the time became more and more widespread in various fields of industry in addition to military technology. In the most developed countries of the world, companies manufacturing special elements have increasingly appeared and developed. Manufacturing plants specializing in a particular product type began to become more widespread, making it possible for suppliers to become large companies.
Due to the high-power density of hydraulics, there is a saying in the 20th century that:

'Hydraulics is the muscle of the 20th century; electronics is the brain.'

Towards the end of the 20th century, with the advent of increasingly modern mechatronic systems, computer control also came to the fore with the use of electrohydraulic components.

2. THE SPREAD OF HYDRAULIC TECHNOLOGY IN TECHNICAL PRACTICE

In the beginning, the hydraulic systems only used the energy of free-flowing fluid, and later, by increasing the pressure (with the help of mechanisms or increasing the temperature) and with the help of different mechanisms, they continuously developed over the millennia and thus hydraulic equipment was formed. In antiquity and the Middle Ages, the use of open-surface water energy dates back to early Mesopotamia, where B. C. VI. millennium, it was used in the field of irrigation and to ancient Egypt, where B. C. II. it has been used for water clocks for millennia. Other early examples of the use of hydropower are the qanat system in ancient Persia and the Turpan water system in ancient China.
In the Hellenistic period (B. C. 336–B. C. 30), the Greeks built highly developed water and hydraulic systems. One example of this is the Eupalinos aqueduct (Samos tunnel), which was the aqueduct channel of the city of Samos.
An early example of the use of the "hydraulic wheel" as a device for draining water is the Perachora wheel (B. C. III. century). This device is the earliest type

of "water lifter" in Europe, which was used to transfer hydraulic media. It was driven by animal power, where the wheel equipped with containers for draining water was driven through two wheels with wooden teeth at right angles to each other.

Notable in the construction industry are the first hydraulic automaton of Ctesibius (Κτησίβιος) (B. C. 270) and the pump of the Egyptian Hellenic machinist and mathematician Heron (10–75). Héron writes of many devices that used hydraulic power, such as the "power pump" - known from many Roman sites - used to raise water in fire trucks. The volume change is caused by the piston moving in the cylinder, the direction of the liquid flow is controlled by self-acting valves. Due to their operating principle, the liquid delivery of piston pumps is not uniform.

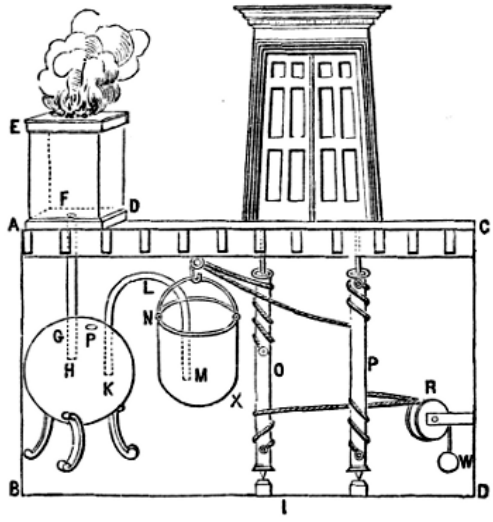

Figure 1. *Automatically opening church door [7]*

In ancient times, priests who possessed knowledge often used their knowledge manipulatively to strengthen faith. One striking example of this is the automatically opening church door. The altar, which opened the door automatically, was connected to a spherical tank approximately half filled with water. The shafts that operated the opening of the door wings, to which hinges were attached and reached all the way down to the floor of the basement under the church. Two chains were wound on the part of the shafts in the basement. A larger weight was attached to the end of one chain, which kept the doors closed, while the other chain was wound onto the shafts from the opposite direction, and a container was attached to its end, the mass of which, when empty, was less than the weight that

kept the doors closed. The vessel was connected by a U-shaped pipe to the container placed under the altar. After igniting the fuel placed on the altar, the temperature increase caused the liquid in the tank to heat up. The heated air increased in volume, exerting pressure on the liquid in the tank. The fluid flowed through the U-shaped tube into the vessel due to the increased pressure, which caused it to descend and open the doors. The diagram of the church opening mechanism is shown in Figure 1.

In ancient Rome, a variety of hydraulic devices were developed, including public water supplies and numerous aqueducts. Water mills were also built to harness the energy of water. The water mill uses water energy as an energy source to drive the mill wheel. The main construction units of the water mill are: the mill wheel, the associated mechanical equipment, and the mill house itself, where grain is most often ground.

Hydraulic mining was used to extract gold in northern Spain. The Las Médulas alluvial gold mine was one of the largest of the mines. They worked with several long aqueducts and used the currents to wash away the soft sediment and then wash the ground of the valuable gold content.

One of the new representatives of hydraulics as a science was Blaise Pascal (1623–1662), who dealt extensively with the physics of liquids. He became known in hydrostatics by creating the law later named after him. He contributed to the development of the natural sciences, designed a mechanical calculator, founded projective geometry, and developed the mathematical theory of probability calculation together with others. He formulated the physical law of moving vessels. At a very young age, he achieved results by examining the pressure conditions of gases and air pressure changes. His famous barometer experiment was actually a remote experiment, as it was carried out by his brother-in-law, Périer. In honour of his work, the pressure unit was named Pascal.

Daniel Bernoulli (1700–1782) was a doctor, mathematician and physicist born in Switzerland. One of his most important scientific results is the Bernoulli equation for stationary flows (he developed it for both compressible and incompressible media). Bernoulli's law states that the sum of the different energies along a streamline in a flowing medium is constant. This law solved many of the physical issues that arose in shipping. His work, Hydrodynamics, is the first literature that discusses the mechanics of liquids with reference to a general principle with the help of analysis.

Many cities in England were so advanced that they used hydraulic networks in the 19th century. in the 20th century for handling machines, such as elevators, cranes, winches, and similar technical achievements.

Similar to other industrial sectors, the 20th century. At the beginning of the 20th century, Hungarian engineers recognized the potential of hydraulics and

successfully used several hydraulic devices in metallurgical, mining, and other plants. As an interesting point, it can be mentioned that between the two world wars, the Budapest Opera House was the first in the world to use stage machinery operated with a hydraulic system. The stage machinery patented by the Asphaleia company, which operated with water hydraulics, was completed based on the design of set designer Josef Kautzky and Robert Gwinner.

The fire disaster at the Ringtheatre in Vienna played a role in the spread of hydraulic technology. He drew attention to the fact that theatres need to be improved from a fire protection point of view. With the help of the hydraulic stage machinery, the set and stage fields were moved by hydraulic cylinders instead of manual force. The stage machinery of the Budapest Opera House also included the hydraulic movement of the circular horizon curtain and the two hydraulic freight elevators, which were also the first in the world to be used in Hungary.

In the middle of the 20th century, Hungarian engineers only rarely had access to specialized literature in which they could learn about new technical results. Due to weak foreign trade, elements were made primarily for domestic machine tool production based on the new technical information. When international relations took off, the Hungarian pneumatics and hydraulics industry was formed at the same time. Modern machines have arrived in our country in increasing numbers, so the demand for specialists who understand this has increased. As a result, pneumatics and hydraulics education was introduced in secondary and higher education from the 1970's.

The education and spread of the theory of hydraulics resulted in the strong development of the industry. As a result, engineers and researchers increasingly came to the introduction of alternating current hydraulic systems. The appearance of alternating current hydraulic drives in written form in the 20th century can be dated to the first quarter of the century.

3. ALTERNATING CURRENT HYDRAULICS IN TECHNICAL PRACTICE

The first publication that can still be found today is attributed to the Romanian researcher George (or Gogu, known by both names) Constantinescu, whose results could already be used for practical implementations. Constantinescu was primarily involved in the design and testing of devices operated with alternating current fluids. In 1910, he emigrated to London, where he was able to focus more on his studies. The single-phase rock drill was able to drill through a hard block of granite quietly and evenly. With the help of this prototype, he illustrated the power of the alternating current system. In Constantinescu's propeller, the generator rotated at high speed, while the propeller (engine) rotated at low speed. A photo of his experimental equipment is shown in Figure 2 [8].

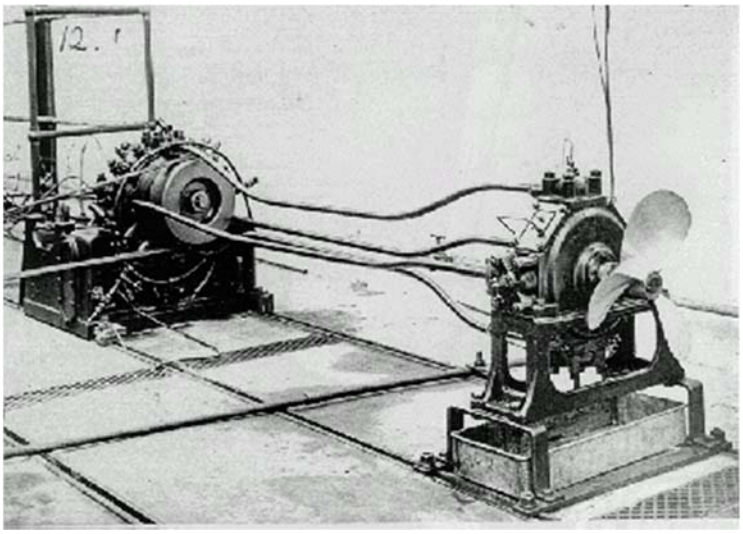

Figure 2. *George Constantinescu's four-phase experimental device for marine use and the structural design of the generator [8]*

With Constantinescu's alternating current devices, the stroke of the phase pistons in each phase could not be modified, i.e., only the drive frequency (generator speed) could be modified. His equipment could have been used on a wider scale if he had also used amplitude control (the possibility of changing the piston stroke).

Bergeron L. (1911–2001) during the graphic analysis of pressure waves examined a water extraction device, which operated the water extraction piston pump by alternating movement of two liquid columns.

In the 1970's, we can find works published by Hibi A., Prokes J. and Prikryl I. on the topic of alternating current hydraulic systems. A. Hibi, a professor at the University of Shizuoka, published the construction of an asynchronous alternating current hydraulic drive (a two-phase system operated with a fixed-stroke generator) and its test results. Prokes J. dealt with the grouping of alternating current hydraulic mechanisms based on electrical analogy. He found that the grouping can be done according to the size of their frequency or the types of connection of the resistors. Prikryl I. established that the so-called hybrid mechanism (Prokes: it can be operated with either direct or alternating current) can be used, for example, as a transformer or even as a current controller. W. M. J. Schlösser, a professor at the University of Eindhoven, deals with synchronous AC hydraulic drives in his work.

In Hungary, synchronous and asynchronous AC hydraulic drives began to be researched in the 1970's at the University of Miskolc.
In the beginning, alternating current hydraulic energy transmission was used as a vibration generating device in the dynamic testing of machine tools. Using the electrical analogy, János Lukács classified alternating current hydraulic drives. He divided AC hydraulic drives into two larger groups: synchronous and asynchronous systems. He examined the typical properties of hydraulic energy transmission and determined the hydraulic power for all types of resistance. From his experiments, he concluded that from a practical point of view, two and three phases and their integer multiples can be used. He performed both no-load and load tests on his two-phase experimental equipment. He determined the movement and flow conditions of synchronous and asynchronous AC hydraulic drives. Later, various alternating current hydraulic drives were implemented, for which a patent was also issued. One of the patented versions of the alternating current hydraulic drive is shown in Figure 3. The alternating movement of the phase piston of the alternating current hydromotor is converted into alternating rotary movement by a mechanical rectifier, or otherwise known as a freewheel [8].

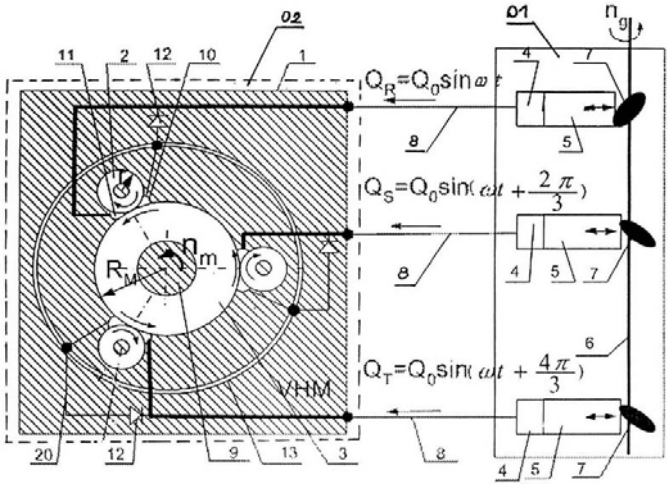

Figure 3. *Diagram of an alternating current hydraulic drive patented by János Lukács [8]*

Breznai A. dealt with dynamic tests of synchronous hydraulic drives and their simulation at a theoretical level but did not prepare experimental equipment and practical measurements in this regard, which would have verified the effectiveness of the calculations.

Dr. Raid Ahmed Smadi designed an alternating current hydraulic clutch and examined its operating principle from a theoretical point of view. performed measurements on it both at idle and under load.

Table 1

Milestones in the research of alternating current hydraulic drives [9]

Year of Publication	Author	Milestones	Country
1913	G. Constantinescu	mechanisms operating with alternating currents of fluids	England
1950	Bergeron L.	pressure waves generated in alternating system hydraulic systems	France
1969	Prokes J.	testing of alternating current hydraulic synchronous drives	Czech Republic
1975	Prikryl I.	testing of alternating current hydraulic synchronous drives	Czech Republic
1970	Lukács J.	examination of synchronous and asynchronous alternating current hydraulic drives	Hungary
1979	Hibi A.	investigation of a three-phase AC hydraulic synchronous drive	Japan

During his research, Dr. Imre Czupy examined asynchronous hydraulic drives. He used the experimental, alternating current linear vibrating equipment, which was also operated under industrial conditions, to remove the stumps left after forestry logging. He determined the relationships between the vertical billet lifting force and the diameter of the billet cutting blade, the laws of billet vibration, and analysed the energy of the vibrating system, respectively. performance conditions. Research in the direction of sperm separation has not yet been fully completed.
Dr. János Erdélyi dealt with the design and construction issues of an asynchronous alternating current hydraulic drive. During his research work, an experimental device was constructed. He examined the power and motion transmission properties of this equipment. He proved that in the case of rigid and hydrodynamically short phase lines, the pressure waves generated in the phase lines do not create dangerous pressure peaks. With the help of the correlations, he showed that the relationship between the pressure and the flow rate of the phase fluid flow of the alternating current asynchronous hydraulic drive can be examined as a concentrated

parameter. He also studied the methods of balancing actuating eccentric disks. There was no investigation of the pressure waves or on the extent and possible effects of the temperature increase that may arise from the pulsating movement of the energy transmitting medium. Table 1 shows the milestones in the research of alternating current hydraulic drives.

REFERENCES

[1] Erdélyi, J. et. al. (2008). A kontrakciós henger konstrukciós és működési tulajdonságai, *Pneumatika, hidraulika, hajtástechnika, automatizálás*, Vol. 12, Nr. 1, ISSN 1587-6853, ISSN 1417-8710.

[2] Erdélyi, J. (2006). Váltakozó áramú hidraulikus aszinkron (A-VAH) hajtás, *OGÉT 2006. XIV. Nemzetközi Gépész Találkozó*, ISBN 9737840100.

[3] Fekete, T. (2014). The alternating current synchronous hydraulic drive, *ANNALS of Faculty Engineering Hunedoara – International Journal of Engineering*, Vol. 12, Nr. 2, ISSN: 1584-2665.

[4] Fekete, T. (2017). Alternating current hydraulic drive the possibility of applying, In: Jármai, K., Bolló, B. (eds) *Vehicle and Automotive Engineering, Lecture Notes in Mechanical Engineering*, Springer, Cham., ISBN 978-3-319-51188-7 https://doi.org/10.1007/978-3-319-51189-4_5.

Fekete, T. (2011). Háromfázisú váltakozó áramú hidromotor forgóelemes fázistér kialakítással, *XXV. microCAD International Scientific Conference*, ISBN: 9789636619633, Miskolci Egyetem.

[5] Fekete, T. (2013). Szinkron rendszerű váltakozó áramú hidraulikus hajtás, *OGÉT 2013. XXI. Nemzetközi Gépész Találkozó*, ISSN 2668-9685.

[6] Andai, P. (1965). *A technika fejlődése az őskortól az atomkor küszöbéig*, Akadémiai Kiadó, Budapest.

[7] Petrescu, R. V. V. et al. (2017). George (Gogu) Constantinescu, *American Journal of Engineering and Applied Sciences*, Vol. 10, No. 4, ISSN 1941-7020, https://doi.org/10.3844/ajeassp.2017.965.979.

[8] Lukács, J. (2005). *Váltakozó áramú hidraulikus hajtás motoregysége forgóelemes fázisterekkel*; használati mintaoltalom, lajstromszám: 3148.

[9] Fekete, T. (2022). Váltakozó áramú hidraulikus hajtás kapacitás változása rugalmas fázisvezetékek alkalmazása esetén, disszertáció, Miskolci Egyetem.

Design of Machines and Structures, Vol. 12, No. 1 (2022), pp. 70–79.
https://doi.org/10.32972/dms.2022.015

MAINTENANCE OF THE N47 INTERNAL-COMBUSTION DIESEL ENGINE

TAMÁS FEKETE

University of Miskolc, Department of Machine Tools
H-3515, Miskolc-Egyetemváros
fekete@uni-miskolc.hu
https://orcid.org/0000-0002-2699-2621

Abstract: The N47 engine debuted in March 2007 in the facelifted BMW 1 Series E87 and E81 and was also available in the BMW 1 Series E82 and E88, which were introduced the same year. The N47 engine replaced the M47 engine that had been in production for 8 years. The M47 construction underwent several modifications, so the injection system was changed, the cylinder head now consists of two parts, and the engine block is made of aluminium. Two main versions of the N47 engine are known: N47D16 (1.6 L) and N47D20 (2.0 L). In the case of both versions, several models with different performances were born. After the distribution of BMW passenger cars equipped with the N47D20 engine, it received a lot of negative criticism due to malfunctions. In this article, I would like to present the maintenance of the engine, which can be used to avoid the failure of passenger cars equipped with the N47D20 diesel engine with huge material damage.

Keywords: *N47, diesel engine, self-ignition, timing chain snaps, DPF, EGR*

1. INTRODUCTION

The appearance of the N47 diesel engine was justified by the desire to reduce fuel consumption and increase engine performance. The first two versions were the smaller 105kW N47D20U0 and the 130kW N47D20O0 engine. After that, the 150kW N47D20T0 with two turbochargers appeared. The motorcycles thus completed set out on their journey in the hope of great popularity. Due to the problems experienced, the manufacturer announced a recall campaign for its engines completed up to March 2011 due to failures related to the timing chain [1]. Table 1 shows the different versions of the N47 diesel engines.

Table 1
The variants of N47 diesel engine [4]

Engine	Displacement	Compression Ratio	Power	Years
N47D16	1.6 L (1598 cm^3)	16.5:1	70 kW (94 hp) at 4000 rpm	2013
			85 kW (114 hp) at 4000 rpm	2012
N47D20	2.0 L (1995 cm^3)	16.5:1	85 kW (114 hp) at 4000 rpm	09/2009
			105 kW (141 hp) at 4000 rpm	03/2007
			120 kW (161 hp) at 4000 rpm	09/2009
			130 kW (174 hp) at 4000 rpm	03/2007
			135 kW (181 hp) at 4000 rpm	03/2010
		16.1:1	150 kW (201 hp) at 4400 rpm	03/2010
		16.5:1	160 kW (215 hp) at 4400 rpm	2011

2. THE MAIN MALFUNCTIONS OF THE N47 ENGINE

The N47 engine family is prone to excessive timing chain wear and premature failure [BBC.co.uk: BMW deny engine failures are due to manufacturing fault, 2013.]. A rattling noise from the rear of the engine indicates the condition. Timing chain failure may require engine replacement or costly repairs. The units most seriously affected and in need of the greatest repair were between 01.03.2007. and 05.01.2009. was produced [1]. However, there have been frequent reports of timing chain failure (Figure 1) in BMW 1, 3 and 5 series diesel engines manufactured from 2004 to at least 2011. The failure occasionally resulted in the engine stalling dangerously while the vehicle was being driven sometimes at relatively high speeds. A "Quality Enhancement" was issued by BMW for some, but not all vehicles, but has since been discontinued.

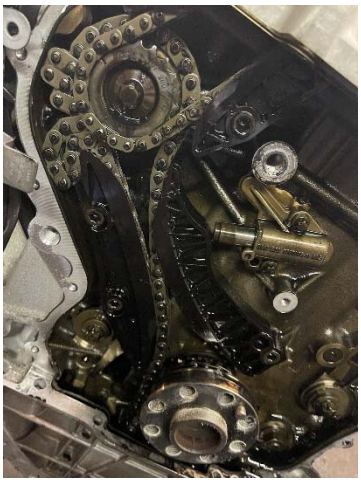

Figure 1. *Timing chain failure (break)*

If the vacuum hose supplying the EGR (Exhaust Gas Recirculation) cooler bypass valve gets a hole rubbed in it, or breaks down from old age and oil spray, the EGR cooler will not get bypassed during the engine warmup period. This causes excessive build-up in the cooler matrix, and when the engine warms up these solid chunks of build-up can detach from the EGR cooler and get sucked into the plastic intake tube, melting holes in the intake tube, causing a massive boost leak and in very rare cases an engine fire (Figure 2). BMW has issued a recall to over 1.6 million vehicles in 2018 for the EGR issues [Braithwaite-Smith G.: Massive BMW diesel engine recall is expanded, Motoring Research, 2019.].

Figure 2. *Vehicle with N47 engine after catching fire*

3. PREVENTIVE MAINTENANCE OF THE MAIN FAULTS OF THE N47 ENGINE

In the case of regular maintenance [3], [6], the N47 engine should be serviced between 200,000 and 300,000 km, unless otherwise indicated. In the case of the N47 engine that I renovated, I examined the following seven segments, and they were repaired (replaced).

3. 1. Timing chain inspection

The first and most important thing is to replace the timing chain and its associated components (sprockets, tensioners, etc.). Since the timing chain is located at the rear of the N47 engine, it is recommended to remove the engine block for professional inspection and repair work (Figure 3).

Figure 3*. The engine compartment without the engine and the removal of N47 engine*

Timing chain elongation can also be determined from the condition of the tension cartridges (Figure 4).
Since the engine block must be disassembled for the inspection, replacement is recommended even if the timing chain is still in good condition. If the timing chain is broken in the block, further tests are suggested to determine the exact damage.

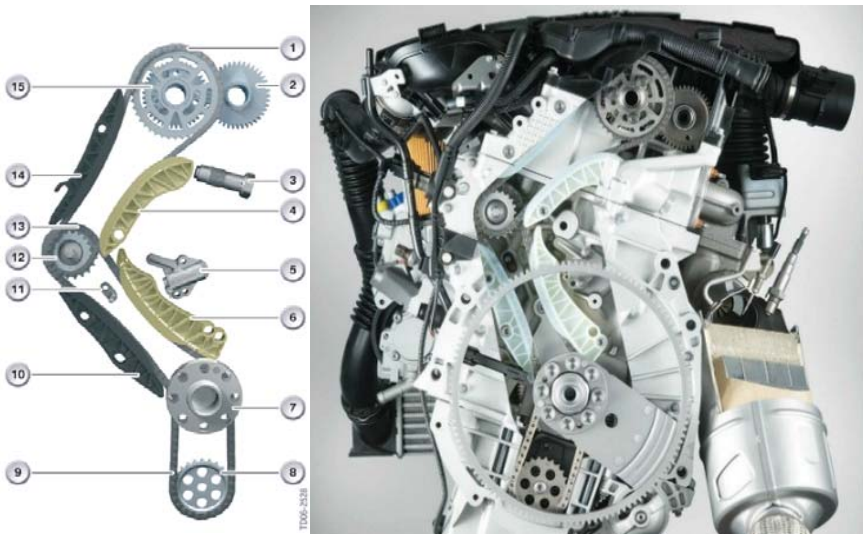

Figure 4. *The timing chain system*
[Tumblr, N47 timing chain, source of a picture]

3. 2. Intake manifold and EGR cooler

The EGR cooler and suction line or the examination of its related elements must be carried out together. An exhaust gas recirculation system is one of the ways to reduce engine emissions. It is an important part of the engine system, and like all heavy-duty components, it must perform in an extremely harsh environment. Exhaust gas recirculation (EGR) reduces combustion temperatures by diluting the air/fuel mixture with a small amount of inert exhaust gas. The EGR cooler is a water-to-air heat exchanger located between the turbo and the EGR valve. The body has a hollow tube or series of tubes through which the hot exhaust passes. Heat from the exhaust system is transferred to the vehicle's cooling system. This excess heat simply escapes through the radiator. Since the EGR cooler connects the engine's exhaust and cooling systems, malfunctions inside the cooler can lead to coolant loss, overheating, and engine damage. Therefore, one of the results can be a decrease in the amount of coolant. In such cases, it is worth cleaning the intake line (Figure 5) and replacing the EGR cooler under warranty. Of course, replacing the EGR cooler under warranty does not solve the problem, because later the above-mentioned problems will reappear.

Figure 5. *Oily soot deposits in the plastic intake pipe*

The leakage of coolant caused by the EGR is only a small element in the set of errors. The first and biggest problem is that the plastic intake manifold, like all direct injection engines, gets oily soot. Only the second stage is the failure of the EGR cooler. If this does not cool the recirculated gases enough, they will easily ignite the deposits in the intake line, which are already at the flash point. Then, due to the turbo pressure, the glowing oil and soot melt the plastic intake pipe. Once it is pierced, it is just a matter of luck as to what the resulting stabbing flame will achieve (0).

Figure 6. *Melting of the cover on the engine as a result of the puncture of the intake pipe*
[Zách D.: Miért gyulladnak ki a BMW-k?, Totalcar 2019. (in Hungarian) source of a picture]

If the complex error of the EGR system occurs on the highway in the summer, the vehicle will most likely catch fire.

3. 3. The puncture of the Diesel Particulate filter (DPF)

The particulate filter (Figure 7), which collects the soot produced by the car's engine, is located directly on the right side of the cylinder bank. The filter must be burned out at certain intervals. This is solved by burning the excess diesel fuel added to the engine, the process starts while driving, typically when driving on the highway. The car does not indicate anything, the driver has no special task. However, the particle filter heats up to a temperature of 600 degrees, and if it has already been punctured, a piercing flame is created through the hole, which easily ignites the surrounding plastic coverings of the engine compartment. There are several of these, the N47D20 is heavily coated from above and below. Based on the experience so far, the punctured filter, which will certainly occur over time, can also cause the car to catch fire.

Figure 7. *Diesel Particulate filter*

3. 4. Inspection of oil filter housing and oil cooler seals

It is worth replacing the oil cooler seal together with the timing chain. A characteristic symptom of seal wear is the formation of oil sludge under the oil cooler. The shaft located at the bottom of the oil filter housing (Figure 8) and oil cooler must be checked, as it is possible that the socket is cracked, which may later lead to premature failure of the engine bearings.

Figure 8. *Oil filter housing shaft. The socket may crack*

3. 5. Checking the generator

The generator can be easily inspected in the case of an advanced engine [4], therefore it is worth checking the condition of the carbon brushes (to be replaced at the voltage regulator) and their bearings. Once the generator has been disassembled for inspection, we can also inspect the freewheel of the pulley.

3. 6. High pressure fuel pump

The task of the diesel high-pressure pump, together with the low-pressure pump, is to deliver fuel from the fuel tank to the vehicle's engine [6]. High pressure pump failure can have a significant impact on engine performance. Signs of diesel high pressure pump failure:

- the engine starts delayed,
- fuel consumption increases,
- high engine temperature,
- the fuel pressure gauge measures a low value.

The easiest way to check is to remove the sensor from the pump and check the condition of the shaft (Figure 9). If we find that, in contrast to the factory shine, it has started to dull (piston, shaft), it is worth refurbishing or replacing it. If the piston rotates relative to the shaft, the fine metal dust coming off the shaft as a result of friction can enter the fuel supply system and cause enormous damage.

Figure 9. *The high-pressure fuel pump, and wear resulting from the sticking of the piston, which results in the entry of metal dust into the system [BMW E91 N47 high pressure pump failure and repair, YouTube, source of picture]*

3. 7. Inspection of the balancing shafts

As previously mentioned, the balancing shafts (Figure 10) of the N47 engine are located inside the crankcase. They are inserted from the front. It is advisable to check the wear of the bushings by moving the balancing shafts, as it can cause strong vibrations, which can lead to further engine failure. It is advisable to check the wear of the bushes by moving the balancing shafts, as it can cause strong vibrations, which can lead to further engine failure.

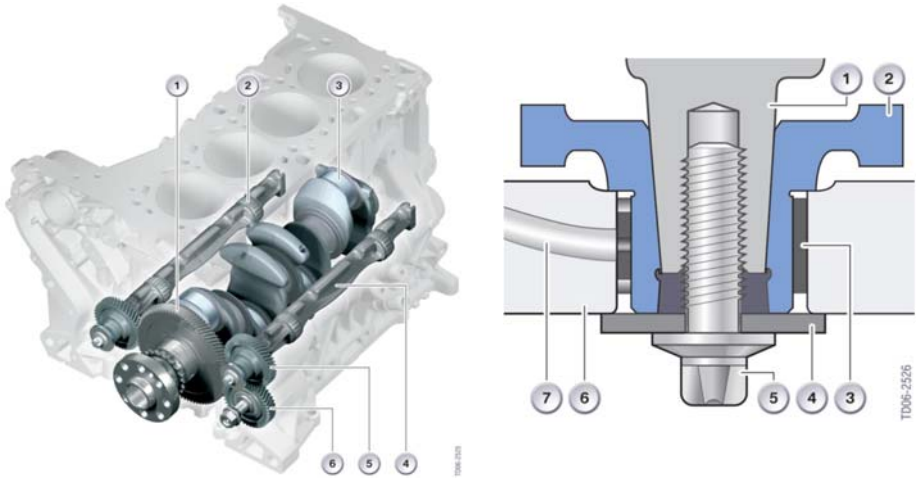

Figure 10. *The balancing shafts and the bush (denoted with number 3) [2]*

4. SUMMARY

As with all vehicles, the most important thing for the N47 engine is regular maintenance and proper operation. We can ensure the lifetime of the timing chain –according to our service experience– by changing the engine oil before the predefined replacement period by the manufacturer (2 years or 30,000 km), but it is recommended after driving between 15,000 and 20,000 km. The N47 engine I dismantled had 235,000 km, but due to regular maintenance and more frequent oil changes, the timing chain was still in good condition and therefore it would not have to be replaced yet. It is unfortunate that the brand dealership gives the answer to replace the timing chain that the brand service can determine, and the brand service does this with noble simplicity based on mileage (as long as there is no noise or other complaints). In this regard, it would be good if the timing chain tension pins were equipped with a transmitter, because the condition of the chain can only be confirmed if the engine is removed and disassembled. The service life of the high-pressure pump is usually 10 years or between 150,000 and 200,000 km, thus it is worth paying attention to this, because in the case of the N47 engine, significant damage can occur due to metal dust. The condition of the DPF filter, EGR cooler and intake manifold must be checked regularly (approx. 50,000 km), because it can lead to the vehicle catching fire. An additional solution against ignition can be if the plastic suction tube is replaced with one made of a material that does not melt under the influence of a flame.

REFERENCES

[1] Őri, P. (2012). BMW N47 dízel motor, *Autotechnika*, ISSN 1588-9858, X-Meditor Kft., Győr.

[2] Krüger, H. (2006). *N47 engine – BMW service*, Bayerische Motoren Werke AG, München.

[3] Wharton, A. J. (1991). *Diesel Engines*, ISBN 9780750602174, Butterworth-Heinemann, London.

[4] Mahon, L. L. J. (1992). *Diesel generator handbook*, ISBN 9780750611473, Newnes, London.

[5] Martyr, A. J. – Plint, M. A. (2012). *Engine testing – The Design, Building, Modification and Use of Powertrain Test Facilities*, ISBN 9780080969497, Butterworth-Heinemann, London.

[6] Heisler, H. (1995). *Advanced engine technology*, ISBN 9780340568224, Butterworth-Heinemann, London.

Design of Machines and Structures, Vol. 12, No. 1 (2022), pp. 80–85.
https://doi.org/10.32972/dms.2022.016

ADDITIVE MANUFACTURING IN THE MILITARY AND DEFENCE INDUSTRY

PÉTER FICZERE

Budapest University of Technology and Economics,
Department of Railway Vehicles and Vehicle Systems Analysis
H-1111 Budapest Műegyetem rkp.3
ficzere.peter@kjk.bme.hu
https://orcid.org/0000-0003-3207-5501

Abstract: The use of additive manufacturing technologies is becoming more widespread. Obviously, such a new and innovative technology should also be used in the defence industry, despite the many strict safety criteria that have to be met in this field. The current paper presents, without being complete, some of the notable military applications where additive technologies are expected to become more significant in the near future.

Keywords: *military industries, additive manufacturing, 3D printing, defence*

1. INTRODUCTION

Thanks to the widespread use of additive manufacturing technologies, more and more areas are exploiting the benefits of the technology. Of course, for real components manufactured using this technology, intended for installation and long-term operation, it is particularly important to have a precise knowledge of the specificities of the technologies. It is also necessary to have the right raw materials at our disposal. Components intended for different applications have different requirements [9]. In many cases, e.g., for medical implants, it is not possible to check the component's ability to perform its function in advance at the final installation site and its load-bearing capacity must be verified in some way beforehand [1], [8], [10]. Additive manufacturing (AM), widely known as 3D printing, can be identified as a key enabling technology for improving industrial competitiveness by allowing fast, decentralised, and flexible production. Additive manufacturing is already being used in various industries, but the armed forces are still far from fully exploiting the potential of the technology. The expected growth of the additive manufacturing market could bring a number of benefits. These include reducing the cost of manufacturing tools and components, improving

design, reducing time to the end user, and increasing technical and commercial competitiveness. In addition, 3D printing can have a significant impact on the maintenance of military equipment through the production of spare parts and equipment components. As air, land and naval defence systems have complex and specific basic structures, the customisation capability of AM and its on-site and on-demand properties are of particular interest to defence. Equally beneficial are weight reduction and increased component strength and durability, which were more difficult to achieve in traditional subtractive manufacturing processes due to processing and time constraints.

In addition, AM technologies can hold great potential for enhancing defence capabilities, such as logistical support to forces deployed in remote or enemy environments. The time between failures and recovery of platform availability, the transport and storage of significant quantities of spare parts can be reduced, with associated cost reductions, reducing the logistical footprint of the operation.

The "Additive Manufacturing Feasibility Study & Technology Demonstration" project successfully installed a 3D printing lab in Zaragoza (Spain) for the third European Advanced Airlift Tactics Training Course (EAATTC 17 3) in June 2017. The successful test flight of the AM lab was key to testing the feasibility of deploying the facilities by air. During the deployment, the AM-lab attracted great interest from multinational units participating in EAATTC 17 3. The deployment also highlighted the high interest and potential of AM technologies across all military branches (pilots, maintenance, technicians, and logistics support), with a high interest in the benefits that 3D printing could bring to their own specialisms. The conclusions drawn from this deployment will help inform the design and requirements of future 3D printing facilities. Awareness of the defence potential of AM is crucial. It will be equally important to create alignment between the materials R&D community and operational military personnel and to help the R&D community understand the capability needs of the defence side. There is also a need for education to make this technology effective and accessible to military users.

On the technological side, further work is expected on the use of additive manufacturing for lightweight ballistic defence. Other key challenges include process standardisation, certification of manufactured parts and legal aspects.

Filling these technological gaps could increase the logistical and operational agility of military forces and provide a decisive competitive advantage for defence in a rapidly changing technological and conflict environment [2].

Additive manufacturing is widely used in a number of sectors, including naval, aerospace and automotive. It is therefore not surprising that it is also increasingly being applied in the defence sector worldwide. In fact, the military 3D printing sector is expected to be worth $1.7 billion by 2027, which illustrates the

importance of the technologies. Considering that the speed, lower weight, and lower costs are all priorities in the military, additive manufacturing will certainly have a role (*www.3dnatives.com*).

2. METHODOLOGY

This paper is a literature review, in which I will show the potential for military applications of additive manufacturing technologies through some of the more well-known and implemented application examples. Of course, this is far from being complete due to the limitations of the scope, as there are many other applications of additive technologies in the military beyond the examples presented here.

3. THE USE OF ADDITIVE MANUFACTURING IN THE DEFENCE SECTOR

3. 1. New 3D printer development

The US military is so convinced of the benefits of additive manufacturing that last year they announced they would even build the world's largest metal 3D printer. The US DEVCOM Army Ground Vehicle Systems Center is working with ASTRO America, Ingersoll Machine Tool, Siemens and MELD Manufacturing at Rock Island Arsenal - Joint Manufacturing and Technology Center to build the printer. The printer will be part of the Jointless Hull project, whose ultimate goal is to print monolithic (one-piece) hulls for combat vehicles. At the time of the announcement, it was estimated that the project would take about 14 months to complete, and the final printer will be capable of printing metal parts 30 feet long, 20 feet wide and 12 feet high (*www.3dnatives.com*).

3. 2. 3D printed runway for the US Air Force

Another application in the military and defence sector comes from ITAMCO (Indiana Technology and Manufacturing Companies), which has developed a runway for military expeditionary airfields using additive manufacturing. These runway mats are an essential component of Expeditionary Airfields (EAFs). Their function is to be implemented on soft ground surfaces to allow military aircraft to land and take off. Previously, a portable runway made of aluminium planks was used, but as this became obsolete, the military had to find an innovative solution. The M290 3D printer from the German company EOS was used to create a much lighter and more durable model for the US Air Force's military equipment (*www.3Dnatives.com*).

3. 3. Military modules, innovative use of additive manufacturing in defence

With the aim of boosting the development of strong and robust 3D printed factory modules, ExOne has joined forces with several partners to realise this challenge. In particular, the Defence Logistics Agency (DLA) contract was valued at $1.6 million. The process used ExOne's Binderjet technology for military applications because its speed, material flexibility and ease of use make it best suited to the critical needs of the military. The 3D printer, designed solely for the military, is said to be capable of binder jetting more than 20 metals, ceramics, and other powder materials - plus its unique housing and other features are said to make it perfect for a military-grade product (*www.3Dnatives.com*).

3. 4. The US Navy is also taking advantage of additive manufacturing

Marines have discovered that 3D printing can be used to create innovative tools for maintaining their vehicles. In particular, the Marine Corps Systems Command, in collaboration with supply battalions and industry partners, has additively manufactured metal steering wheel removal tools, helping to solve a common problematic operation that often needs to be solved during naval vehicle service [3], [7]. With the benefits of reduced maintenance time and increased readiness, additive manufacturing is highly profitable, especially when considering that the actual waiting time for such component parts is about 25 days [4], [6], (*www.3Dnatives.com*).

3. 5. The additive manufacturing propeller demonstrates the progress made in the French defence sector

The prestigious French company Naval Group has been using 3D printing for several years to meet different needs. In 2021, thanks to additive manufacturing, more specifically the WAAM (Wire Arc Additive Manufacturing) process, Naval Group 3D printed a propeller. The propeller, consisting of five 200 kg blades, was installed on the minesweeper Andromeda. The teams behind the project explained that by using the technology, they drastically reduced manufacturing time and minimised the number of materials used [5].

Figure 1. *3D printed boat propeller (www.3dnatives.com)*

4. CONCLUSIONS

It is also clear from the examples presented that the use of additive manufacturing technologies in the defence industry is still in its infancy. At the same time, however, it can be seen that it is being experimented with and its potential applications investigated in a number of areas. With its obvious advantages in terms of the ability to produce customised geometries, manufacturing flexibility, weight and cost reduction, logistical support and component supplies, it is evident that its application will be introduced in an increasing number of areas.
It is important to note that for military applications (priority safety criteria), specific requirements (technical and legal adequacy) have to be met in terms of processes and materials used. These take more time to meet, and their introduction may be slower than in the general market.

REFERENCES

[1] Ficzere, P. (2018). Design Questions of the Individual Medical Implants, *Proceedings of 4th International Interdisciplinary 3D Conference: Engineering Section*, ISBN 978-963-429-267-8, Pécsi Tudományegyetem.

[2] Lopez Vicente, P. (2017). Additive manufacturing in defence, *European defence matters*, Vol. 11, Nr. 14, ISSN 1977-5059.

[3] Alzyod, H. – Ficzere, P. (2022). Finite Element Modelling of Additive Manufacturing in Case of Metal Parts, *Periodica Polytechnica Transportation Engineering*, Vol. 50, Nr. 4, ISSN 0303-7800, https://doi.org/10.3311/PPtr.19242.

[4] Ficzere, P. et al. (2013). Economical investigation of rapid prototyping, *International Journal for Traffic and Transport Engineering*, Vol. 3, Nr. 3, ISSN 2217-5652 (online), https://doi.org/10.7708/ijtte.2013.3(3).09.

[5] Ficzere, P. (2022). The Impact of the Positioning of Parts on the Variable Production Costs in the Case of Additive Manufacturing, *Periodica Polytechnica Transportation Engineering*, Vol. 50, Nr. 3, ISSN 0303-7800, https://doi.org/10.3311/PPtr.15827.

[6] Ficzere, P. (2021). Effect of 3D printing direction on manufacturing costs of automotive parts, *International Journal for Traffic and Transport Engineering*, Vol. 11, Nr. 1, ISSN 2217-5652 (online), http://dx.doi.org/10.7708/ijtte.2021.11(1).05.

[7] Alzyod, H. – Ficzere, P. (2022). Using Finite Element Analysis in the 3D Printing of Metals, *Hungarian Journal of Industry and Chemistry*, Vol.: 49, Nr.: 2, ISSN 2450-5102, https://doi.org/10.33927/hjic-2021-24.

[8] Ficzere, P. (2022). Research on and Practice of Additive Manufacturing Technologies, *Hungarian Journal of Industry and Chemistry*, Vol. 49, Nr. 2, ISSN 2450-5102, https://doi.org/10.33927/hjic-2021-23.

[9] Ficzere, P. – Borbás, L. (2019). Experimental dynamical analysis of specimens' material properties manufactured by additive technologies, *Materials Today: Proceedings*, Vol. 12, Nr. 2, ISSN 2214-7853, https://doi.org/10.1016/j.matpr.2019.03.135.

[10] Alkentar, R. – Mankovits, T. (2022). A Study on the Shape and Dimensional Accuracy of Additively Manufactured Titanium Lattice Structures for Orthopedic Purposes, *Periodica Polytechnica Mechanical Engineering*, Vol. 66, Nr. 4, ISSN 0324-6051, https://doi.org/10.3311/PPme.20382.

Design of Machines and Structures, Vol. 12, No. 1 (2022), pp. 86–95.
https://doi.org/10.32972/dms.2022.017

DESIGN AND BUILD PROTOTYPE OF AUTOMATIC CURTAIN MOVING SYSTEM

PÁLMA KAPITÁNY

University of Miskolc, Robert Bosch Department of Mechatronics
H-3515, Miskolc-Egyetemváros
mrbpalma@uni-miskolc.hu
https://orcid.org/0000-0001-6826-2371

Abstract: The paper deals with an automatic curtain moving system. Here shown the process of design and build prototype. Solution of problem included design of mechanical construction, electric circuit and program of control. Nowadays is so popular to build houses by sandwich panel. This building method allows quick and modular process of building of halls. In this paper found a possible way for also quick and modular automatic curtain moving system. Chapters deal with initial known and added parameters and the problem. Furthermore, paper says about curtain cornice solutions, sliding ways, design of sheet metal components, DC motor choice, microcontroller and communication preparing. At the end found the conclusion of first prototype.

Keywords: *curtain moving, automatization, Arduino Uno*

1. INTRODUCTION

Today, modular construction is becoming more and more common, because it allows quick implementation, and unique assemblies can be created [1-3]. In this paper found a solution for an automatic curtains problem in a big hall. Figure 1 is shown one of the five windows, which need automatic curtains. The hall's inner height is 9 meters, the distance between columns is 5.5 meters, the depth is 15 centimetres, and the special curtain will be 2.3 meters vertical-long with 700 grams per m^2 weight.

2. MOVING TECHNIQUE

First, there was walked around question of curtain cornice and sliding ways [4-6]. There exist two class based on the curtain moving direction: vertical moving direction created by roller blinds, the horizontal one is the traditional curtains.

Because of the fire safety part of window, there was chosen the horizontal moving direction. Figure 2 presents the main two class of the traditional one. Figure 2, part a) shows 'rod with hoops' technic, while Figure 2, part b) shows 'rail track with sliders' solution. The version b) is compact, but in this length would have required a custom order and caused complication in automatic moving process. Therefore, the design continued with the 'rod with hoops' technic.

Figure 1. *One of the windows in the hall inside and outside*

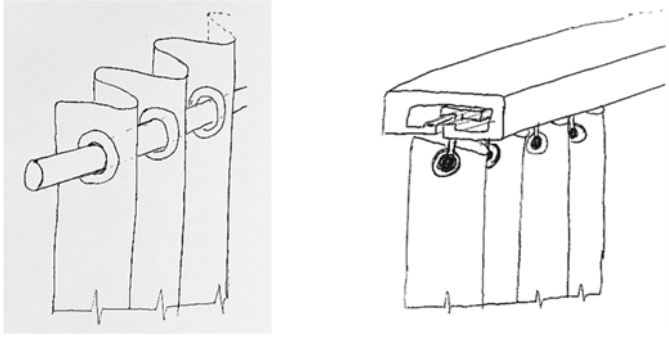

a) b)

Figure 2. *Horizontal moving direction classes*

Cost-effect solution kept in mind, the designed construction become steel wire rope with metal hoops and plastic sliders [7]. Compared to the sliding track, the rod material is 50 percent cheaper, while compared to the rod material, the steel wire together with the tensioners turned out to be financially more favourable. Figure 3 shows sheet metal consoles on the wall and the steel wire rope solution. The consoles were designed by 3D software Autodesk Inventor and was produced by 3 mm steel material and production by the company AR-Robotics in Debrecen. The consoles were fixed with concrete dowel screws because the columns are made of reinforced concrete. The sheet metals included extra holes, because of the iron shank in the concrete column and other connecting elements.

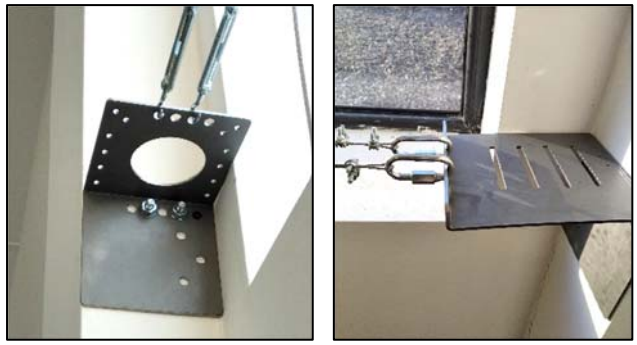

Figure 3. *Steel wire with tensioners and the consoles on the wall*

Figure 4. *First prototype with weight representation*

First prototype was built in laboratory at the Institute of Machine Tools and Mechatronics. In this case consoles were fixed at the other direction on the wall, because of the possibilities. It is a difference between the first prototype and the final structure. Sacks filled with salt were hung at the bottom of the curtain strip, which were represented the weight of the 2.3 meters vertical-long curtain, it is shown in Figure 4. This prototype was 'two side closing' layout due to the centrally located fire safety window-part. In fire-case, this layout is the most fastest opening way.
At the 'one wire solution' was necessary to support it in the middle, because otherwise it would hang too much, furthermore the two curtain sides must overlap. Figure 5 included two used consoles in the middle. The left one is made of aluminium profile with a rectangular cross-section with two fixed screws. In this case the one wire was hung on screws, its benefit is the quick installation. The right one is built from three holed steel L-profile, this solution was not required a custom manufacturing, but the wire was threaded into holes.

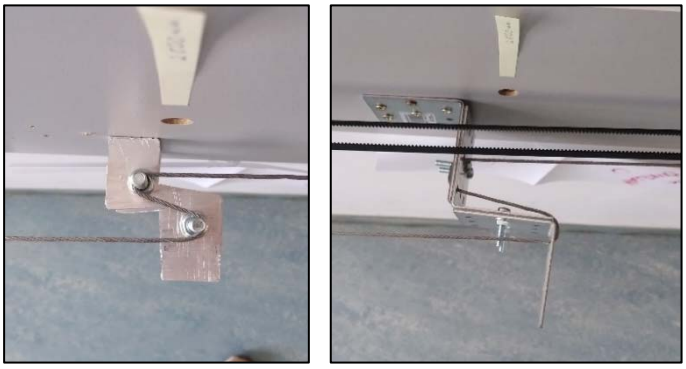

Figure 5. *Wire support in the middle and the overlapping*

Taking additional options and simplicity into account, at the end, there were used the 'two wire solution'. It gave a simple holder in the middle and some extra holes on the end-consoles. One extra steel wire tensioner was acceptable for cost-effect solution.
Automatization of the opening and closing can be solved by controlled electric motor. This motor could rotate a drum and pull rope, its needed pulley and appropriate rope fixing and way. Figure 6 presents an example for it. It is known that the motor can be installed by its own weight stretching the rope. On the other hand, we can build a space-saving solution with stretched ribbed belt.

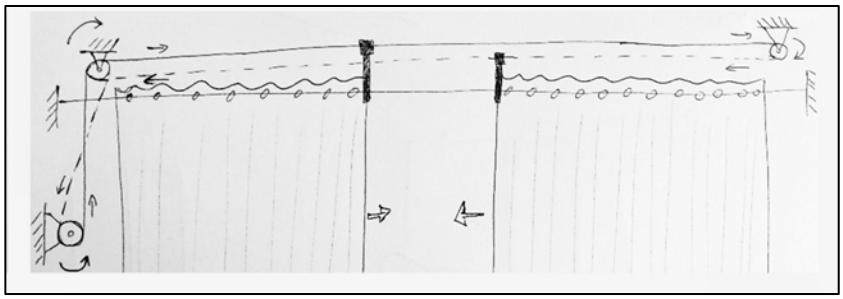

Figure 6. *Curtain moving by motor with drum, pulley and rope*

The pulling with ribbed belt contact with the electric motor shaft via rib wheel, on the opposite side we can create a ribbed belt stretching structure on the consol. Figure 7 present this structure made by Bosch-profile with groove nuts, fixing screws, threaded stem, ribbed idler element, and an extra perpendicular aluminium part. The ribbed idler is rotating free, the groove nuts can slide in the groove. Stepless tensioning is achieved by the threaded stem in the threaded aluminium element with locknuts.

Figure 7. *Stretching structure of ribbed belt*

It is needed to note, compared to the prototype built at the department, in the case of the finally installed version rotated by 90 degrees, such a tension could be achieved with the steel ropes that it was not necessary to fix them in the middle, and the overlap was realized with two steel ropes. During the tests, it was found that the aluminium hoops dragged on the steel rope wear out, so a towing hoop

made of wear-resistant plastic rod was applied with the help of a quick connector. This from and connection element shown in Figure 8.

Figure 8. *Wear-resistant plastic and connection between the rope and belt*

3. MOTOR SELECTION

During the building of prototype were tested four different direct current motors. As Figure 9 shows the first was an 12V DC motor without gearbox. Rib wheel was fixed on the shaft by a fixing screw. This motor was proved to be underpowered. The next DC motor was a windscreen wiper motor, because of enough power. At the same time was tested the third motor, which were moved electric controlled window of car. Both turned out good power to moving the automatic curtain, but due to the availability and validity of the warranty, a fourth solution was created.

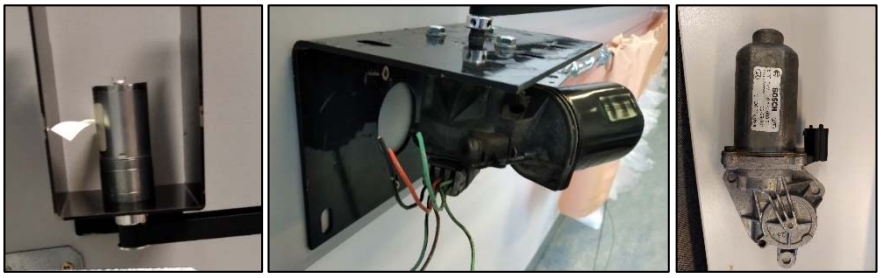

Figure 9. *Tested direct current electric motors*

Since there was looking for the right power, the ability to change the direction of rotation and the right gear ratio, the installation of a hand drill proved to be an obvious solution. Thus, the customer purchased five PARKSIDE brand hand drills. This drill has a threaded connection, which were suitable for attaching an

extra pliers. There was designed next sheet metal component to fixing the drill used this connection opportunity. Furthermore, the starter switch and the direction change handle were electrically wired out.
Next testing period focused on accuracy, repeatability, and operational stability. The conclusions of tests were as follows: reduce the distance between the ribbed belt and steel rope; curtain-dragging carriage to build higher. Moreover, it was necessary to put a bearing on the shaft of the rotating rib wheel, because it was bent due to the tension of ribbed belt.
Figure 10 shows the fixed hand drill by thread connection place, wired out electric points, tensioned ribbed belt and tensioned steel rope.

Figure 10. *Application of hand drill with ribbed belt and wired out electric points*

There were two ideas for put a bearing onto the shaft of the rotating rib wheel. One of them is a turned element, the other one is building a structure by sheet metal parts. It was chosen sheet metal structure because manufacturer of this project was suggested a solution, which is shown in Figure 11. The shaft diameter was caused by the parameter of rib wheel, it was necessary to have chamfer for the fixing screw. On this shaft could put the bearings. Position of bearings determined by height and width of sheet metal.
Accuracy of fitting is ensured by laser-cutting of sheet metal, which punctuality is 0.1 mm. The bearing SKF 608 has 7 mm width, it could be achieved by 3+1.5+3 mm metals; 8 mm inside diameter, it is enough for the shaft; and 22 mm outside diameter, it is possible to produce by laser cutting.

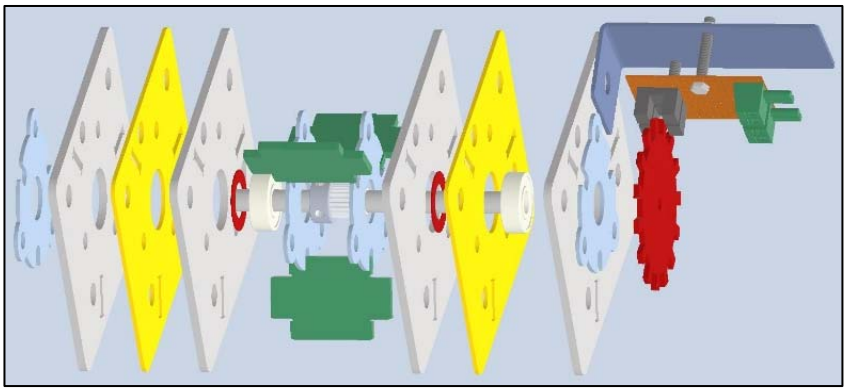

Figure 11. *Bearing and speed measurement*

Assembly process is as follows. Put the bearing (colour white) into the fixed sheet metals, fixing the sheet metals (colour grey, yellow and grey) by plates (colour blue) and screws. Put the rib wheel onto the shaft, fix by screw. Put the fixed bearings onto ends of shaft. Take spacer plates (colour green) into and between fixed sheet metals. Use long through screw to fixing sides. Applicate this structure on the consoles.
After it is possible to put up the optical speed measuring part, which included two opto-gate and one encoder dial. The encoder dial could be fixed with threaded nut onto the shaft.

4. MOVING CONTROL

The automatic curtain is open by default, the idea of control process is as follows. When the customer gives a signal of closing task via Ethernet, which included slow or fast motion. Arduino Uno receives the signal and interprets it, gives a command to the H-bridge with PWM and logical high and low signal pairs. It will cause an intermittent supply voltage corresponding to the speed and well direction of rotation.
At the same time, two opto-gate give to microcontroller a square wave signal arriving with a phase difference. So, the controller could check the speed and intervene if necessary. Figure 12 shows the system of microcontroller, sensors, and actuators. It can be seen, there are sensors for case of closed, case of opened and case of fire. Opening and closing processes work until the respective sensors are switched on.

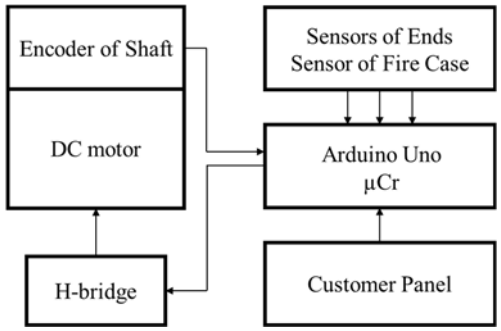

Figure 12. *System of microcontroller, sensors and actuators*

In fire case, the middle part of window automatically starts opening by a linear direct current motor. There is only 800 msec to react this opening signal by the curtain moving controller. At the right side of Figure 13 shown a test circuit and program for Arduino Uno, which fulfilled the control tasks. At the left side of figure can be seen a validated hand drill with motor control h-bridge. It is worth noting that the end-switches had to be placed further away from the wall consoles, so that in the case of fast moving, overrunning due to momentum would not cause a problem.

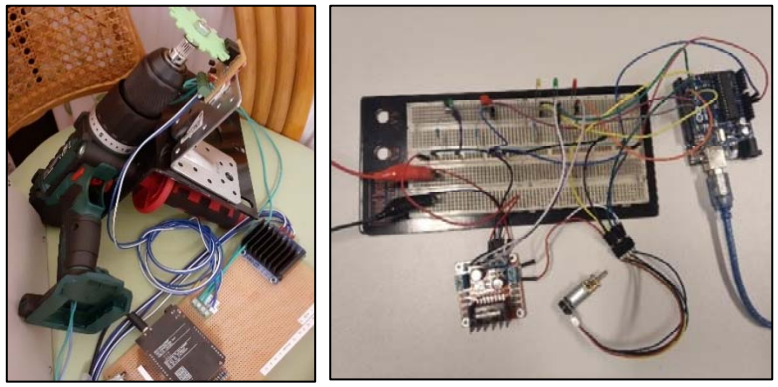

Figure 13. *Validation of electrical circuit and Uno programming*

5. SUMMARY

This paper deals with design and prototype an automatic curtain moving system. It says about how was chosen technique of sliding structure, designed and manufactured sheet metal elements, test circuit of microcontroller, sensors and controlled direct current motor. Here was presented choice of respective electric

motor. There were designed own sheet metal structure for bearings, furthermore a system of opto-gate with dial-plate for works as encoder. The presented system is suitable for opening with a sufficiently fast reaction in the event of a fire

ACKNOLEDGEMENT

This research was supported by company of AR-Robotics Ltd. in Debrecen and volunteers from Faith Church Miskolc.

REFERENCES

[1] Milinkovic, O. et al. (2017). Multi-criteria decision-based approach to selecting the type of industrial halls used in food industry, *Ekonomika Poljoprivrede*, Vol. 64, No. 1, ISSN 2334-8453 (online), https://doi.org/10.5937/ekoPolj1701081M.

[2] Lin, C. et al. (2022). Revealing the sound insulation capacities of TPMS sandwich panels, *Journal of Sound and Vibration*, Vol. 540, ISSN 1095-8568, https://doi.org/10.1016/j.jsv.2022.117303.

[3] Kang, L. et al. (2022). Mechanical and vibro-acoustic performance of sandwich panel with perforated honeycomb cores, *The Journal of the Acoustical Society of America*, Vol. 152, No. 3, ISSN 0001-4966, https://doi.org/10.1121/10.0013997.

[4] Pieren, R. et al. (2018). Sound absorption of textile curtains - Theoretical models and validations by experiments and simulations, *Textile Research Journal* Vol. 88, No. 1, ISSN: 1746-7748 (online), https://doi.org/10.1177/0040517516673337.

[5] Fang, D. (2001). A study of the U-factor of a window with a cloth curtain, *Applied Thermal Engineering*, Vol. 21, No. 5, ISSN 1359-4311, https://doi.org/10.1016/S1359-4311(00)00071-5.

[6] Hamida, H. – Alshibani, A. (2021). A multi-criteria decision-making model for selecting curtain wall systems in office buildings, *Journal of Engineering Design and Technology*, Vol. 19, No. 4, ISSN 1726-0531, https://doi.org/10.1108/JEDT-04-2020-0154.

[7] Onur, Y. A. (2019). Theoretical investigation of rope strand subjected to axial tensile load, *International Review of Applied Sciences and Engineering*, Vol. 10, No. 2, ISSN 2062-0810, http://doi.org/10.1556/1848.2019.0017.

Design of Machines and Structures, Vol. 12, No. 1 (2022), pp. 96–102.
https://doi.org/10.32972/dms.2022.018

DESIGN OF A FORCE MEASURING UNIT FOR ROBOTIC APPLICATIONS

LÁSZLÓ RÓNAI

University of Miskolc, Institute of Machine Tools and Mechatronics
H-3515, Miskolc-Egyetemváros
ronai.laszlo@uni-miskolc.hu
https://orcid.org/0000-0002-1717-1493

Abstract: The paper deals with design process of a force measuring unit, which is capable to mount onto a robot or to integrate into a measuring device. The main element is a beam type load cell equipped with strain gauges in Wheatstone bridge configuration. In order to measure the force only in one direction a linear guide rail is used to lock the degrees of freedom. The unit will have a microcontroller board to process and transfer the data to a personal computer. Furthermore, the system will be capable to intervene processes thanks to the digital inputs and outputs of the electric board. The paper introduces the 3D model of the device, and its components.

Keywords: *load cell, linear guide rail, force measurement*

1. INTRODUCTION

Nowadays measuring and data acquisition is an important tool to investigate a phenomenon of a process or make sure of the correctness of operations, e.g., at industrial environment. Force measurement is required in many fields, e.g., hydraulics, pneumatics, robotics etc.
In robotics there are commercially available force and torque sensors, which can give feedback on the forces during the process [1], but they are expensive and most of them cannot ensure flexible programming capability to make the robot intelligent. Several publications deal with the development of special purpose robotic end-effectors, which consist of force sensors to measure the force of a specific process. In [2] a self-developed end-effector containing flexible element equipped with strain gauges is developed, which is suitable for polishing process performing with industrial robot. The unit includes a 6-axis force/torque sensor. A low cost 6 axis capacitor-based force sensor is developed in [3], which can be suitable for robotic applications especially at human-robot interactions.

Not only for industrial robotics, but also for other fields, force measuring can be necessary, e.g., in [4] a self-devised low cost, modular 3 degree of freedom (DOF) force sensing unit is investigated, which serves wrist rehabilitation purposes. The authors used beam type load cells equipped with HX711 Analog/Digital converter unit.
The main aim of this paper is to develop a force measuring unit, which can be integrated into a robotic cell or a special purpose testing device. Previously another version of the unit was designed and manufactured, which was mounted onto an industrial robot to serve force measurements during assembling tasks [5]. The unit had two thin sheet metals [6] to prevent the unwanted force components. The new device will have linear guide rail instead of sheet metals.
The remainder of this paper is organized as follows. Section 2 introduces the sketch of the planned force measuring unit with its main elements. Furthermore, the necessary requirements of the measurement unit are also detailed in this Section. The 3D model of the device is introduced in Section 3. The concluding remarks and the plans for the future are given in the last Section.

2. REQUIREMENTS AND SCHEMATIC PRESENTATION OF THE UNIT

The main goal is to develop a force measurement unit, which can be used in robotics and other fields. The system would be capable to intervene in processes depending on the measuring task. Therefore, an ATmega328 based microcontroller (μC) is placed to provide the decision capability of the system. An HX711 24-bit resolution analogue-digital (A/D) module is integrated to transform the bridge voltage of the load cell to digital data.
Necessary hardware and software demands of the measuring system can be formulated, which are the following:

- Overload protection needs to be solved.
- Provide an opportunity to save the measured force values for post processing.
- The system must be reprogrammable depending on the measurement task to be performed.
- Existence of intervention in processes.
- The structure should be compact and lightweight.
- Assembling and disassembling should be not complicated.
- Provide a 1-way force measurement.

A robotic intelligent end-effector, which is capable to use it during assembling tasks was previously developed [7] and it was used with an industrial robot to perform an intelligent assembling operation [5].

The system to be developed contains the same aluminium alloy beam type load cell, which has 200 N capacity. The data of the load cell can be seen in Table 1. The main difference between the previously developed and current device is the elimination technique of the unwanted force components. The current system will use a linear guide rail unit to lock the DOF. The type of the unit is a MGN12H 12 mm with a linear carriage. The scheme of the system can be seen in Figure 1.
A pneumatically actuated Gimatic GS25 gripper will be mounted to make the availability of grasping.

Table 1
Specification of the load cell

	Value
Dimensions (LxWxH)	80 mm x 12.7 mm x 12.7 mm
Capacity	200 N
Safe overload	~240 N
Hysteresis	0.03 %
Excitation voltage	5 V
Number of strain gauges	4
Range of the operating temperature	-20°C–65°C

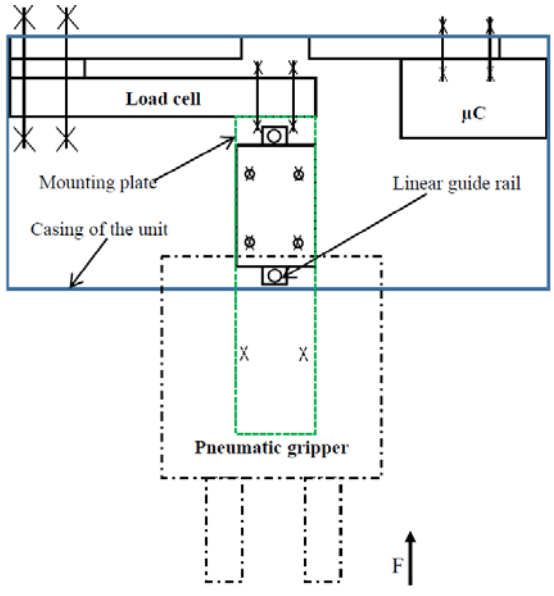

Figure 1. *Scheme of the measuring unit*

3. DESIGN PROCESS OF THE UNIT

The modelling of the system is performed in the Autodesk Inventor Professional 2018 software. The 3D model of the system is shown in Figure 2 and Figure 3, respectively. The main elements of the unit according to Figure 2 and Figure 3 are the following: 1) Mounting plate; 2) Load transferring elements; 3) Electronics board; 4) Pneumatic gripper; 5) Connection element; 6) Load cell; 7) Overload protection; 8) Linear guide rail with the carriage.

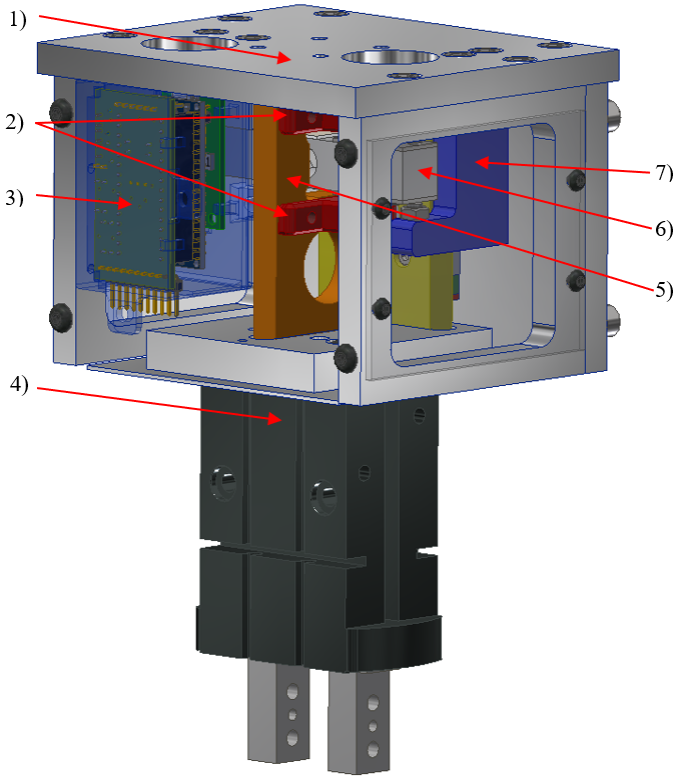

Figure 2. *The 3D model of the system 1*

The electronics of the system consists of an ATmega328 microcontroller-based Arduino Nano development platform, the HX711 A/D converter, and a special purpose board, which contains optocoupler units for voltage levelling. The electronics of the unit will get a self-devised 3D printed casing. The overload protection is ensured by a horseshoe shaped element, which was introduced in the previous system [7]. It has set screws to adjust the limit force of the load cell.

A connection element is necessary in order to join the gripper with the carriage and to design the connections of the load transferring elements, and the overload protection element.

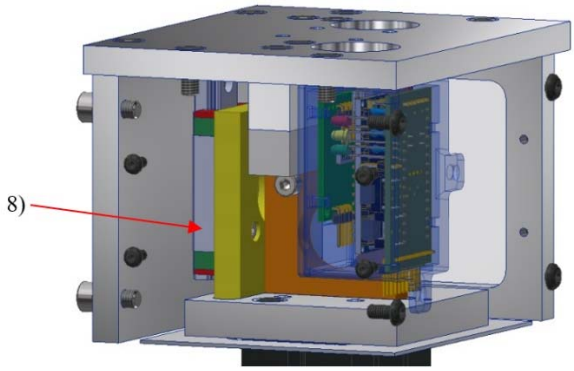

Figure 3. *The 3D model of the system 2*

The drawing of the connection element with the dimensions can be seen in Figure 4. The element will be manufactured from aluminium. In order to fulfil the requirements of the measuring unit, weight reduction is performed. Bores are placed to connect the load transferring elements and to mount the connection element to the carriage with the gripper and its mounting plate.

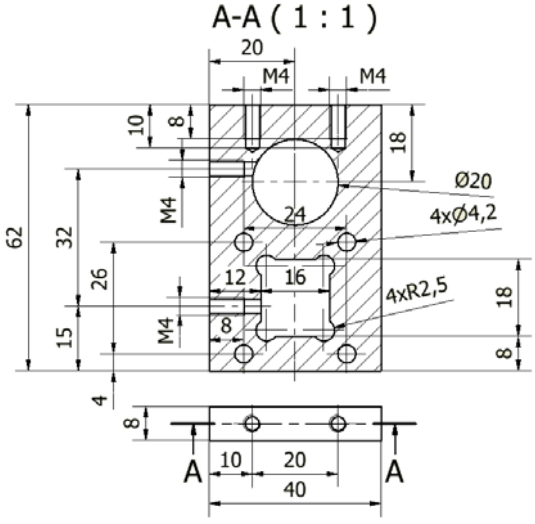

Figure 4. *Technical drawing of the connection element*

The load cell will contain two steel plates (see Figure 5), which prevent the set screws of the overload protection element and the set screws on the load transfer element from being pushed into the aluminium beam. The ends of the set screws of the load transfer element will be machined to cone.

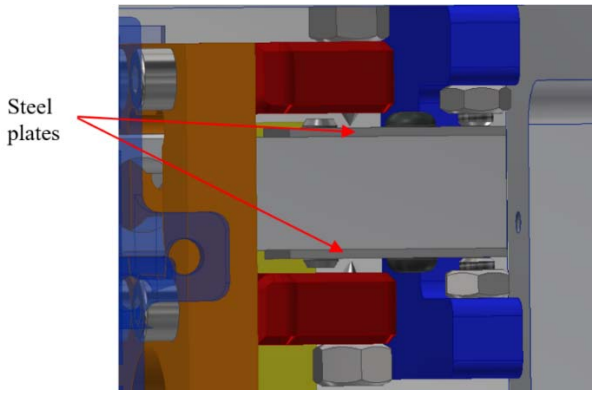

Figure 5. *Load transferring elements and the overload protection*

Since the load cell has 0.1063 mm elastic deflection at 200 N load [6], precise adjustment of the screws is essential.

4. SUMMARY

A force measuring unit was designed, which is capable to use in robotic applications or in test systems to perform force measurements. The 3D model was created in Autodesk Inventor Professional software. In addition to force measurements, the unit will also be suitable for intervention since the electronics panel includes both digital outputs and inputs with optocouplers.
In the future the system will be manufactured and integrated to a Rexroth compact module in order to perform force measurements.

REFERENCES

[1] Loske, J. – Biesenbach, R. (2014). Force-torque sensor integration in industrial robot control, *15th International Workshop on Research and Education in Mechatronics (REM)*, ISBN 978-1-4799-3029-6, http://doi.org/10.1109/REM.2014.6920241.

[2] Ren, C. et al. (2016). Theoretical analysis of a six-axis force/torque sensor with overload protection for polishing robot, *23rd International Conference on Mechatronics and Machine Vision in Practice (M2VIP)*, ISBN 978-1-5090-2764-4, http://doi.org/10.1109/M2VIP.2016.7827338.

[3] He, Z.; Liu, T. (2021). Design of a three-dimensional capacitor-based six-axis force sensor for human-robot interaction, *Sensors and Actuators A: Physical*, Vol. 331, Article ID 112939, ISSN 0924-4247, http://doi.org/10.1016/j.sna.2021.112939.

[4] Mayetin, U. – Kucuk, S. (2021). A low cost 3-DOF force sensing unit design for wrist rehabilitation robots, *Mechatronics*, Vol. 78, Article ID 102623, ISSN 0957-4158, http://doi.org/10.1016/j.mechatronics.2021.102623.

[5] Rónai, L. – Szabó, T. (2020). Modeling and Robotic Handling of a Snap-Fitting Box Buckle, *Pollack Periodica*, Vol. 15, No. 2, ISSN 1788-1994, http://doi.org/10.1556/606.2020.15.2.9.

[6] Rónai, L. (2018). Design Aspects of a Robotic End-effector, *Design of Machines and Structures*, Vol. 8, No. 2, ISSN 2064-7522 (online).

[7] Rónai, L. – Szabó, T. (2019). Intelligens robotmegfogó fejlesztése, *Multidiszciplináris tudományok*, Vol. 9, No. 4, ISSN: 2786-1465 (online), https://doi.org/10.35925/j.multi.2019.4.40.

Design of Machines and Structures, Vol. 12, No. 1 (2022), pp. 103–109.
https://doi.org/10.32972/dms.2022.019

LASER INTERFEROMETRIC MEASUREMENT OF MACHINE TOOLS

LÁSZLÓ RÓNAI[1] – JÓZSEF LÉNÁRT[2]

University of Miskolc, Institute of Machine Tools and Mechatronics
H-3515, Miskolc-Egyetemváros
[1]ronai.laszlo@uni-miskolc.hu, [2]lenart.jozsef@uni-miskolc.hu
[1]https://orcid.org/0000-0002-1717-1493, [2]https://orcid.org/0000-0002-2268-3434

Abstract: This paper deals with a positioning accuracy measurement on a machine tool to perform calibration. The principle of laser interferometric measurement is introduced, a Renishaw XL-80 laser interferometer is applied to perform measurements. The methodology of using the system is presented through a practical measurement. The deviations in certain positions are determined, thus the pitch error table of the machine tool can be refreshed. Thereafter a test running is performed in order to check the accuracy of the machining centre.

Keywords: *laser interferometer, backlash, positioning accuracy*

1. INTRODUCTION

Nowadays the production of dimensionally accurate workpieces is indispensable [1]. This aspect can be provided by the use of numerically controlled machine tools. These machines, e.g., milling station or turning machine can provide the production of high precision parts. However, after a certain period of operation, the machines need to be checked, calibrated. Since there are many parameters, which have an effect on the accuracy of a machine tool, e.g., heat, lubricants, vibrations etc., therefore planned maintenance is essential.
Lasers (Light amplification by stimulated emission of radiation) are widely used not only in laboratory purposes, but also for industrial measurements. There are several types of lasers, e.g., gas-, solid-state-, fiber-, and semiconductor lasers. Laser interferometers [2–4] are good tools to determine the positioning accuracy of a machine tool. These devices contain a high monochromatic and coherent laser beam source ensured by stimulated emission, a stabilizer/compensator, and a stationary-, moving mirror.
The main goal of the article is to present the methodology of measuring with a Renishaw XL-80 [5], laser interferometric system. The unit is capable to

communicate with computers through an USB cable in order to establish the possibility of data acquisition. This laser interferometer is applicable in the field of machine tool calibration. A compensation unit called XC-80 is used, which consists of temperature, pressure, and humidity sensors. Aligning the measuring mirrors and the laser head unit requires a great deal of care. The measurement of positioning accuracy of a Mazak VTC-800 machining centre is essential, since the accuracy of recent parts produced on the machine tool was no longer adequate. The axis x to be measured has 3000 mm distance, during the measurement 40 mm position increments are applied.
The paper is organised as follows: Section 2 describes the structure and elements of the measurement. A practical measurement is discussed in Section 3. The positioning error of the Mazak machining centre is measured and analysed. Knowing the deviations, the correction of the error is performed with the pitch error compensation table of the machine. The concluding remarks are given in the last Section.

2. METHODOLOGY OF MEASUREMENTS

Laser interferometric measurements usually contain a laser head unit, a stationary mirror, and a moving mirror as it is shown in Figure 1. The principle of laser interferometer measurements is based on the phenomenon of interference. The moving mirror must be placed on the object to be measured, and then the stationary mirror must be placed in a stable fixed place. Then, the laser beam emitted by the head unit is divided into two parts perpendicular to each other, but with equal intensity, thanks to the beam splitter. Then one laser beam will return to the head unit from the stationary mirror, while the other will return from the moving mirror. The amount of displacement is obtained from the interference of the laser beams arriving from two different paths.

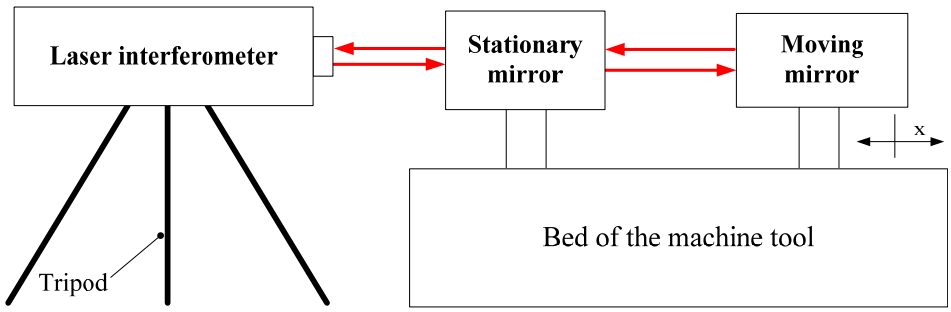

Figure 1. *Scheme of the measurement*

A Renishaw XL-80 laser interferometer (see Figure 2) is used to perform measurements, the specification of the unit can be seen in Table 1. A compensator unit is essential to get accurate measurement data, therefore it consists of intelligent sensors, which can measure the air temperature, the pressure, and the relative humidity [5]. It is a key factor to get precise displacement values in the course of measurement.

Table 1
Specification of the Renishaw XL-80

Name	**Value**
Linear resolution	~1 nm
Range	0-40 m (expandable to 80 m)
Heating up time	< 6 minutes
Compensator unit	XC-80
Dynamic capture rate	50 kHz
Travel velocity	up to 4 m/s

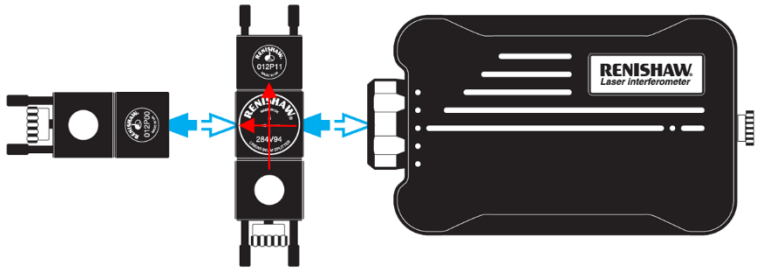

Figure 2. *Renishaw XL-80 interferometer and its mirrors with the directions of the laser beams (Source: XL laser system user guide, Renishaw plc)*

2. 1. Setup of the measurement

Before starting the measurement, the system must be set. Accurate adjustment (see Figure 3) of the measuring system often takes more time than the entire measurement. In order to be able to measure accurately, it is important that the path of the laser beam from the laser unit to the moving mirror and back to the laser head should be coaxial.
Therefore, it is necessary to pay attention to the placement of the units, which can be performed with the help of eye gauge, the XL-80 unit and the optics must be aligned.

After the appropriate placement, turn on the laser to make sure that the laser beam is exactly parallel to the movement to be measured. To check this, caps can be attached to the mirrors, which make the point visible, where the beam reaches the cap. Then, the following steps must be followed:

- targeting the point on the moving mirror with the laser at the far end of the measurement,
- moving the machine (and the moving mirror) to the nearest point of the measurement,
- if the laser beam has moved away from the target area, then readjustment is needed with the set of the appropriate knobs in the proper direction and magnitude,
- check again at the far point and - if necessary - correction.

Once this is done, the system is ready to perform machine calibration.

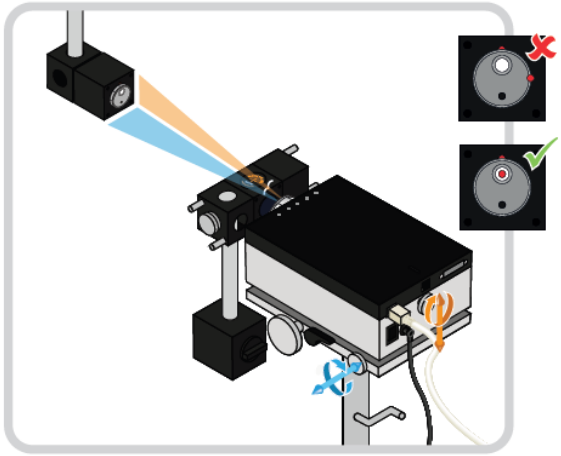

Figure 3. *Adjustment of the laser beam and the mirrors (Source: XL laser system user guide, Renishaw plc)*

3. PERFORMING CALIBRATION ON A MACHINE TOOL

A Mazak VTC-800 machining centre is analysed. The set-up of the measuring system is shown in Figure 4. The positioning accuracy will be determined, and the backlash will be also checked.

The LaserXLTM/Linear Measurement software is used to capture the measurement data. Before measurement several tasks need to be performed. The first-, last targets must be defined, the interval size, measurement type are also important to give. When the measurement is performed in the position increments, the

minimum period halt, stability of reading, tolerance window, and overrun step size must be also necessary, an example is shown in Figure 5. After setup, the measurement can be started.

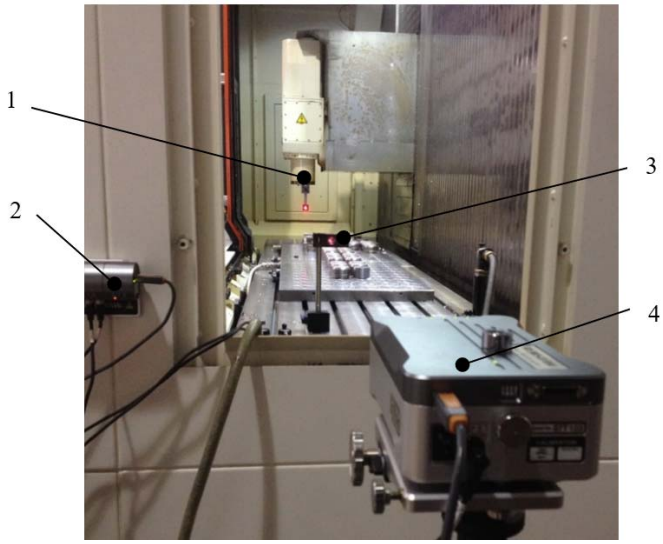

Figure 4. *The set-up of the measurement system: 1 – moving mirror placed on the spindle; 2 – XC-80 compensator; 3 – stationary mirror; 4 – laser interferometer head unit*

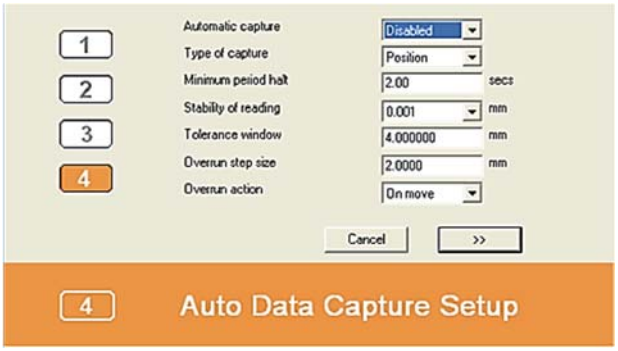

Figure 5. *Fourth step of measurement settings*

The measurement values are displayed and saved in an .rtl file format. Thereafter the Pitch-error table on the machine tool must be filled in with the correction values. A rounded value must be given in microns, e.g., 1 µm, and then the correction

must be checked with another measurement. If the results are worse than they were either changing the sign will solve the problem since the type of transmitter can also determine the measurement or the data form must be changed (incremental, absolute forms).

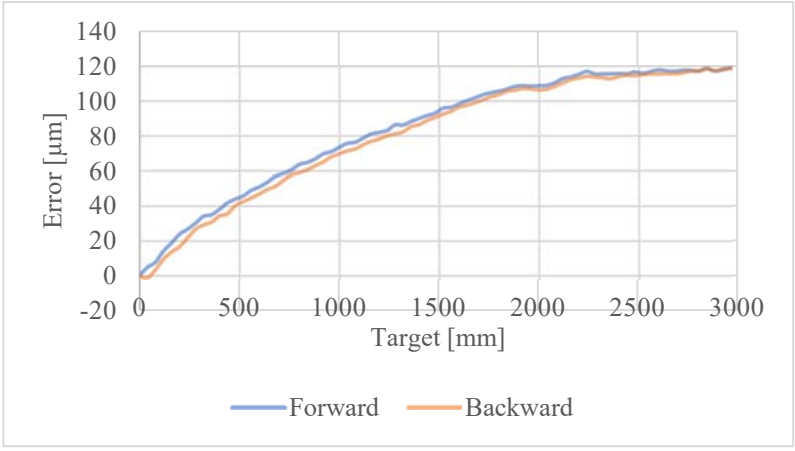

Figure 6. *Measurement result without calibration of the machine tool*

The results of a bidirectional measurement are shown in Figure 6, which is performed on a Mazak VTC-800 machining centre. The deviations of axis x of the machine are measured, 40 mm displacement increment is used. The length of the axis is 3000 mm, the total measurement points are 75.

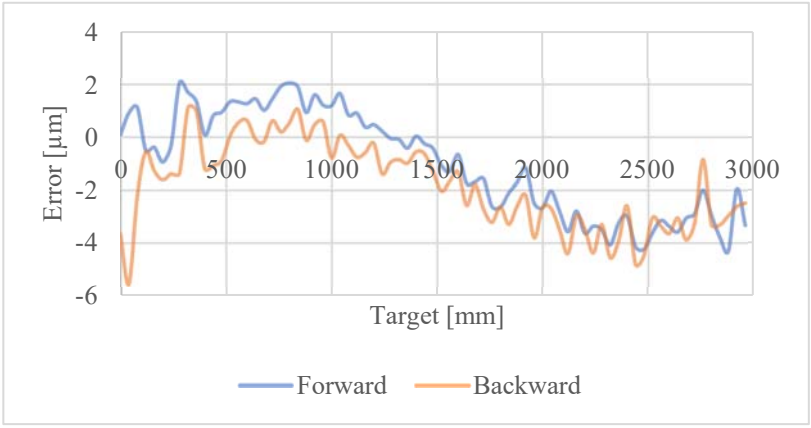

Figure 7. *After calibration*

It can be seen that the machining centre has relatively high deviations (> 100 µm) from the desired positions at the travelling distance of axis x. Therefore, corrections are essential.
After refreshing the pitch error table, a test measurement is performed, which is shown in Figure 7. The bidirectional measurement shows that the deviations became smaller. Thereafter, trial production followed, which showed that the accuracy of the machine tool is satisfactory.

4. SUMMARY

The article dealt with a laser interferometric measurement of a machining centre, which used a Renishaw laser interferometer. The principle of laser interferometry was briefly introduced. The methodology of the measurement was presented. The positioning accuracy of the Mazak VTC-800 machining centre was checked. The results, and quality of the produced workpieces showed that calibration is needed. The correction data was determined and typed to the pitch error table of the control unit. Thereafter test production was performed, which proved to be adequate.

REFERENCES

[1] Marek, J. et al. (2020). *Geometric Accuracy, Volumetric Accuracy and Compensation of CNC Machine Tools: Machine Tools – Design, Research, Application*, ISBN 978-1-83962-351-6, IntechOpen, London, http://doi.org/10.5772/intechopen.92085.

[2] Rónai, L. (2016). Further Development of a Laser Interferometer, *Recent Innovations in Mechatronics*, Vol. 3, No. 1-2, ISSN 2064-9622, http://doi.org/10.17667/riim.2016.1-2/12.

[3] Béres, M. – Paripás, B. (2017). Comparison of Two Laser Interferometric Methods for the Study of Vibrations, In: Jármai, K., Bolló, B. (eds) *Vehicle and Automotive Engineering, Lecture Notes in Mechanical Engineering*, Springer, Cham., ISBN 978-3-319-51188-7, https://doi.org/10.1007/978-3-319-51189-4_20.

[4] Begović, E. et al. (2014). Laser Interferometry – Measurement and Calibration Method for Machine Tools, *3rd Conference "MAINTENANCE 2014" Conference Proceedings*, ISSN 1986-583X.

[5] Slamani M. et al. (2012). Assessment of the positioning performance of an industrial robot, *Industrial Robot*, Vol. 39, No. 1, ISSN 1758-5791, https://doi.org/10.1108/01439911211192501.

Design of Machines and Structures, Vol. 12, No. 1 (2022), pp. 110–119.
https://doi.org/10.32972/dms.2022.020

COMPARISON OF PROGRAMMING ANSYS AND COSMOS/M FINITE ELEMENT SYSTEMS

FERENC JÁNOS SZABÓ

University of Miskolc, Department of Machine and Product Design
H-3515, Miskolc-Egyetemváros
machszf@uni-miskolc.hu
https://orcid.org/0000-0002-6694-8959

Abstract: A simple optimization task is programmed by using the built- in programming possibilities of two finite element systems: ANSYS APDL (Parametric Design Language) and COSMOS/M built-in macro language. The same program is written in the two different programming language and the resulting program listings is compared. The demonstration optimization problem is to find the minimum safe radius of an L-shape model, loaded by a uniform surface pressure. The program to solve this optimization task builds the model, solves the finite element problem, and iteratively improves the radius until the optimum solution. In both cases, when the program running ends, we will see the optimum structure on the screen, and we can use the menu possibilities of the finite element system to see any details of the optimized model or listing the values of the parameters.

Keywords: *programming FEM systems, ANSYS, COSMOS/M, ANSYS APDL, COSMOS Built in macro language*

1. INTRODUCTION

In this paper an optimization problem is solved by using the internal programming possibilities of two different finite element program systems (COSMOS/M and ANSYS). In COSMOS/M system, the internal programming is possible by a macro language, which is similar to FORTRAN, in the ANSYS system this is possible by the APDL. Both these programming languages give the possibility to build the 3D model, mesh it, defining material properties, boundary conditions, loads and solve the finite element task. After the finite element run, in both systems it is possible to access to the displacement and stress solutions (and many more results) and using the IF structures, loops and GOTO structures it is possible to check the availability and safety factor of the structure. If the structure is feasible for the applied load, it is possible to think about the weight reduction or

improve other important characteristic of the structure, which will lead us to the optimization world. In this case it is possible to build up an optimization algorithm and by using this algorithm it is possible to define an optimization process. This complex process (build model- solve FEM task- check the feasibility of the model- change the model, iterate- optimize) can be integrated into one program inside of the finite element system, using the internal programming language and when running this complex problem, this process will be automatically played by the system just like a film, showing the self- improving and self- optimizing process of the model. When the optimum solution is reached, the program will stop showing the optimum solution and we can see any characteristics or results more detailly (stress and displacement contours, value of the parameters used during the running of the program, etc), by using the possibilities given by the menu of the finite element program system.
In the paper the reader can find the listing of both programs, therefore it is possible to compare the most important commands, used for the build-up of the model and for some iterative situations during the optimization process. The conclusion of this comparison could be that the programming languages, keywords and the logic of the commands are very similar, but in some details of the model building one can find some differences, which may need a time to understand or translate. The programming possibility of finite element systems is very useful during the analysis [1], [5], optimization [2], [5], and multidisciplinary optimization [3], [4] of structures.
It is necessary to comment that the CATIA Integrated CAD- FEM system bought the COSMOS/M program system, therefore in order to run the program listing given in this paper, it is necessary to use an earlier version of COSMOS/M, which is dated before this integration.

2. DESCRIPTION OF THE MODEL TO BE OPTIMIZED

The optimization task is to minimize the radius in the corner of an L-shape element (see Figure 1), which is loaded by a pressure of 1.15 MPa and it is supposed to be bonded to a wall at its backside surface (fixed support). The maximum permissible stress in the model can be 56 MPa, this is an implicit constraint of the optimization. 56 MPa will assure that the final result of the optimization is safely inside of the permissible region and it will be easy to test the working of the optimization algorithm. The explicit constraint is that the radius should be between 1 and 10 mm. For simplicity reasons, this optimization task is a one- variable optimization problem, in order to show by very short and easy to understand programming segments, the thinking and programming of the optimization process.

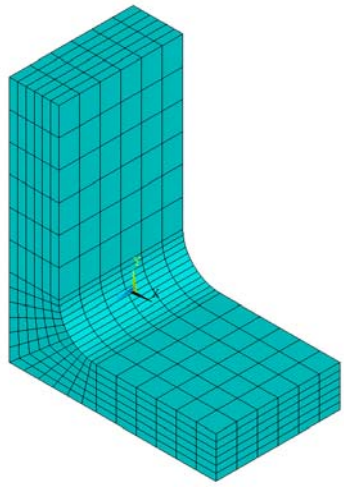

Figure 1. *The model to be optimized*

The model contains two brick shape blocks (a horizontal, towards x direction and a vertical, towards y direction) and in the corner a radius. The horizontal block has a length described by the parameter AA, the vertical one BB. Extrusion towards z direction is CC. The thickness of vertical block is DD and of horizontal block EE. Material of the model is structural steel, the vertical block has fixed support at the backside surface and the horizontal block is loaded in y direction. The program listing of the model in COSMOS/M macro language can be found in Figure 2, and in ANSYS APDL in Figure 3. In the program listings it is possible to identify the numerical values of the parameters.

Both of the program listings show the build- up the model, setting the material data and the boundary conditions of the finite element running (displacement constraint and load), they mesh and solve the model. After the running of these programs, in the memory of the computer there will be ready the displacement and stress results, so it will be possible to read them and check if the structure fulfils the feasibility conditions or not.

Since the optimization is a very simple, one variable minimization problem, the optimum searching algorithm is also very simple. Starting from a 'big' enough radius (for example 9 mm) which gives feasible structure so the maximum equivalent stress is under the permissible stress (56 MPa), by using a step of 1 mm we decrease the radius step by step and in each step we check the maximum equivalent stress. If this stress is higher than the permissible stress, then the radius is too small and the previous radius was the optimum.

```
PARASSIGN,AA,REAL,0.050
PARASSIGN,BB,REAL,0.060
PARASSIGN,CC,REAL,0.030
PARASSIGN,DD,REAL,0.012
PARASSIGN,EE,REAL,0.010
PARASSIGN,RR,REAL,0.009
PARASSIGN,GG,REAL,AA-DD-RR
PARASSIGN,K1,REAL,0.707107
PT,1,0.0,0.0,0.0
PT,2,AA-GG,0.0,0.0
PT,3,AA,0.0,0.0
PT,4,AA-GG,EE,0.0
PT,5,AA,EE,0.0
PT,6,AA-GG-RR*K1,EE+RR*(1-K1),0.0
PT,7,0.0,EE+RR,0.0
PT,8,DD,EE+RR,0.0
PT,9,0.0,BB,0.0
PT,10,DD,BB,0.0
PT,11,AA-GG,EE+RR,0.0
CRARC,1,4,6,11,RR
CRARC,2,6,8,11,RR
CRLINE,3,1,2
CRLINE,4,1,7
SF4PT,1,2,3,5,4,0
SF2CR,2,1,3,0
SF2CR,3,2,4,0
SF4PT,4,7,8,10,9,0
VLEXTRUDE,1,4,1,Z,CC
M_VL,1,4,1,8,4,4,10,1,1,1
DSF,21,AL,0,21,1
PSF,8,1.15E+06,8,1,1.15E+006,1.15E+006,4
NMERGE,1,1100,1,0.0001,0,0,0
MPROP,1,EX,2.1E+11,EY,2.1E+11,EZ,2.1E+11,GXY,0.8E+11,G&XZ,0.8E+11,GYZ,0.8E+11
MPROP,1,DENS,7850
EGROUP,1,SOLID,0,1,0,0,0,0,0,0
R_CHECK,STATIC
R_STATIC
```

Figure 2. *The program listing in COSMOS/M macro language (build and solve the model)*

```
!!! MODEL TO BE OPTIMIZED
/RGB,INDEX,100,100,100,0
/RGB,INDEX,0,0,0,15
! Isometric view
/VIEW,1,1,1,1
/ANG,1
/REP,FAST
! Define constant parameters
! Units: m, N
ELAST=2E5
NU=0.3
P1=6
P2=8
!!SETUP: element types, material
KEYW,PR_STRUC,1 ! Pref / Struct
/PREP7
ET,1,SOLID185
MPTEMP,1,0
MPDATA,EX,1,,ELAST
MPDATA,PRXY,1,,NU
AA=0.050
BB=0.060
CC=0.030
DD=0.012
EE=0.010
RR=0.009
GG=AA-DD-RR
K1=0.707107
K,1,0.0,0.0,0.0
K,2,AA-GG,0.0,0.0
K,3,AA,0.0,0.0
K,4,AA-GG,EE,0.0
K,5,AA,EE,0.0
K,6,AA-GG-(RR*K1),EE+RR*(1-K1),0.0
K,7,0.0,EE+RR,0.0
K,8,DD,EE+RR,0.0
K,9,0.0,BB,0.0
K,10,DD,BB,0.0
K,11,AA-GG,EE+RR,0.0
LARC,4,6,11,RR
LARC,6,8,11,RR
L,1,2
L,1,7
L,1,6
L,7,8
L,2,4
L,2,3
L,3,5
L,4,5
L,7,9
L,8,10
L,9,10
AL,3,7,1,5
AL,5,2,6,4
A,2,3,5,4
A,7,8,10,9
VEXT,1,4,1,,,CC
*DO,III,3,13
LESIZE,III,,,6
*ENDDO
*DO,III,18,21
LESIZE,III,,,6
*ENDDO
LESIZE,25,,,6
LESIZE,26,,,6
LESIZE,30,,,6
LESIZE,31,,,6
LESIZE,36,,,6
VMESH,1,4,1
DA,21,ALL,0
SFA,17,1,PRES,1.15e+06
FINISH
/SOL
SOLVE
/POST1
PLNSOL,S,Y,2,1.0
```

Figure 3. *Program listing in ANSYS APDL (build and solve the model)*

If the equivalent stress is smaller as the permissible stress, it means that the structure is feasible and the radius can be decreased by 1 mm as the next step. In the case when the equivalent stress is equal to the permissible stress, this means that this is the optimum radius. When the optimum is reached, the program will delete

the model and build it and solve it once more for the optimum radius and it will stop showing the optimum structure. Applying the menu possibilities of the finite element system, it is possible to see the stress and displacement contours or list the values of the parameters, in order to check all the results of the running process.

In order to perform the optimization process, a main program is necessary, controlling every step of the search and setting the actual values for the parameters and calling the model building program segment (newana). This main program is shown in Figure 4. Figure 5 and Figure 6 show the stress contours in both of finite element systems.

```
ROPT=0.0
MAXITER=8
VONMIS=0.0
VONADM=0.55e+08
LEPES=0.001
RR=0.009
*DO,JJJ,1,MAXITER
/INPUT,C:/Users/ff/Desktop/newana,txt,,,,
*GET,VONMIS,PLNSOL,0,MAX,,
*IF,VONMIS,GT,VONADM,THEN
ROPT=RR+LEPES
RR=ROPT
*ELSEIF,VONMIS,EQ,VONADM,THEN
ROPT=RR
RR=ROPT
*ELSE
RR=RR-LEPES
*ENDIF
*ENDIF
/INPUT,C:/Users/ff/Desktop/töröl,txt,,,,
*ENDDO
RR=ROPT

/INPUT,C:/Users/ff/Desktop/newana,txt,,,,
```

```
PARASSIGN,ROPT,REAL,0.0
PARASSIGN,MAXITER,INT,8
PARASSIGN,VONMISES,REAL,0.0
PARASSIGN,VONADM,REAL,0.55E+08
PARASSIGN,LEPES,REAL,0.001
PARASSIGN,RR,REAL,0.009
#LOOP CIMKE1 MAXITER
FILE,F:\DOKUMENTUMOK\ff\NEWANA.GEO
PARASSIGN,VONMISES,REAL,VON(1|ND|0)
#IF (VONMISES > VONADM)
PARASSIGN,ROPT,REAL,RR+LEPES
#GOTO CIMKE2
#ELSE
#IF (VONMISES == VONADM)
PARASSIGN,ROPT,REAL,RR
#GOTO CIMKE2
#ELSE
PARASSIGN,RR,REAL,RR-LEPES
#ENDIF
#ENDIF
FILE,F:\DOKUMENTUMOK\ff\TOROL.GEO
#LABEL CIMKE1
#LABEL CIMKE2
FILE,F:\DOKUMENTUMOK\ff\TOROL.GEO
PARASSIGN,RR,REAL,ROPT
FILE,F:\DOKUMENTUMOK\ff\NEWANA.GEO
```

Figure 4. *Program listings (main), left ANSYS APDL, right: COSMOS/M macro language*

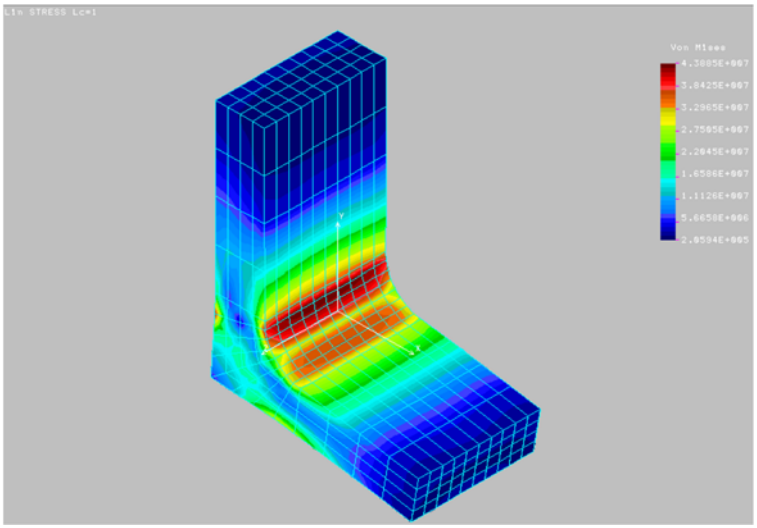

Figure 5. *Stress contours in COSMOS/M*

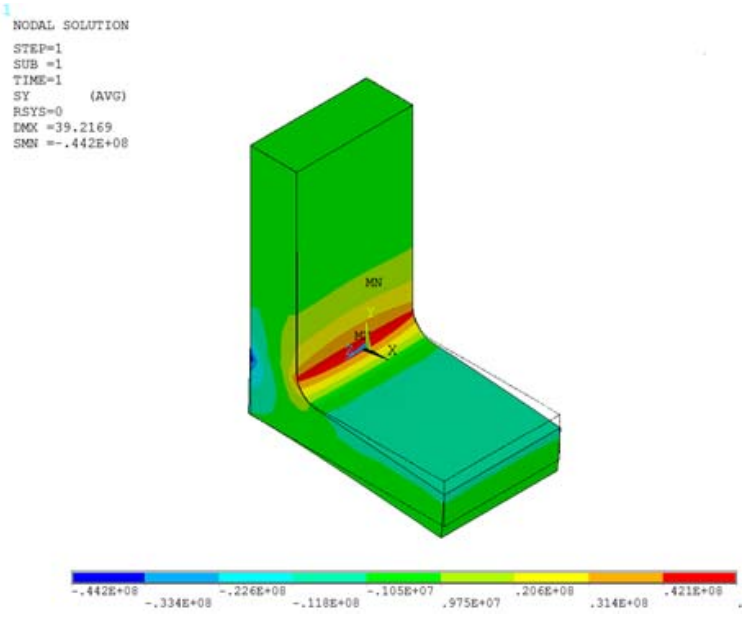

Figure 6. *Stress contours in ANSYS Mechanical*

Figure 5 and Figure 6 show the stress contours on the deformed shape. Figure 7 shows the displacement contours of the optimized model in ANSYS Mechanical finite element system.

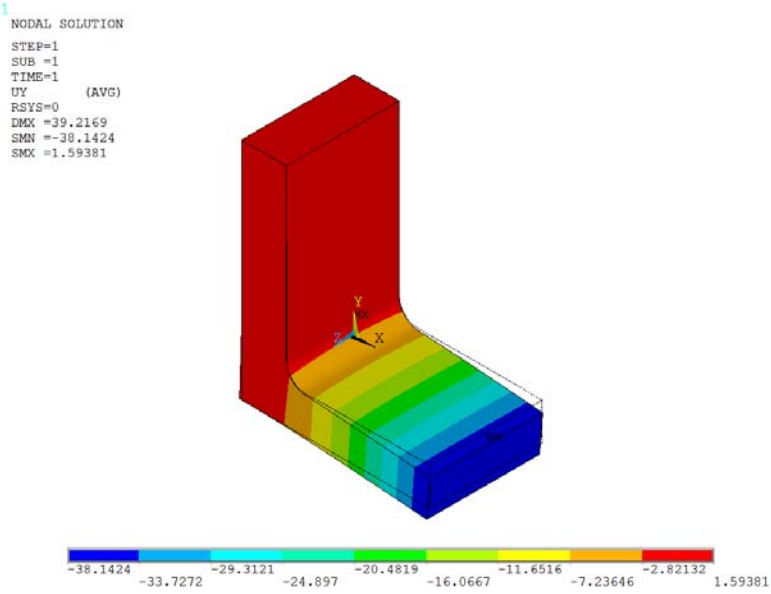

Figure 7. *Displacement contours in ANSYS Mechanical*

3. COMPARISON OF THE PROGRAMS

Comparing the program listings, the first thing what we can conclude is that the ANSYS APDL program is 60 % longer than COSMOS/M macro language program. This is because of more comments, which can help the understanding, and there are some differences concerning the 3D model building keywords and the meshing. The length of the main program is almost the same, ANSYS APDL program is shorter. This is because the COSMOS/M program is using GOTO and LABEL statements, but in the APDL program it was easier to solve the decision-making procedure without GOTO statement. The logic and the syntax of the model building and solution keywords are very similar, easy to understand. All these characteristics make very easy to translate one program into another programming language. The history of these programs is that first the COSMOS/M program was written and later the APDL program was built by translating the macro language commands into APDL commands or into similar commands which can do the required steps. The final results of the optimization are shown

in Table 1. These results are the optimum results in both programs, in COSMOS/M and in ANSYS, too.

Table 1
Optimum results

Param	R_{opt} [mm]	Vonadm [MPa]	Vonmis [MPa]	Step No.
Value	5	56	55.61	5

4. SUMMARY

Optimization problem and its solution is shown for a three-dimensional, L shape element, solved by programming the finite element program systems COSMOS/M and ANSYS Mechanical. In COSMOS/M the built-in macro language is used, in ANSYS the APDL (ANSYS Parametric Design Language) is applied. In both programming language, the full program listing is shown for the optimization process. This program listing contains the model building and finite element solving program segment and the optimum process controlling main program, which calls the model building segment as a subroutine. The optimum design task is a one variable problem with one explicit and one implicit constraint.
Running the programs, when they successfully finish the optimum searching, they stop showing the optimum structure and it is possible to see all the details and parameters by using the menu system of the given program system. Comparing the programs, as a conclusion it is possible to say that the logic and the build- up of the programs is very similar, however it is possible to find some differences during the model building and solution setting commands.

REFERENCES

[1] Szabó, F. J. (2019). Finite element study of rotating elements of a ventilator, *International Review of Mechanical Engineering*, Vol. 13, Nr. 6, ISSN 1970-8734, https://doi.org/10.15866/ireme.v13i6.17145.

[2] Kovács, B. et al. (2001). A generalized shape optimization procedure for the solution of linear partial differential equations with application to multidisciplinary optimization, *Structural and Multidisciplinary Optimization*, Vol. 21, Nr. 4, ISSN 1615-1488 (online), https://doi.org/10.1007/PL00013280.

[3] Szabó, F. J. (2016). Multidisciplinary optimization of journal bearings, using a RVA evolutionary type optimization algorithm, *Acta Polytechnica*

Hungarica, Vol. 13, Nr. 7, ISSN 1785-8860, https://doi.org/10.12700/APH.13.7.2016.7.10.

[4] Szabó, F. J. (2008). Multidisciplinary optimization of a structure with temperature dependent material characteristics, subjected to impact loading, *International Review of Mechanical Engineering*, Vol. 2, Nr. 3, ISSN 1970-8734.

[5] Szabó, F. J. (2008). Finite element analysis and optimization of a car seat under impact loading. In: Jármai, K., Farkas, J. (eds): *Design, Fabrication and Economy of Welded Structures, International Conference Proceedings*, Woodhead Publishing Ltd., ISBN 978-1-904275-28-2.

Design of Machines and Structures, Vol. 12, No. 1 (2022), pp. 120–125.
https://doi.org/10.32972/dms.2022.021

ENGINEERING APPLICATION OF REVERSE ENGINEERING TECHNOLOGY

DÁNIEL TÓTH

University of Miskolc, Department of Machine Tools
H-3515, Miskolc-Egyetemváros
toth.daniel@uni-miskolc.hu
https://orcid.org/0000-0001-8928-4633

Abstract: Scanners operating on the optical principle are devices for recording the physical geometry of bodies suitable for non-contact measurement which work in the visible light range. These use the difference in contrasts and the strength of the reflected light for the measurement, by using the classic triangulation principle. This article focuses on reverse engineering technologies and optical scanning process.

Keywords: *digitization, scanning, optical scanner*

1. INTRODUCTION

The two main units of the optical scanner are the projector and the video camera. The projector projects contrast on the object to be examined by projecting a "light-dark" net consisting of increasingly thin bands. The change of border areas of brightness and contrast grid creates comparison data. The difference between the angle of reflection and incidence gives the extent and shape of the object measured at a given point. Averaging principle based on differences creates data, that is, in contrast to 2-dimensional cameras, measurement results without data distortion can be obtained. The surfaces of the object scanned with bright-dark contrast and the reflected light are recorded by one or more colour digital camera. The resolution of the received image, i.e., the digital copy of the object, changes depending on the CCD, i.e., the imaging chip of the digital camera [1], [2].

2. SCANNING PROCEDURE

The Department of Machine Tools of the University of Miskolc has a Breuckmann Smart Scan 3D-HE type three-dimensional optical scanner, with the help of which it can carry out such scanning tasks [3]. A high-resolution scanner alone does not

guarantee that the obtained point cloud accurately shows every detail of the object to be scanned. It happens that due to the particularity of the object, we receive confusing or incomplete information (noise) from the surface of the object. Professional software are needed for the correction of these. To carry out the reparation with software the Geomagic Studio software can be used well. top-quality Smart Scan 3D-HE mobile scanner can provide high-precision 3D coordinates of any object within seconds [4]. The size of the object can vary within wide limits thanks to different sets of lenses, the device also handles shapes with complex geometry excellently. In addition to recording points with a positional accuracy of even less than a hundredth of a millimetre, the system can also recognize and record the colour of the object in the 3D digital file. The scanner works in the range of visible light and collects information about the surface of objects by non-contact sampling. Its main parts are the camera system which consists of two 5 megapixel cameras each, and the central projector which illuminates the objects. Figure 1 shows the image of the illuminated object.

Figure 1. *Illuminated object*

The central projector projects a continuously thickening contrast grid to the surface which consists of vertical ‘dark’ and ‘light’ lines. The distortion of this light grid on the surface of the scanned object provides information about the appearance of the surface. The distorted light grid is photographed by the two cameras, after which the 3D point cloud is created by the software belonging to the device. The cameras have an exchangeable lens system, with the help of which the size of the field of view can be changed. The images taken one after the other are stitched together by software, so we get a complete 3D image of the body to be scanned. The scanning control and data collection software is Optocat. After the scan, a common section of the images in the field of view of the camera system is

displayed on the computer. The images taken one after the other are placed in the software's own global coordinate system, so they have a different orientation than the recordings of the previous scans. The program therefore does not automatically join the images, this task must be performed ‘manually’. Figure 2 shows the consecutive recordings in the unstitched state.

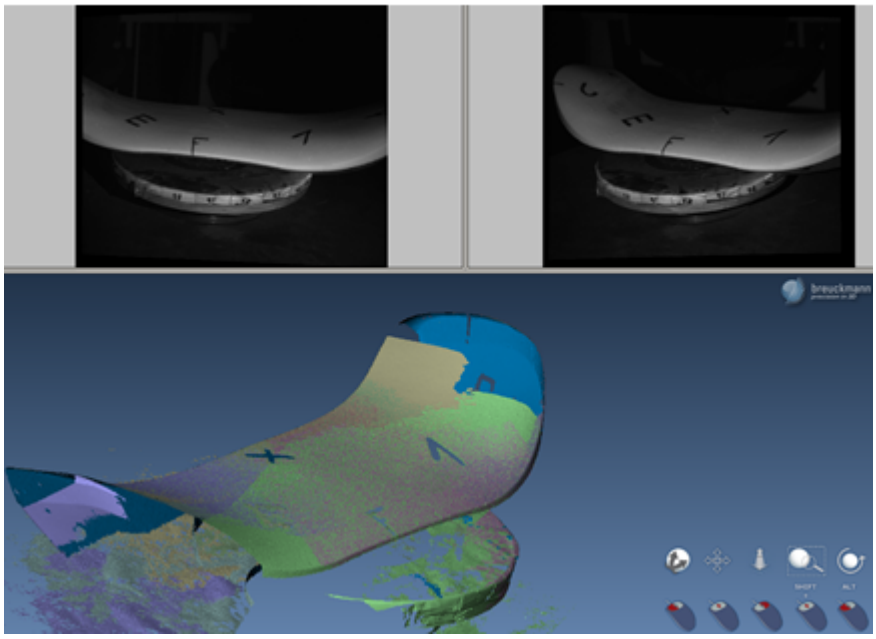

Figure 2. *Scanned objects*

In every case, the more recent pictures must be matched to the previous shots to get the full body model. Stitching is done using markers, as shown in Figure 3.

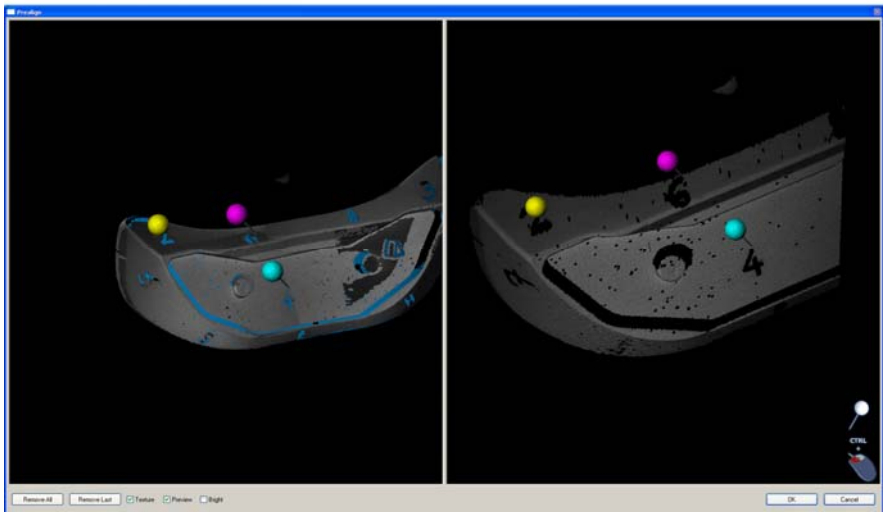

Figure 3. *Connecting 3D objects*

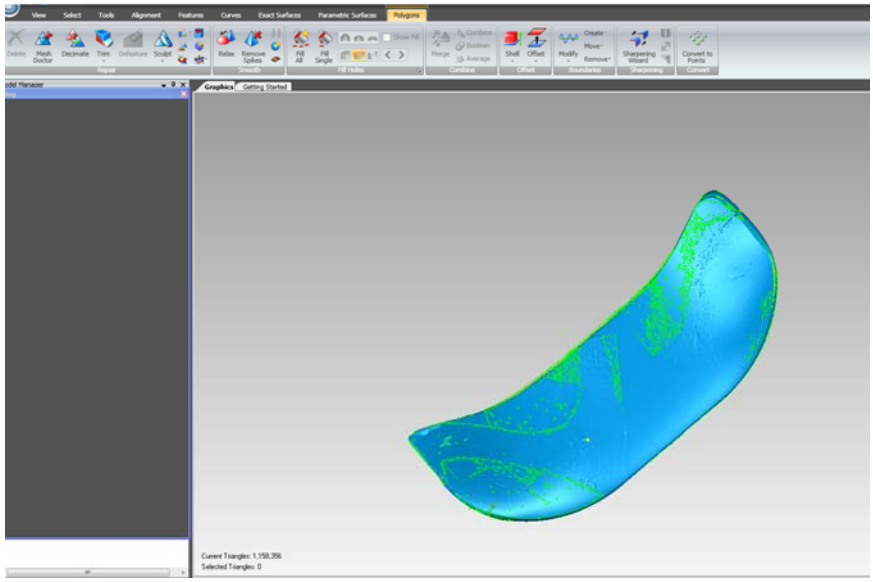

Figure 4. *Correction of model*

The software compares the points in the vicinity of the 'manually' placed markers on the two images (the last scanned part and the previously joined details) and expands the model by assigning the matches to each other. Thus, we get the 3D point cloud corresponding to the entire body. The Geomagic fits surface for the point cloud saved from the Optocat software, in this way the modification and the correction is easier. As it can be seen in Figure 4, with the help of the program, we can remove surface protrusions, unnecessary points, created surface markings and we can eliminate possible continuity gaps.
After this, the corrected model (see Figure 5) saved in a suitable file format can be used for CAD software or RPT technologies.

Figure 5. *Correct model*

3. CONCLUSION

The modern procedure using 3D optical scanning provides an effective tool for size and shape checking, in addition, it can be a good help during finalization of production program and technology objects with complicated surfaces.

ACKNOWLEDGEMENT

The described article was carried out as part of the EFOP-3.6.1-16-2016-00011 "Younger and Renewing University – Innovative Knowledge City – institutional development of the University of Miskolc aiming at intelligent specialisation" project implemented in the framework of the Szechenyi 2020 program. The realization of this project is supported by the European Union, co-financed by the European Social Fund.

REFERENCES

[1] Zhang, Y. (2003). Research into the engineering application of reverse engineering technology, *Journal of Materials Processing Technology*, Vol. 139, Nr. 1-3, ISSN 0924-0136, https://doi.org/10.1016/S0924-0136(03)00513-2.

[2] Patkó, Gy. et al. (2010). A process for establishing the remanent lifetime of rolling element bearings, *XXIV. microCAD International Scientific Conference*, ISBN 9789636619169, Miskolci Egyetem.

[3] Takács, Gy. et al. (2006). Development of Mechatronic Systems at the Institute for Mechatronics at the University of Miskolc, *IEEE International Conference on Mechatronics*, Budapest.

[4] Breuckmann, B. (2003). State of the art of topometric 3D-metrology, In: Grün, A., Kahmen, H. (eds) *Proceedings of the 6. Conference on Optical 3D Measurement Techniques*, Vol.:2, ETH Zürich.

Design of Machines and Structures, Vol. 12, No. 1 (2022), pp. 126–132.
https://doi.org/10.32972/dms.2022.022

INVESTIGATION OF BEARING FAILURES USING VIBRATION ANALYSIS

DÁNIEL TÓTH

University of Miskolc, Department of Machine Tools
H-3515, Miskolc-Egyetemváros
toth.daniel@uni-miskolc.hu
https://orcid.org/0000-0001-8928-4633

Abstract: Bearings are important components of most machinery and their working conditions influence the operation of the entire machinery. Even if bearings are being used under excellent conditions, sooner or later material fatigue will occur. Besides other things poor operating environment contaminated or peculiarly moist areas and improper handling practices cause premature failures. This article focuses on vibration analysis methods for detecting bearing failures and presents a special lifetime test procedure.

Keywords: *bearing, vibration analysis, signal processing*

1. INTRODUCTION

Bearings can be found extensively in domestic- and industrial applications. Bearing failures can cause machine malfunction and even lead to dangerous accidents. In order that prevent these damages, defects should detected as soon as possible. Several methods are used to diagnosis and detection of bearing failures. Investigation of vibration signals is a very important technique for monitoring the condition of machine components [1]. Vibration analysis methods benefit from accurate results and specific information. Vibration signals collected from bearings have detailed information [2]. Different techniques are used to the experimental analysis of bearings.

2. BEARING FAILURES

Almost all bearing defect creates its own characteristic sign. Failures may grouped into secondary and primary ones in many cases. Secondary failures such as cracks and flaking are rooted in primary ones. Primary defects for example smearing, wear, indentations, corrosion, surface distress and the passage of electric current.

A defective bearing usually indicates a combination of primary and secondary failures [3], [4]. Table 1 contains the most common bearing failures and possible causes.

Table 1
Bearing faults and causes [4]

Failure modes with characteristics \ Possible causes			Operating						Environ-mental factor					Lubriction						Mounting								Other						
			Overload	Overspeed	Excessive freq. of load/speed changes	Vibrations	Shaft/housing deflection	Temperature too high/low	Dust and dirt ingress	Water ingress	Electrical leakage	Wrong viscosity	(Consistency) additives selection	Lack of lubricant	Excess of lubricant	Impurities	Incorrect handling (shock loads)	Mounting procedures	Fit too tight	Fit too loose	Tilting/misalignment	Incorrect setting	Incorrect locating (clamping)	Storage	Transportation (vibration/shock)	Bearing selection	Equipment design	Manufacturing concerns	Material concerns
Fatigue		Flaking, spalling, peeling	•				•	•				•	•	•			•	•	•													
		Burnishing, microcracks		•	•	•		•	•	•	•	•	•	•	•	•		•				•		•		•	•			•			•
Wear	Abrasive	Excessive wear		•	•	•	•	•	•	•	•	•	•	•		•			•	•	•	•	•			•				•			•
		Scratches, scores		•	•				•				•			•	•	•							•								
	Adhesive	Seizing marks, smearing	•		•		•	•				•	•	•	•			•	•	•	•					•	•	•	•				
		Hot runners	•	•	•		•	•				•	•	•	•			•	•		•	•	•			•	•	•	•				
Corrosion		Moisture corrosion								•			•			•		•						•	•		•					
		Fretting corrosion	•		•	•	•													•	•	•	•			•	•	•					
		False brinelling			•	•							•							•				•	•	•							
Electrical		Craters, fluting									•																•						
Plastic deformation		Depressions	•				•	•							•		•	•	•		•	•	•	•	•	•	•						•
		Debris indentation							•							•	•	•									•	•					
		Nicks, gouges															•	•										•					
Fracture & cracking		Forced fracture	•	•				•									•	•	•		•	•	•			•	•	•	•				
		Fatigue fracture	•	•	•	•	•													•	•	•	•			•	•	•	•				
		Thermal cracking	•	•	•			•				•		•	•			•	•			•					•						

3. TEST EQUIPMENT

Bearing condition monitoring can be perform by using a test device at laboratory conditions. Such an equipment is located at University of Miskolc, Department of Machine Tools [5]. This device used to execute measurements and fatigue of bearings. Figure 1 shows the test equipment in measuring position.

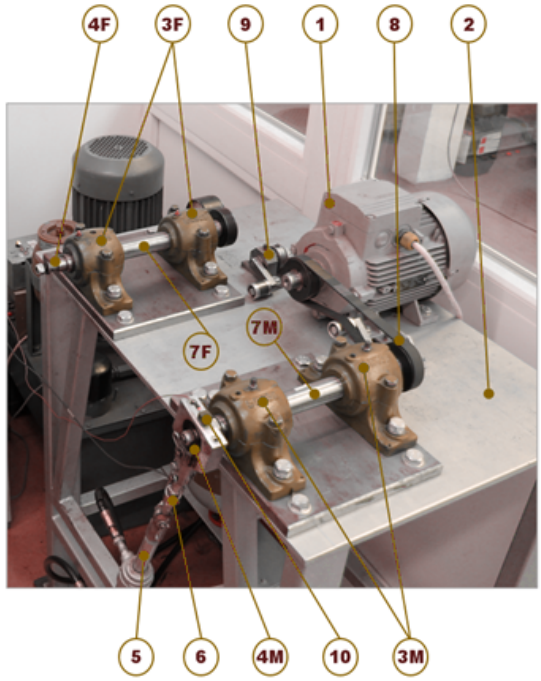

Figure 1. *Bearing test device*

The special symbols have the following meanings:

- 10: piezoelectric vibration accelerometer (Kistler 8632C),
- 9: belt tensioner,
- 8: three-phase motor,
- 7F: fatigue test shaft,
- 7M: measurement test shaft,
- 6: double-acting hydraulic cylinder,
- 5: load cell, the adjustment of hydraulic load,
- 4F: fatigued bearing,
- 4M: measurement position,
- 3F: supporting bearings of fatigue side,
- 3M: special supporting plain bearings of measurement side,
- 2: length ribbed belt,
- 1: rigid table.

During the fatigue cycles the loading shaft (7F) works at the given rotational speed (1500 min^{-1}), while the hydraulic cylinder (6) exerts artificial load (6 kN) for the bearing (4F). The measurements performed after each fixed-term fatigue cycles.

During the measurement cycles the shaft works (7M) at the given rotational speed (1500 min^{-1}), while the hydraulic cylinder (6) exerts artificial load (1 kN) for the examined bearing (4M).

4. EXPERIMENTS AND ANALYSIS

Generally, two proceedings are used experimental analysis of bearings. One method is produced artificial failure(s) on elements of bearings. Another technique is fatigue tests when bearings operate until they get permanent damage. This research focuses on fatigue test of bearings. The above-mentioned bearing test device used to examine 6303-2RS, ball bearing. During the experiments, the vibration patterns measured from bearing using Kistler 8632C, piezoelectric vibration accelerometer. The fixed-term fatigue cycles on average 4 hours long. After each fatigue cycles, vibration signals were taken from the bearing and time-domain tests were done during which stochastic indexes have been calculated. The measurement cycles are performed at 9,6 kHz sampling frequency. Five vibration samples and 16,384 element samples measured within each measuring cycle. During fatigue tests always set on 1500 min^{-1} rotational speed and the equivalent dynamic bearing load is 6000 N. Stochastic features calculated based on sampled values. These indexes computed by a program code, which runs in Maple software. Consequently, the tested bearing (6303-2RS) has near 160 hours lifetime with described data. Peak-to-peak value is a local extreme value in the time signal of the acceleration signal. It is the maximum acceleration in the signal amplitude. Lifetime curve is the temporal dependence of the statistical indexes. Figure 2 shows the change of peak-to-peak value.

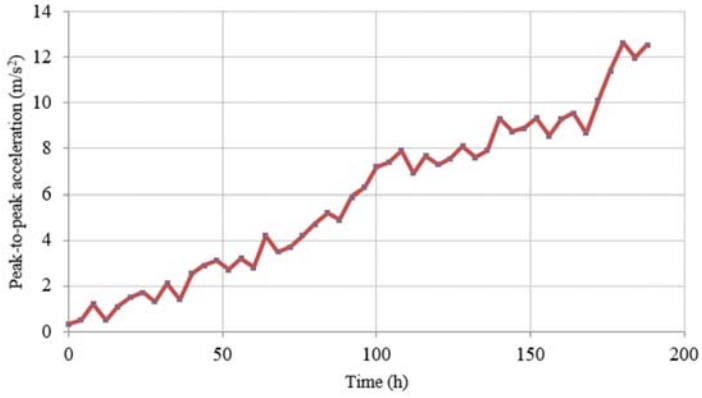

Figure 2. *Lifetime curve of Peak value*

It is visible that the passage of time the acceleration values increased. At be-tween 172 and 188 hours there is a sudden increase in the graph. This might be due to intense bearing exhaustion or the emergence of defects at one of the sur-faces. The Root Mean Square (RMS) history of vibrations is given in Figure 3. The RMS graph seems quite similar to the peak graph.

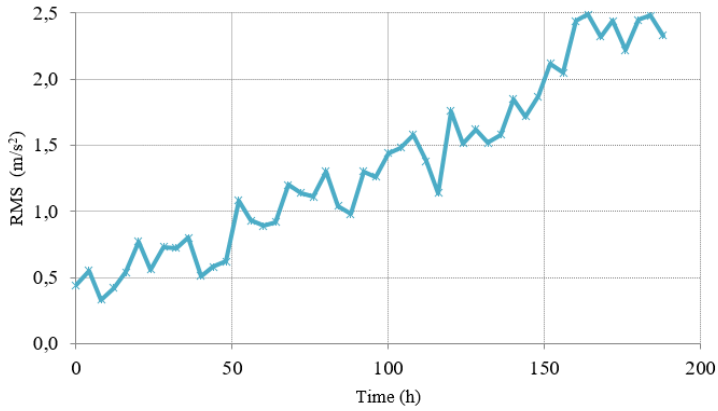

Figure 3. *Lifetime curve of Root Mean Square (RMS)*

Crest factor is one of the scalar measures that used to disclose the faults in bear-ings. If the Crest factor value is more than 5, there might be a fault in ball bearings [6]. Figure 4 shows the Crest factor change. After 140 hours Crest value is above 5.

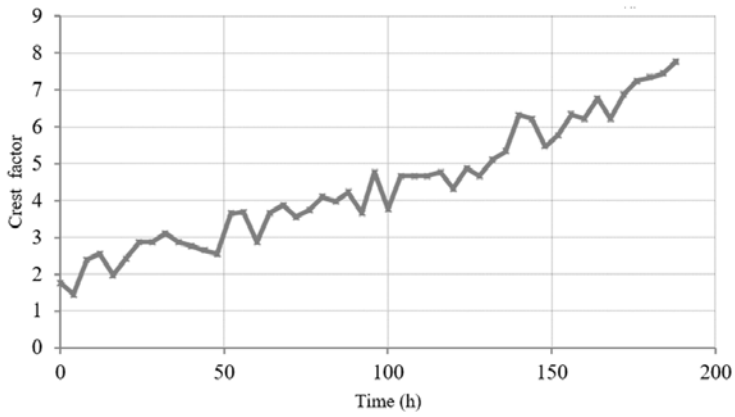

Figure 4. *Lifetime curve of Crest factor*

After the results of the time domain analysis indicated and the bearing noise increased, the bearing was taken apart to pieces. As predicted the time domain analysis after 188 fatigue hours the bearing indeed had a defect. The main reason of bearing failure was the inner ring defect. Figure 5 shows the smeared inside surface.

Figure 5. *Failure of inner ring*

5. CONCLUSION

Vibration based methods are well established for the condition monitoring of bearings, although they are not so effectual in detecting early defects in the bearing. This article shows that vibration analysis methods, especially time domain techniques can perfectly use in condition monitoring of bearings. Statistical analysis methods are accurate tools, and they make possible quick data processing.

ACKNOWLEDGEMENT

The described article was carried out as part of the EFOP-3.6.1-16-2016-00011 "Younger and Renewing University – Innovative Knowledge City – institutional development of the University of Miskolc aiming at intelligent specialisation" project implemented in the framework of the Szechenyi 2020 program. The realization of this project is supported by the European Union, co-financed by the European Social Fund.

REFERENCES

[1] Tóth, D. et al. (2018). Methods for the detection and analysis of bearing failures, *Design of Machines and Structures*, Vol. 8, No. 1, ISSN 2064-7522.

[2] Tóth, D. et al. (2015). Overview of analysis methods of rolling element bearings, *Design of Machines and Structures*, Vol. 5, No. 1, ISSN 2064-7522.

[3] Patkó, Gy. et al. (2010). A process for establishing the remanent lifetime of rolling element bearings, *XXIV. microCAD International Scientific Conference*, ISBN 9789636619169, Miskolci Egyetem.

[4] Tóth, D. et al. (2019). Analysis of methods to detect bearing failures, *7th International Scientific Conference on Advances in Mechanical Engineering*, ISCAME 2019, ISBN 978-963-490-168-6, University of Debrecen.

[5] Takács, Gy. et al. (2006). Development of Mechatronic Systems at the Institute for Mechatronics at the University of Miskolc, *IEEE International Conference on Mechatronics*, Budapest.

[6] Williams, T. et al. (2001). Rolling element bearing diagnostics in run-to-failure lifetime testing, *Mechanical Systems and Signal Processing*, Vol. 15, No. 5, ISSN 0888-3270, https://doi.org/10.1006/mssp.2001.1418.

Design of Machines and Structures, Vol. 12, No. 1 (2022), pp. 133–145.
https://doi.org/10.32972/dms.2022.023

MECHANICAL SIMULATION OF SPRING-BASED TUBE COMPENSATOR

LAURA TRAUTMANN[1] – ATTILA PIROS[2] – KÁROLY SZILÁGYI[3] – BALÁZS KOMÁROMI[4]

[1]Budapest University of Technology and Economics,
Department of Machine and Product Design
H-1111, Budapest, Műegyetem rkp. 3.
[2]John von Neumann University,
Department of Innovative Vehicles and Materials
H-6000, Kecskemét, Izsáki út. 10.
[3]C3D Engineering Consultant Ltd.
H-1106, Budapest, Fehér út 10.,
[4]ESZO Kft.
H-2451, Ercsi, Öreghegyi út 2867 hrsz.
[1]trautmann.laura@gt3.bme.hu, [2]piros.attila@gamf.uni-neumann.hu
[3]szilagyi.karoly@c3d.hu, [4]komaromib@eszokft.hu
[1]https://orcid.org/0000-0001-9230-4949, [2]https://orcid.org/0000-0002-0829-8062

Abstract: This article deals with the examination of a new product family of tube holders. FEA analysis and analytical calculation also provided information on displacements due to force. The article introduces a simplified mathematical model to substitute the complicated numeric simulations. The results have shown that appropriate calculations are accurate and can replace the simulation of fully detailed model.

Keywords: *Tube Compensator, FEA simulation, Displacement*

1. INTRODUCTION

The project described in the article was prepared for the support of ESZO Kft. ESZO Szerelőipari Kereskedelmi és Szolgáltató Kft. was founded in 2006 as a limited liability company. The purpose and activity of the Company are to provide technological tube, steel structure, and machine assembly services for the chemical, oil, energy, and food industry sectors by employing free, valuable, and experienced labour in the Central Hungary region. This information is based on the Product Information Brochure of ESZO Kft. from 2020.

ESZO Kft. has developed its products: spring tube holders. It contains four tube types and nine assemblies of them. There were previous simulations for the tube support and analytical strength calculations of the spring since the spring is essential in these products. It performs the compensation if there is a displacement in the tubing. These calculations gave information about the geometry and the stiffness of the spring; thus, it is known how it will react to the different displacements and with what force it will respond.
The spring is only one part of the product, and there were no calculations for the other parts, however, these are also very informative. Besides these, the available report did not explain the contact goals and places, and the model distribution and the result are also insufficient.
The main question in this research is, how much does the tube holder deform under a specific load? This information about the compensators can help the designers.
The parts of this study were:

- tube holder strength simulation in full detail,
- simplification (geometric transformations),
- simplified analytical calculations,
- design guide.

In order to find these deformities, Finite Element Analysis (FEA) was used, which is usually "used to find stress distribution for complex geometries" [1].

2. METHODS

The compensators are designed to compensate for vertical displacements caused by thermal expansion [2]. Here they can be divided into two main groups: five drawn and four compressed systems.
As a first step, the obtained Solidworks CAD models were converted to STP format by using PTC Creo7, and then the (.asm) Creo assemblies were created in PTC Creo6 (Figure 1).

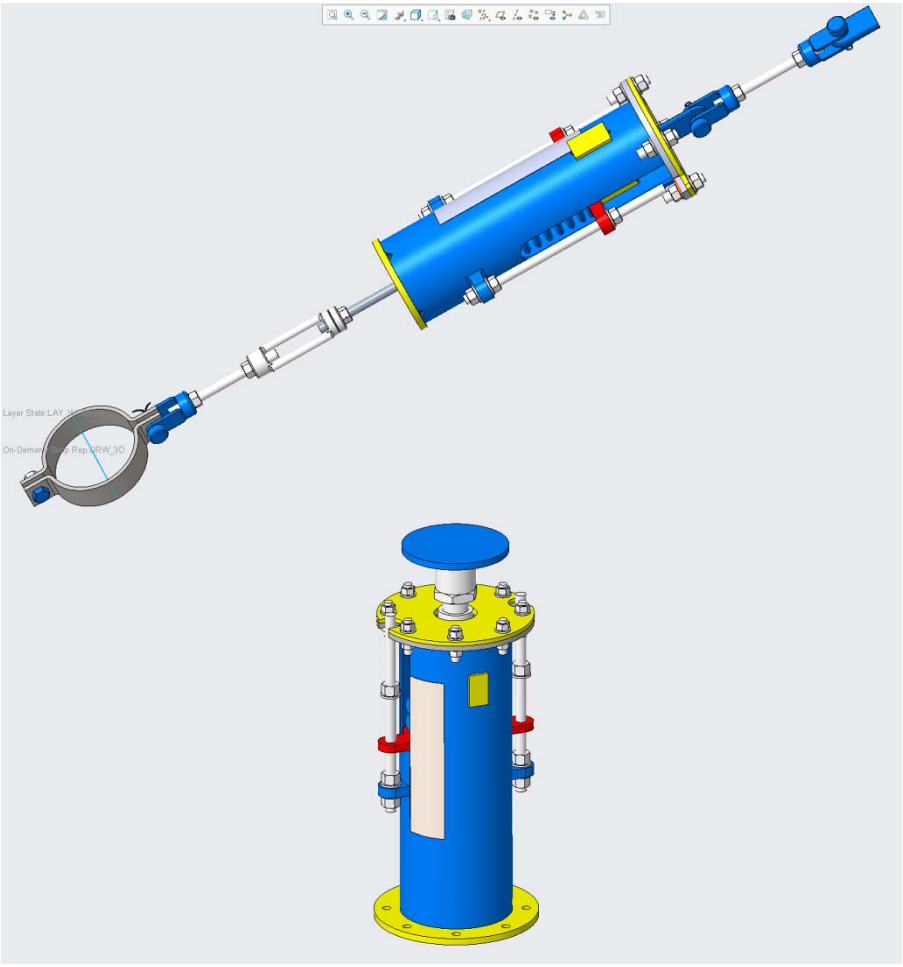

Figure 1. *Fully detailed geometries in PTC Creo 7*

The geometric threads were removed from the threaded parts, and cylinder/bore shapes were created with the same nominal diameter.
An assembly state (Simp Rep [3]) optimized for finite element analysis was created, in which the unnecessary parts were excluded in the force flow, and formal simplifications were performed on the remaining parts (removal of chamfers, roundings, etc.) (Figure 2).

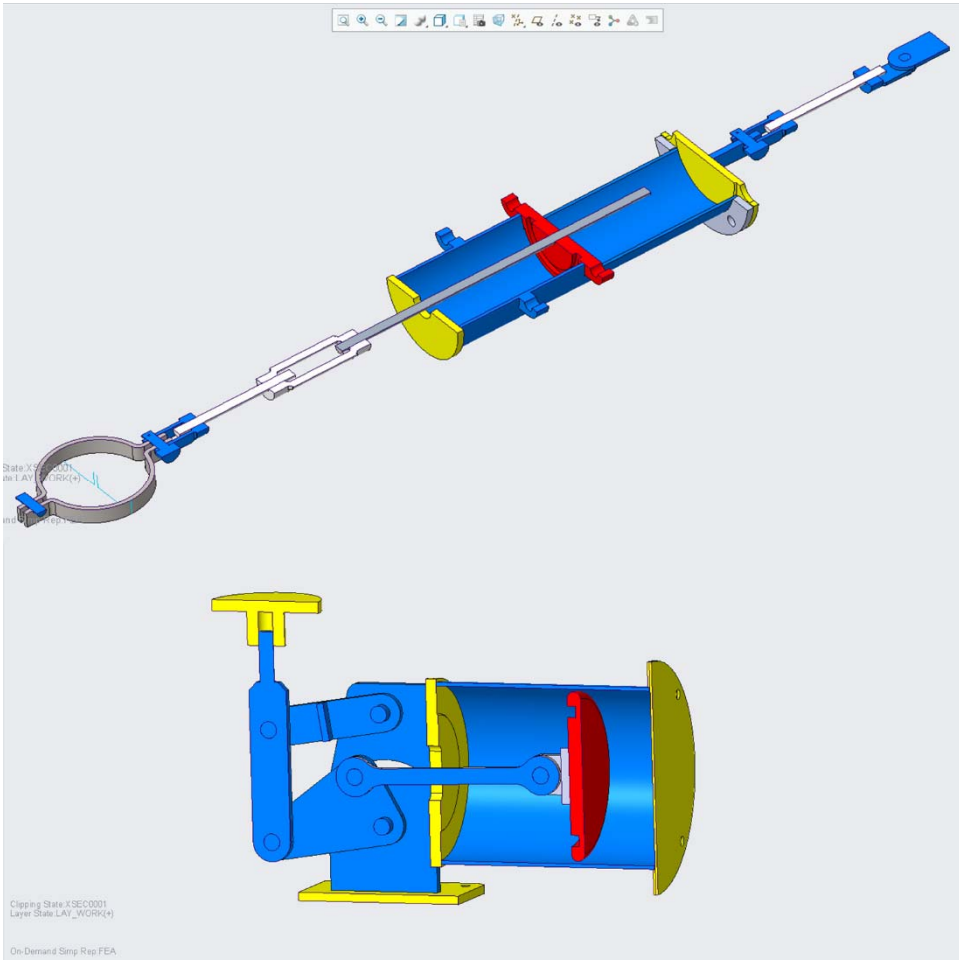

Figure 2. *Simplified geometries in PTC Creo 7*

The compensators can be divided into two subassemblies, between which the spring transfers the load. The subassemblies can be examined separately, thus the assembly states optimized for finite element examination have been created for them as well (Figure 3).

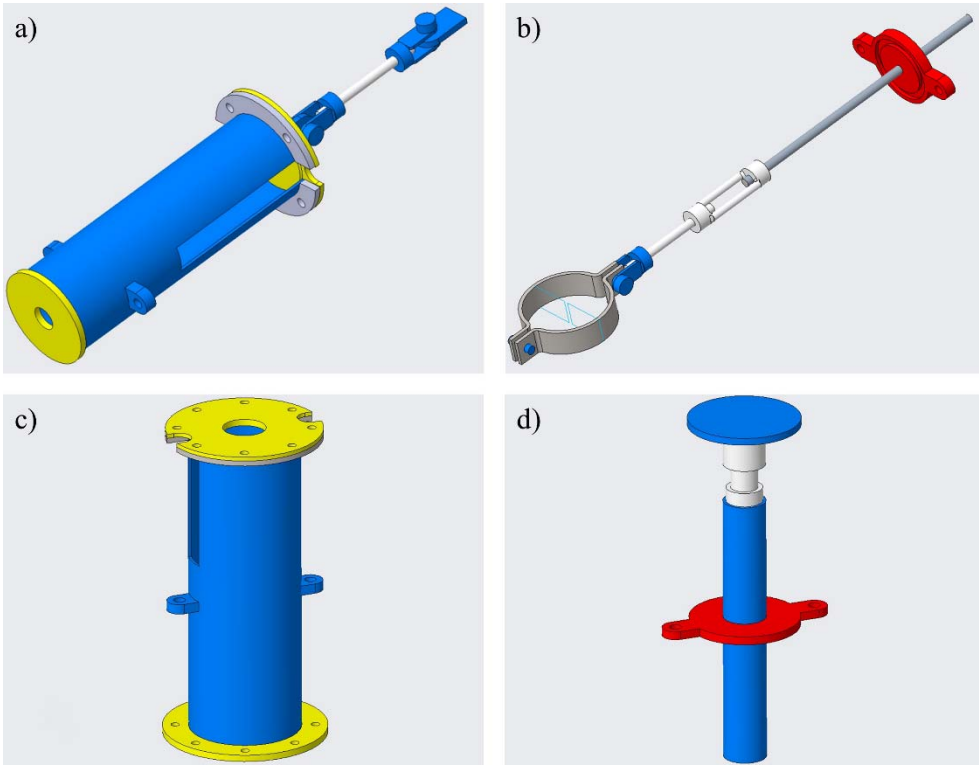

Figure 3. *Separated subassemblies for FEA simulation*
a) Compensator top assembly
b) Tube holder subassembly
c) Housing subassembly
d) Spring holder subassembly

The main assemblies are simulated under maximum load, in which case the two subassemblies are also in physical contact with each other. This can occur at the specified maximum load capacity or during the exceeding of the maximum load capacity (overload) (Figure 4). Four arrangements were selected from the eight types of the manufacture's products. The concerning manufacturer ID's are A, B, E, G.
At the maximum load or overload, the compensator is geometrically terminated to protect the spring inside [4].

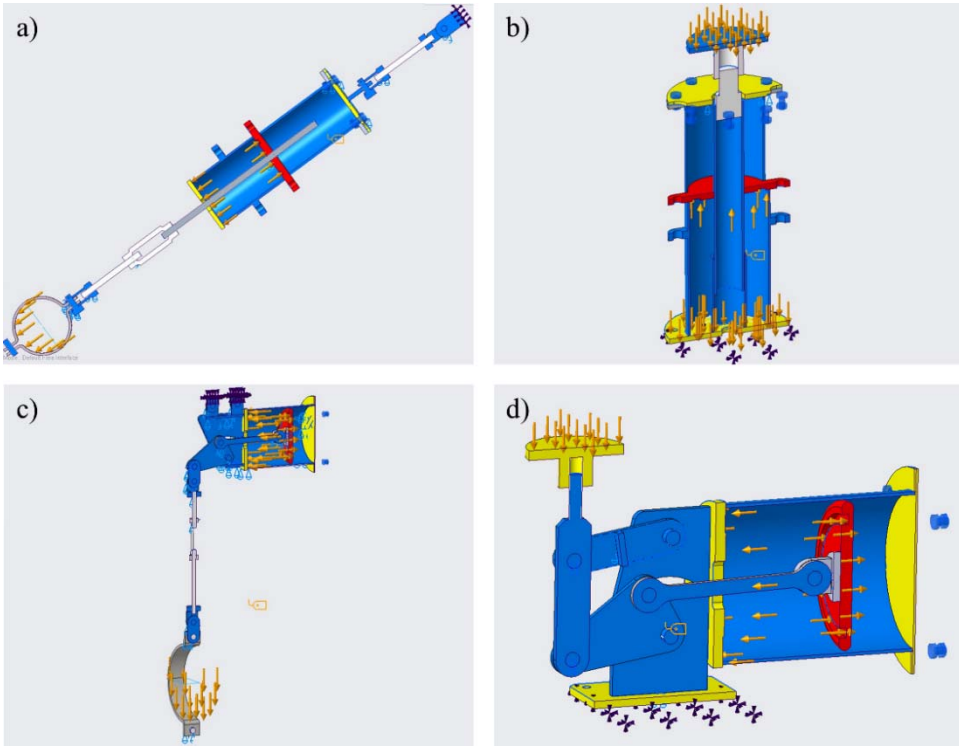

Figure 4. *Load cases of four different top assemblies*
a) Type A
b) Type B
c) Type E
d) Type G

Simulation of subassemblies in 4 positions:

- minimum working load (the spring plate just touches the spring housing cover but does not yet apply a load to it),
- intermediate load (half the range of movement of the spring plate),
- maximum working load (either the specified maximum load - the two subassemblies does not contact with each other; or the value below the specified maximum load - the two subassemblies just contacts with each other, there is no load transfer at the point of impact),
- overload (either the specified maximum load is exceeded - the two subassemblies contact with the help of an overload; or the specified maximum

load - the two subassemblies are contacted with each other, there is a load transfer at the point of collision).

The static component was fixed (all degrees of freedom were 0) in each load case. The fasteners were substituted with special boundary conditions.

Illustration of the simulation result for main assemblies and subassemblies at overload (Figure 5).

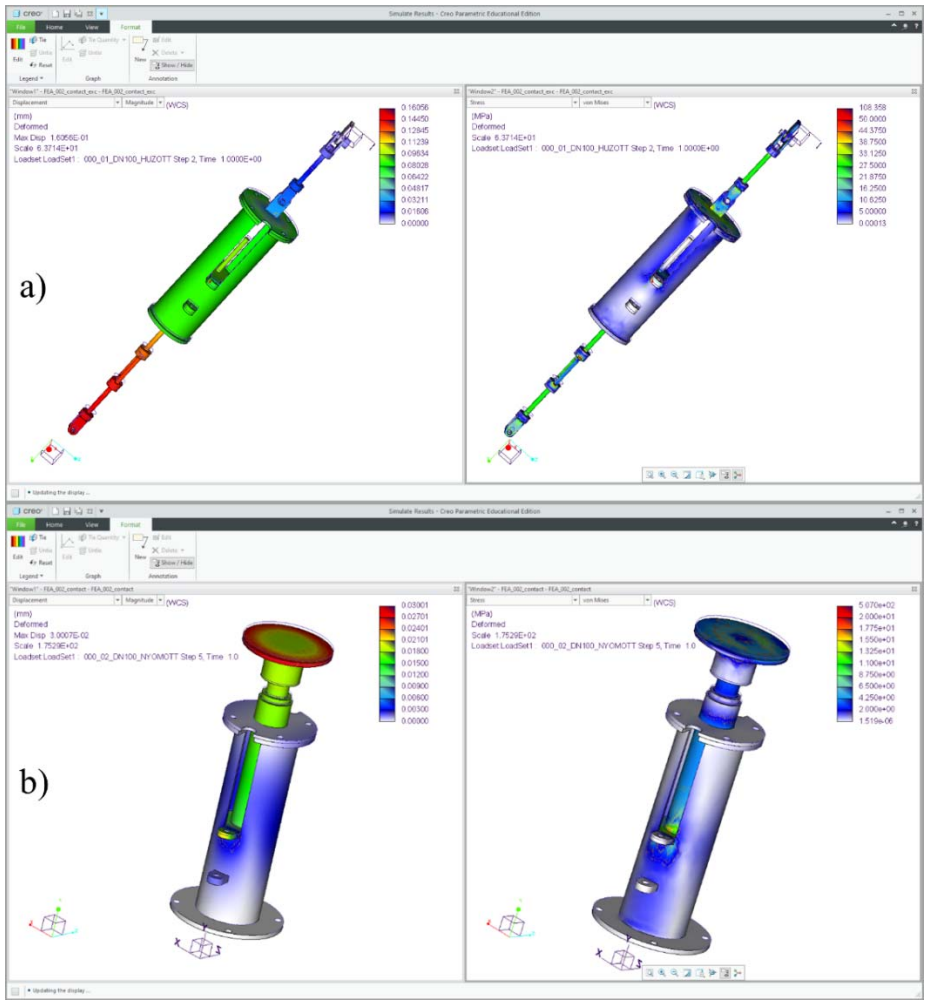

Figure 5. *FEA results in case of overload*
a) Type A
b) Type B

Simplified CAD models [5] were also created from the nine tube compensators, which designed as a reference point for the analytical calculation. The subassemblies were modelled and simulated as components (Figure 6).

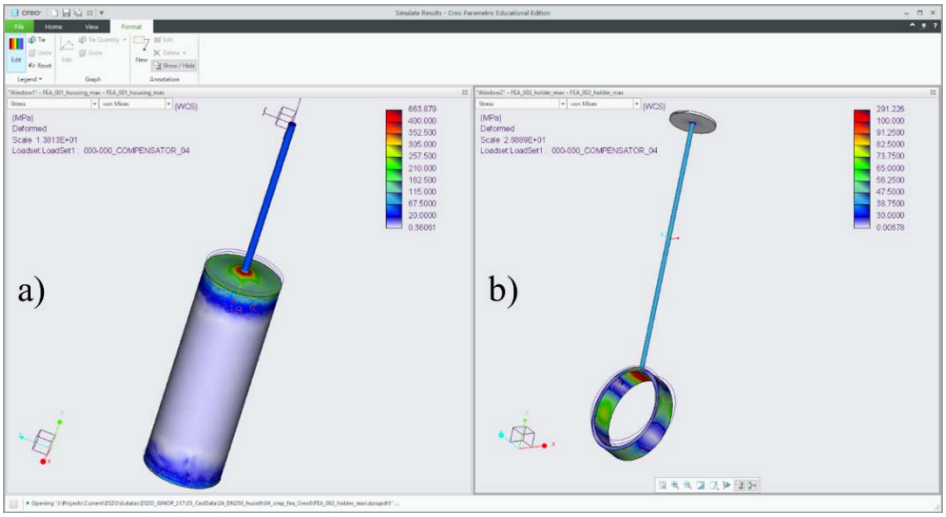

Figure 6. *FEA results on simplified CAD models*
a) Simplified model of housing
b) Simplified model of tube holder

Unfortunately, this method was not accurate enough. Therefore, the full simulations were used as a reference for the analytic calculations.
In parallel with the processes described so far, an Excel spreadsheet was continuously developed, in which, first, the data of the tube compensators were collected, and then various calculations were performed using these data.
In the four situations examined during the simulations, the following was determined:

- the amount of compression of the springs measured at rest (ΔL),
- the force required for the given compression (F_r),
- the length of the compressed spring measured under the given load (L).

The original and simplified models were also prepared. The deformation of the simplified models was calculated analytically as well, considering the main geometries (rod, tube) as spring models.

3. RESULTS

The Table 1 shows the results in summary, where the loads were given (F_{max}), and Max. Fr is the force required for the collision. For example, in the first case, it can be seen that the spring plate will contact the housing sooner than the maximum load. In the fourth case, it appears that it will not contact under maximum load, but only in the event of overload.

Table 1

Values of maximum loads

LOADS - until contact

	min. ΔL	**min. F_r**	**rug. L**	**mid. ΔL**	**mid. F_r**	**rug. L**	**max. ΔL**	**max. F_r**	**rug. L**	**F_{max}**
1	65,0	545,0	350,0	157,5	1320,6	257,5	250,0	2096,2	165,0	3000
2	60,5	507,3	354,5	155,5	1304	259,5	250,5	2100,4	164,5	3000
3	23,0	26,5	257,0	116,0	133,6	164,0	209,0	240,8	71,0	1000
4	83,0	2093,7	460,0	174,5	4401,9	368,5	266,0	6710,0	277,0	6136
5	83,0	2093,7	460,0	174,5	4401,9	368,5	266,0	6710,0	277,0	6136
6	166,0	4447,8	357,0	214,3	5740,6	308,8	262,5	7033,4	260,5	7566
7	166,0	4447,8	357,0	214,3	5740,6	308,8	262,5	7033,4	260,5	7566
8	109,0	6449,8	444,0	198,5	11745,7	354,5	288,0	17041,6	265,0	14000
9	108,0	6390,6	445,0	175,5	10384,7	377,5	243,0	14378,9	310,0	14000
	[mm]	[N]	[mm]	[mm]	[N]	[mm]	[mm]	[N]	[mm]	[N]

These results are also clearly visible in the figures (Figure 7). Where there is a fracture, the contact occurs because the system's rigidity changes significantly. This is spectacular in Example 3 since where the housing and the plate contact, there is a more significant fracture, and then the whole system stretches under the influence of force (F_{max}).

Figure 7. *Comparison of simulated and calculated results*

The research revealed that if we perform the simulation with significantly simplified geometry, the behaviour of the geometry will be very different so we will get very different results. However, calculations and simulations from the original model produce nearly identical results for elongation. This may be because the metal plate's elongation is not calculated, but it is included in the simulation.

The simplified analytical calculation is where geometries have been replaced by elongating rods or tubes. The housing was a tube, and the holder parts were rods. For example, Figure 8 shows that only the holder will stretch in the calculations. In conclusion, the more straightforward analytic calculation was more proportional to the full detailed finite element simulation than the behaviour of the simplified finite element model.

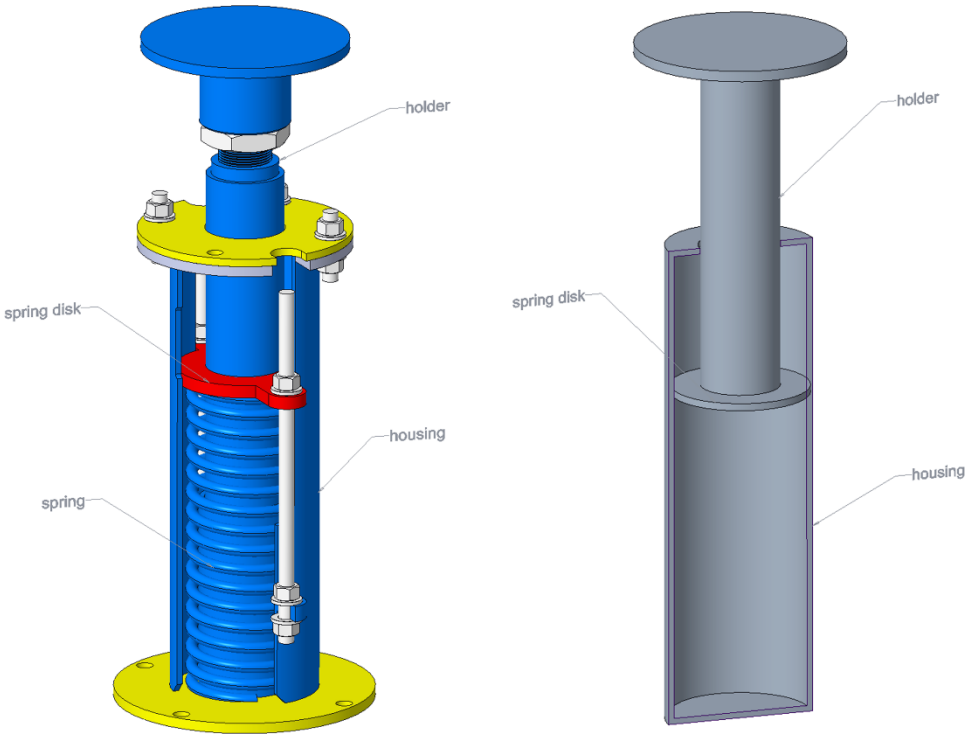

Figure 8. *Simplified geometry for analytic calculation*

Multiplying the calculated result by a specific factor gives the original values, which are 1.22 on average for pulling and 0.98 for pressure. When pulling, the deviation may be due to varying cross-sections. This result means that under a reasonable accuracy there is not needed to simulate the whole model, but the usage of analytical calculations provides accurate results for further design.
Based on these results, a design guide was also developed in SMath opensource software. The program used to perform the analytical calculations was of great help in calculating the desired mathematical operations using the appropriate formulas, instead of paper-based manual calculations. Arranging the four states

detailed above into matrices could be performed as a single operation. Compared to paper-based calculations, the chances of human omission (accounting) could be significantly reduced. Not least, the formula, once made, could be applied to the nine types of compensators (with the help of copying), which significantly speeded up the calculations. SMath can also export a .exe application from the calculations, which allows you to change the parameters of a particular compensator type. The application performs the operations with the changed parameters and prints the result in the appropriate location.

4. CONCLUSION

In order to investigate the deformity of the tube holders, three steps were presented in this project: tube holder strength simulation in full detail, simplification (geometric transformations), simplified analytical calculations.
The result shows that there is no need to simulate the entire model, the application of analytical calculations provides accurate results for further design. In specific circumstances this simplified mathematical model substitutes the more complex FEA analysis well. This kind of calculation can be the calculation of displacements in a wide range tube network.

ACKNOWLEDGEMENT

ESZO Kft.'s application for support under the Economic Development and Innovation Operative Program of GINOP registered with the identification number 2.1.7-15-2016-00764 was considered worthy of approval. Within the framework of the project, the company developed and then manufactured the pipe holder product family with the EMARUG name.
The research reported in this paper is part of project no. BME-NVA-02, implemented with the support provided by the Ministry of Innovation and Technology of Hungary from the National Research, Development and Innovation Fund, financed under the TKP2021 funding scheme.

REFERENCES

[1] Mills, N. (2007). *Polymer Foams Handbook*, ISBN 9780080475448, Butterworth-Heinemann.

[2] Klobucar, R. – Acko, B. (2016). Experimental Evaluation of Ball Bar Standard Thermal Properties by Simulating Real Shop Floor Conditions, *International Journal of Simulation Modelling*, Vol. 15, Nr. 3, ISSN 1726-4529, https://doi.org/10.2507/IJSIMM15(3)10.356.

[3] Stoll, H. W. (1999). *Product Design Methods and Practices*, ISBN 9780824775650, CRP Press, Boca Raton, https://doi.org/10.1201/9781482276800.

[4] Knauf, G. – Kulgemeyer, A. (2015). *Major Standards for Line Pipe Manufacturing and Testing*, Wiley Online Library, https://doi.org/10.1002/9781119019213.ch16.

[5] Horváth, I. et al. (2005). *Advanced Design Support*, ISBN 7-5062-7444-2, Delft University of Technology.

Design of Machines and Structures, Vol. 12, No. 1 (2022), pp. 146–152.
https://doi.org/10.32972/dms.2022.024

HISTORY OF GLEASON WORKS SPIRAL BEVEL GEAR TECHNOLOGY

MIKLÓS GÁBOR VÁRKULI[1] – GABRIELLA BOGNÁR[2]

University of Miskolc, Department of Machine and Product Design
H-3515, Miskolc-Egyetemváros
[1]machvmg@uni-miskolc.hu, [2]v.bognar.gabriella@uni-miskolc.hu
[1]https://orcid.org/0000-0003-4435-7629, [2]https://orcid.org/0000-0002-4070-1376

Abstract: The paper deals with the history of Gleason Works history in regard for their bevel gear manufacturing technology. In spiral bevel gear technology Gleason is a leading company, with many patterns and research studies in this field. The focus of this paper is to show the development of the technology provided by Gleason over the past more than 100 years.

Keywords: *spiral bevel gear, Gleason production machinery, Gleason production methods*

1. INTRODUCTION

In the gear manufacturing industry, three large companies played a decisive role in the development of bevel gears. The three major companies, Gleason, Klingelnberg and Oerlikon laid the foundations for the production and theoretical background of modern bevel gears. Today, a significant portion of the bevel gears are manufactured using Gleason technology.

Figure 1. *Gleason spiral bevel-gear pair [source: internet]*

2. HISTORY OF GLEASON WORKS

William Gleason founded his first machine tool manufacturing workshop in the United States in 1865, in Rochester, which later grew into what is now known as Gleason.

Figure 2. *Gleason Works 1865 [source: internet]*

In 1874, he created the first milling machine suitable for the production of bevel gears. In 1905, the first Gleason factory was built on University Avenue in Rochester, also the headquarter of the parent company. From 1913, the company began the active development of spiral bevel gears. In 1919, a Gleason milling machine called Generator No. 16 was created. It was designed to meet the production needs of the bevel gears in the automotive industry at the time. The machine was built by Paul Böttcher in 1910, It was developed on the basis of James Gleason's 1913, milling machine [2].
In 1928, Brandenberger developed a new type of profile milling machine that was suitable to produce normal and spiral bevel gears.
Before 1930, the idea of the tilted cutter head production machines, and the first working Gleason's model based on this principle was born. In 1956, the Gleason No. 116 Hypoid Generator was introduced, which is already equipped with a tilting cutting head and drive elements can be replaced. Thanks to this, more kinematic setups were possible during production [3], [4].

Figure 3. *Generator No.16 [source: internet]*

Figure 4. *Gleason No. 116 Hypoid Generator [source: internet]*

In 1977, Gleason introduced its PLC-controlled production equipment called the Gleason No. 641 Generator, which was able to create gears in a single workflow.

Figure 5. *Gleason No.641 Generator (PLC controlled) [source: internet]*

In 1986, the company presented its first CNC-controlled bevel gear production equipment. In 1988, a production machine called Phoenix was created. It was the first 6-axis CNC-controlled milling machine suitable for the manufacture of spiral bevel gears [7], [8].
In 2000, the Phoenix II. was introduced, which was already directly driven by a spindle drive it had higher productivity and faster grinding.

Figure 6. *Phoenix II. second gen. 6 axis Gleason bevel gear cutter [source: internet]*

Figure 7. *Gleason Genesis 210H (New Genesis series) [source: internet]*

In 2006, the company introduced the 'New Genesis' family of milling and grinding machines. In 2011, in cooperation with Heller, 5-axis gear machining centres were established to produce large gears. In 2014, their 'New Phoenix 280G' machining machine will be released, which will significantly improve the tooth grinding performance of the bevel gear.
In 2016, the 500CB analyser, and manufacturing equipment has been completed. The equipment is suitable for the manufacture and inspection of the machining heads.[5][6]

Figure 8. *Gleason 500CB [source: internet]*

In 2017, the Genesis 400HCD milling machine was introduced. This new machine was able to use cornering and delineating in parallel.

Figure 9. *Gleason 400HCD [source: internet]*

In 2018, Gleason began integrating KiSSsys design and FEM software with GEMS design and manufacturing software. This allows immediate action and communication between the design and manufacturing sides.
As we can see Gleason has created a solid knowledge base and a wide range of manufacturing tools to meet the growing demand for high-end bevel gears.

REFERENCES

[1] Stadtfeld, H. J. (1993). *Handbook of bevel and hypoid gears: Calculation, manufacturing, optimization*, Rochester Institute of Technology, Rochester.

[2] Litvin, F. L. (1997). *Development of Gear Technology and Theory of Gearing*, NASA Lewis Research Center, Cleveland.

[3] The Gleason Works. (1950). *The Gleason Works 1865-1950*, Rochester.

[4] Woodbury, R. S. (1958). *History of the Gear-cutting machine – A historical study in geometry and machines*, ISBN 9780262730013, Technology Press MIT.

[5] Hotchkiss, R. G. (1990). *The application of the face milling and face hobbing processes on the Gleason Phoenix universal generator*, Gleason Works, Rochester.

[6] Krenzer, T. – Yunker, K. (1990). *Understanding the Phoenix universal bevel and hypoid generator*, Gleason Works, Rochester.

[7] Goldrich, R. N. (1989). *Theory of 6-Axis CNC Generation of Spiral Bevel and Hypoid Gears*, American Gear Manufacturers Association.

REVIEWING COMMITTEE

GY. HEGEDŰS
Institute of Machine Tools and Mechatronics
University of Miskolc
H-3515 Miskolc-Egyetemváros, Hungary
hegedus.gyorgy@uni-miskolc.hu

K. JÁLICS
Institute of Machine and Product Design
University of Miskolc
H-3515 Miskolc-Egyetemváros, Hungary
machijk@uni-miskolc.hu

ZS. KONCSIK
Institute of Materials Science and Technology
University of Miskolc
H-3515 Miskolc-Egyetemváros, Hungary
zsuzsanna.koncsik@uni-miskolc.hu

J. LÉNÁRT
Institute of Machine Tools and Mechatronics
University of Miskolc
H-3515 Miskolc-Egyetemváros, Hungary
lenart.jozsef@uni-miskolc.hu

ZS. LUKÁCS
Institute of Materials Science and Technology
University of Miskolc
H-3515 Miskolc-Egyetemváros, Hungary
zsolt.lukacs@uni-miskolc.hu

L. RÓNAI
Institute of Machine Tools and Mechatronics
University of Miskolc
H-3515 Miskolc-Egyetemváros, Hungary
ronai.laszlo@uni-miskolc.hu

F. SARKA
Institute of Machine and Product Design
University of Miskolc
H-3515 Miskolc-Egyetemváros, Hungary
machsf@uni-miskolc.hu

F. J. SZABÓ
Institute of Machine and Product Design
University of Miskolc
H-3515 Miskolc-Egyetemváros, Hungary
machszf@uni-miskolc.hu

K. SZABÓ
Institute of Machine Tools and Mechatronics
University of Miskolc
H-3515 Miskolc-Egyetemváros, Hungary
szabo.kristof@uni-miskolc.hu

I. SZTANKOVICS
Institute of Manufacturing Science
University of Miskolc
H-3515 Miskolc-Egyetemváros, Hungary
istvan.sztankovics@uni-miskolc.hu

Á. TAKACS
Institute of Machine and Product Design
University of Miskolc
H-3515 Miskolc-Egyetemváros, Hungary
takacs.agnes@uni-miskolc.hu

Z. TOMORI
Institute of Machine Tools and Mechatronics
University of Miskolc
H-3515 Miskolc-Egyetemváros, Hungary
tomori.zoltan@uni-miskolc.hu

Á. TÖRÖK
KTI – Institute for Transport Sciences
H-1119 Budapest, Hungary
Than Károly u. 3-5
torok.adam@kti.hu

I. TÜSKE
Institute of Machine Tools and Mechatronics
University of Miskolc
H-3515 Miskolc-Egyetemváros, Hungary
tuske.istvan@student.uni-miskolc.hu